Universität Hamburg
DER FORSCHUNG | DER LEHRE | DER BILDUNG

Universitätsklinikum Hamburg-Eppendorf

Investigating the role of the transcription factor TCF-1 in the tissue adaptation of Th17 cells in renal autoimmune disease

Dissertation with the aim of achieving a doctoral degree, *Dr. rer. nat*, at the Faculty of Mathematics, Informatics and Natural Sciences

Department of Biology of University of Hamburg

Submitted by

Amirrtavarshni Sivayoganathan

Hamburg 2025

This work was done during the period of 1st October 2020 and 31st December 2024 in the group of Prof. Dr. med. Christian Krebs in the III. Medical Clinic of the Universitätsklinikum Hamburg-Eppendorf.

Gutachter 1: Prof. Dr. Tobias Lenz

Gutachter 2: Prof. Dr. med. Christian Krebs

Datum der Disputation: 29.05.2026

Sometimes life is like a dark tunnel. You can't always see the light at the end of the tunnel, but if you just keep moving... you will come to a better place.

- Uncle Iroh

Dedication

To my parents, for their unwavering support, sacrifices and encouragement throughout my life.

And to myself, for coming this far.

Acknowledgment

The journey of my PhD was a long and rocky road, but along the way, I gained invaluable skills and met wonderful people who made it worthwhile. First and foremost, I would like to express my sincere gratitude to my “Doktorvater”, Prof. Dr. med. Christian Krebs, for not only providing me with this incredible opportunity but also for guiding me through the entire process. His commitment to me and this project, especially through our weekly meetings, gave me the constant guidance and feedback I needed to complete my PhD.

Furthermore, I would like to thank Prof. Dr. Tobias Lenz who agreed to be my second supervisor and provided me guidance.

I would also like to give a special thanks to Prof. Dr. med. Ulf Panzer and Prof. Dr. med. Samuel Huber for the possibility to perform my thesis within the SFB1192 and allowing me to join lab meetings that were always filled with insightful scientific discussions.

A big thank you goes to Alina Borchers, who assisted me with every single one of my experiments. Alina was a guiding hand throughout my journey; my experiments would not have run so smoothly without her expertise. She is the sunshine of our group, always pushing all of us to achieve our best. Alina is the biggest supporter of all AG Krebs scientists.

I would also like to thank all the medical students of the AG Krebs: Jens Kleiner, Tobias Neben, Arthur Hube and Vincent Piegsa, who I had the pleasure of working with and who also helped me immensely on this journey. Jens and I started this scientific journey together and established our protocols. Once my mouse line was ready, Tobias aided me on all my experimental days and ensured my experiments ran smoothly. Vincent joined much later on in my journey, but with his bioinformatical insight helped me finalise my figures. A very special thank you to Arthur who not only assisted with my experiments, results and bioinformatical analysis but was always open to critical discussions about my helping me shape the narrative of my project with his scientific mind.

A special shout out also goes to my dear friends Dr. rer. biol. hum. Apurva Shrivastava whom I met whilst she was also embarking the PhD journey. She is an incredibly supportive friend who shared her wisdom with me and always had an open ear to listen to me and advise me.

I would also like to express my gratitude to Dr. rer. nat. Saskia Jauch-Speer who helped me in processing my single cell samples for sequencing.

Lastly and most importantly, I would like to thank my family and friends without whom I would not be here today. My parents and sister who showered me with love and made me believe I could make it this far. My friends – the “BioSquad”, the “Earlsdon Housemates” and my CHSA girls - thank you for believing in me and supporting me through this journey.

Table of Contents

Acknowledgment v
List of Figures iii
List of Tables v
Abstract 1
Zusammenfassung 2
1 Introduction 3
1.1 The immune system 3
1.2 T cells 5
1.3 Th1 and Th2 Cells 6
1.4 Treg Cells 7
1.5 Th17 Cells 7
1.5.1 Th17 plasticity 8
1.6 Autoimmune kidney disease 10
1.7 The role of Th17 in the kidney and intestine 12
1.8 Tcf7 13
1.9 *Tcf7* and Th17 cells 13
1.10 Hypothesis and aim 15
2 Materials and Methods 16
2.1 Materials 16
2.1.1 Mice 16
2.1.2 Primers for Genotyping 16
2.1.3 Antibodies 17
2.1.4 FACS Antibodies 17
2.1.4 Buffers, Solutions and Media 18
2.1.5 Chemicals and consumables 19
2.1.6 Plasticware 20
2.1.7 Kits 21
2.1.8 Equipment 21
2.1.9 Software 23
2.2 Methods 24
2.2.1 Genotyping of transgenic mice 24

2.2.2 Histological tissue preparation 26
2.2.3 Induction of nephrotoxic nephritis (NTN) 29
2.2.3 Urine sample collection and proteinuria determination 30
2.2.4 Isolation of cells from murine kidneys 30
2.2.5 ELISA of renal albumin 31
2.2.6 Determination of renal creatinine 34
2.2.7 Quantification of blood urea nitrogen 35
2.2.8 Induction of anti-CD3 induced duodenitis 35
2.2.9 Isolation of cells from murine duodenum 35
2.2.10 Staining for FACS analysis 36
2.2.11 Flow cytometric cell sorting 38
2.2.10 Whole kidney tissue dissociation 38
2.2.12 Single Cell Sequencing 38
2.2.13 Bioinformatical analysis 40
3 Results 41
3.1 Single cell & single nuclei sequencing data 41
3.1.1 Renal leukocytes from cGN induced and control mice 41
3.1.2 Th17 cells from cGN induced and control mice 46
3.1.3 Pseudotime analysis of Th17 cells 49
3.1.4 ATAC-seq data from cGN induced mice 52
3.2 Functional *in vivo* FACS data 56
3.2.1. Establishment of transgenic mice for experimental purposes 56
3.2.2 *In vivo* FACS analysis in crescentic glomerulonephritis 58
3.2.3 *In vivo* FACS analysis in anti-CD3 induced duodenitis 62
3.3 Whole kidney analysis 66
3.3.1 scRNA-seq of the whole kidney from control and cGN induced mice 66
4 Discussion 70
4.1 Single cell sequencing analysis 70
4.1.1 High expression of TCF-1 in Th17 cells from murine kidneys 70
4.1.2 Differential expression of distinct sub-clusters revealed within renal murine Th17 cells 72
4.1.3. Inverse expression of RORγT and TCF-1 within the Th17 cell pseudotime trajectory 74
4.1.4 High RORγT chromatin accessibility in Th17 and Th1 cells 77
4.2 Functional *in vivo* analysis 79

4.2.1 Increased expression of IL-10 in Th17 cells of cGN induced mice 79
4.2.2 Reduced expression of IL-10 in Th17 cells in duodenitis induced mice ... 80
4.3 Whole kidney scRNA-seq analysis 82
4.3.1 High expression of IL-10 receptors in endothelial cells 82
Conclusion 85
References 87
List of Abbreviations 98
Curriculum Vitae 101
Eidesstattliche Erklärung/Affidavit 103

List of Figures

Figure 1: Brief overview of immune cell subtypes 4

Figure 2: Differentiation pathways of T lymphocytes 6

Figure 3: Th17 plasticity 8

Figure 4: The kidney and the physiology of the nephron 11

Figure 5: GEM generation in chip 38

Figure 6: Generation of cDNA from GEMs 39

Figure 7: Generation of gene expression library 39

Figure 8: GEMs of ATAC protocol 40

Figure 9: Overview of cell sorting, clustering and cell group distribution analysis of leukocytes from the cGN model. 42

Figure 10:Differential expression of key markers in cGN and control groups. 45

Figure 11:Analysis of Th17 cluster within the cGN leukocyte dataset 46

Figure 12: Visualization of Gene Expression on UMAP Integrated into the Monocle3 Pipeline. 49

Figure 13: Analysis of Th17 Cell Differentiation Using Seurat and Monocle3. 50

Figure 14: Overview of cell sorting, clustering and integration of ATAC-seq data of cGN induced mice 53

Figure 15: Integration and analysis scRNA-seq and ATAC-seq data 55

Figure 16: Genetic modification and validation of experimental mouse lines. 57

Figure 17: Experimental crescentic glomerulonephritis model and disease severity assessment. 59

Figure 18: Quantification of YFP^+ cells in cGN. 60

Figure 19*:* Cytokine expression profiles in cGN across $CD4^+$ T cell subsets. 61

Figure 20: Anti-CD3 induced duodenitis model and disease severity assessment 62

Figure 21: Quantification of YFP^+ cells in anti-CD3 induced duodenitis. 63

Figure 22: Cytokine expression profiles in anti-CD3 induced duodenitis across $CD4^+$ T cell subsets..... 65
Figure 23: Clustering analysis of single cell RNA-seq data from the whole kidney..... 66
Figure 24: Analysis of signalling pathways and IL-10 receptor expression in the whole kidney 69

List of Tables

Table 1: PCR master mixes 24

Table 2: Genotyping PCR steps 25

Table 3: PAS rehydration and deparaffinisation 27

Table 4: PAS dehydration 27

Table 5: ELISA dilution determination 33

Table 6: ELISA standard concentrations 34

Table 7: Creatinine standard concentrations 35

Table 8: FACS antibody staining panel for extracellular staining 37

Table 9: FACS antibody staining panel for intracellular and intranuclear staining 37

Table 10: FACS antibody staining panel for cell sorting 38

Abstract

Chronic kidney diseases affect approximately 10-12% of the world population and ranks among the top ten causes of death globally. One of these kidney diseases is crescentic glomerulonephritis which accounts for 15% of these patients in severe cases leading to irreversible kidney failure. $CD4^+$ T cells, Th17 cells in particular, are key drivers of immune mediated renal tissue damage. Th17 cells have shown to exhibit tissue adaptation capabilities, potentially worsening or ameliorating the disease outcome.

In this study, the role of the transcription factor, TCF-1, in the plasticity of Th17 cells was investigated. Using *Il17A*^{cre} *x R26*^{eYFP} and *Tcf7*^{flox} x *Il17A*^{cre} *x R26*^{eYFP} mouse lines in *in vivo* experiments, it was revealed that in the absence of TCF-1 renal IL-17A producing cells produce more of the anti-inflammatory cytokine IL-10. Additionally, single cell RNA sequencing revealed the heterogeneity of Th17 cells by identifying various subsets of renal Th17 cells with different cytokine expression profiles. Furthermore, a pseudotime analysis using the single cell data of the renal Th17 cells revealed an inverse relationship of the expression of the transcription factors TCF-1 and RORγT, revealing TCF-1 to be a negative regulator of renal Th17 cells.

These findings could potentially lead to discovering more strategic and efficient therapeutic approaches in crescentic glomerulonephritis by targeting pathogenic Th17 cells, triggering an anti-inflammatory response in the kidney to avoid further tissue damage.

Zusammenfassung

Chronische Nierenerkrankungen betreffen etwa 10-12 % der Weltbevölkerung und gehören weltweit zu den zehn häufigsten Todesursachen. Eine dieser Nierenerkrankungen ist die halbmondförmige Glomerulonephritis, die bei 15 % der Patienten auftritt und in schweren Fällen zu irreversiblem Nierenversagen führt. CD4+ T-Zellen, insbesondere Th17-Zellen, sind die Hauptverantwortlichen für die immunvermittelte Schädigung des Nierengewebes. Es hat sich gezeigt, dass Th17-Zellen die Fähigkeit zur Gewebeanpassung besitzen, was den Krankheitsverlauf möglicherweise verschlimmern oder verbessern kann.

In dieser Studie wurde die Rolle des Transkriptionsfaktors TCF-1 bei der Plastizität von Th17-Zellen untersucht. Mit der Verwendung von *Il17A*^{cre} *x R26*^{eYFP} und *Tcf7*^{flox} x *Il17A*^{cre} *x R26*^{eYFP} Mauslinien in In-vivo-Experimenten zeigte sich, dass in Abwesenheit von TCF-1 17A-produzierende Zellen in der Niere mehr des entzündungshemmenden Zytokins IL-10 produzieren. Darüber hinaus zeigte die Einzelzell-RNA-Sequenzierung die Heterogenität der Th17-Zellen, indem verschiedene Untergruppen von Th17-Zellen in der Niere mit unterschiedlichen Zytokin-Expressionsprofilen identifiziert wurden. Darüber hinaus ergab eine Pseudozeitanalyse unter Verwendung der Einzelzelldaten der renalen Th17-Zellen eine umgekehrte Beziehung zwischen der Expression der Transkriptionsfaktoren TCF-1 und RORγT, was darauf hindeutet, dass TCF-1 ein negativer Regulator der renalen Th17-Zellen ist.

Diese Erkenntnisse könnten möglicherweise dazu führen, dass strategischere und effizientere Therapieansätze für die sichelförmige Glomerulonephritis gefunden werden, indem die pathogenen Th17-Zellen ins Visier genommen und eine entzündungshemmende Reaktion in der Niere ausgelöst werden, um weitere Gewebeschäden zu vermeiden.

1 Introduction

1.1 The immune system

Living organisms are constantly exposed to harmful invaders, including pathogens and other foreign substances. In order to counteract such attacks against the host's body, a complex network of cells, plasma-proteins, tissues and organs act as a defence mechanism. This is known as the immune system. Its primary function is to recognise and eliminate these threats while maintaining tolerance to the body's own cells and tissue.

The immune system contains a diverse range of cell types (Figure 1) and it consists of two main branches: the innate and adaptive immune response (Delves & Roitt, 2000). The two branches originate based on their myeloid or lymphoid lineage (Niroula et al., 2021). The innate immune system is the first line of defence when exposed to a pathogen. Starting with physical barriers, such as the skin or mucus membrane extending to rapid and nonspecific defence mechanisms such as short-lived immune cells, including macrophages and neutrophils, (Turvey & Broide, 2010). The cellular components of the immune system recognise and eliminate pathogens and foreign antibodies via various mechanisms, including phagocytosis and cytotoxicity. Furthermore, the innate immune system relies on molecular mediators, including complement proteins and antimicrobial peptides, which act synergistically to enhance the clearance of pathogens and promote inflammation (Cruvinel et al., 2010).

In contrast to the innate response, the adaptive immune response offers a slower but more specific and targeted response with long-term memory. The two central cell types involved in the adaptive response are B and T lymphocytes (Deets & Vance, 2021). B cells are named after the bursa of Fabricius, which is the site of hematopoiesis in birds since B cells were first identified in the Fabricius birds (Cooper et al., 1966). In contrast, T cells are termed after their location of development which is the thymus (Miller, 1961). These cells can recognise specific pathogens and create an immunological memory of past infections, enabling these cells to

mount a more rapid and more precise response upon re-exposure to the same pathogen. B cells differentiate into plasma cells when exposed to antigens. These plasma cells secrete antibodies tailored to the specific antigen (Arpin et al., 1995). The secreted antibodies, also known as immunoglobulins, bind to antigens with high specificity, marking them for destruction by other immune cells or neutralising their effects (Hoffman et al., 2016). In comparison, T lymphocytes undergo clonal expansion and differentiate into a range effector and memory cells depending on the pathogen (Adams et al., 2020).

Cell	Image	% in adults	Nucleus	Functions	Lifetime	Main targets
Macrophage	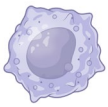	Varies	Varies	Phagocytosis Antigen presentation to T cells	Months – years	Various
Neutrophil	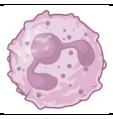	40-75%	Multi-lobed	Phagocytosis Degranulation	6 hours – few days	Bacteria Fungi
Eosinophil		1-6%	Bi-lobed	Degranulation Release of enzymes, growth factors, cytokines	8 – 12 days (circulate for 4 -5 hours)	Parasites Various allergic tissue
Basophil	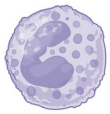	< 1%	Bi- or tri-lobed	Degranulation Release of histamine, enzymes, cytokines	Lifetime uncertain (likely a few hours – few days)	Various allergic tissues
Mast cell	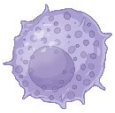	Common in tissues	Central, single-lobed	Degranulation Release of histamine, enzymes, cytokines	Months to years	Parasites Various allergic tissues
Lymphocyte (T cells)		20-40%	Deeply staining, eccentric	T helper (CD4+) cells: immune response mediators Cytotoxic (CD8+) cells: cell destruction	Weeks to years	Th cells: intracellular bacteria Cytotoxic T cells: virus infected and tumour cells
Monocyte		2-6%	Kidney shaped	Differentiate into macrophages and dendritic cells to elicit an immune response	Hours – days	Various
Natural killer cell	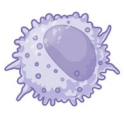	15% of circulating lymphocytes and tissue	Single-lobed	Tumour rejection Destruction of infected cells Release of perforin and granzymes which induce apoptosis	7 – 10 days	Viruses Tumour cells

Figure 1: Brief overview of immune cell subtypes (adapted from Marshall et al., 2018 using Biorender)

Two other noteworthy groups of immune cells are innate lymphoid cells (ILCs) (Spits & Di Santo, 2011) and unconventional T cells (Godfrey et al., 2015). ILCs are types of innate immune cells that resemble T helper cells in function but lack antigen-specific receptors. Their role is the rapid response to infection and tissue damage, with their main location being mucosal surfaces. There are three main groups of ILCs: ILC1, ILC2 and ILC3, with each group mirroring the function of Th1, Th2 and Th17 cells, respectively (Klose et al., 2016). On the other hand, unconventional T cells are not dependent on the classical MHC-restricted activation like other T cells. Some examples of unconventional T cells are: γδ T cells, invariant natural killer (iNK) cells and mucosal-associated invariant T (MAIT) cells (Brenner et al., 1986; Makino et al., 1995; Treiner et al., 2003). These act as a bridge between the innate and adaptive immunity response and contribute to tissue homeostasis and immune surveillance.

1.2 T cells

T lymphocytes, also known as T cells, are an essential part of the adaptive immune system and are the key players of cell-mediated immune reactions. These cells mature in the thymus, hence why they are called “T” cells, even though they originate from the bone marrow (Miller, 1961). In the thymus, these cells undergo a rigorous selection process that ensures both self-tolerance and functional competence. Once the cells have matured, they migrate to secondary lymphoid organs and await exposure to antigens (Luckheeram et al., 2012).

T cells can be grouped into functionally distinct populations based on their cell surface protein expression, the main examples being CD4 and CD8 (Kortekaas Krohn et al., 2022). The cell surface protein expression determines the later fates of the T lymphocytes. T cells that are characterised by a $CD8^+$ expression are also known as cytotoxic T cells. These cells specialise in killing infected and abnormal cells in the body by releasing perforin, granzymes and granulysin which trigger cell apoptosis. These cells play a critical role in eliminating intracellular pathogens as well as tumour cells (Andersen et al., 2006).

T cells characterised by a $CD4^+$ cell surface protein expression are called T helper (Th) cells. These cells are crucial for orchestrating immune responses. Once activated, they differentiate into various subtypes (Figure 2), including Th1, Th2, Th17 and T regulatory cells. Each of these cells are uniquely characterised by their specific cytokine profiles and effector functions (Kortekaas Krohn et al., 2022; Luckheeram et al., 2012).

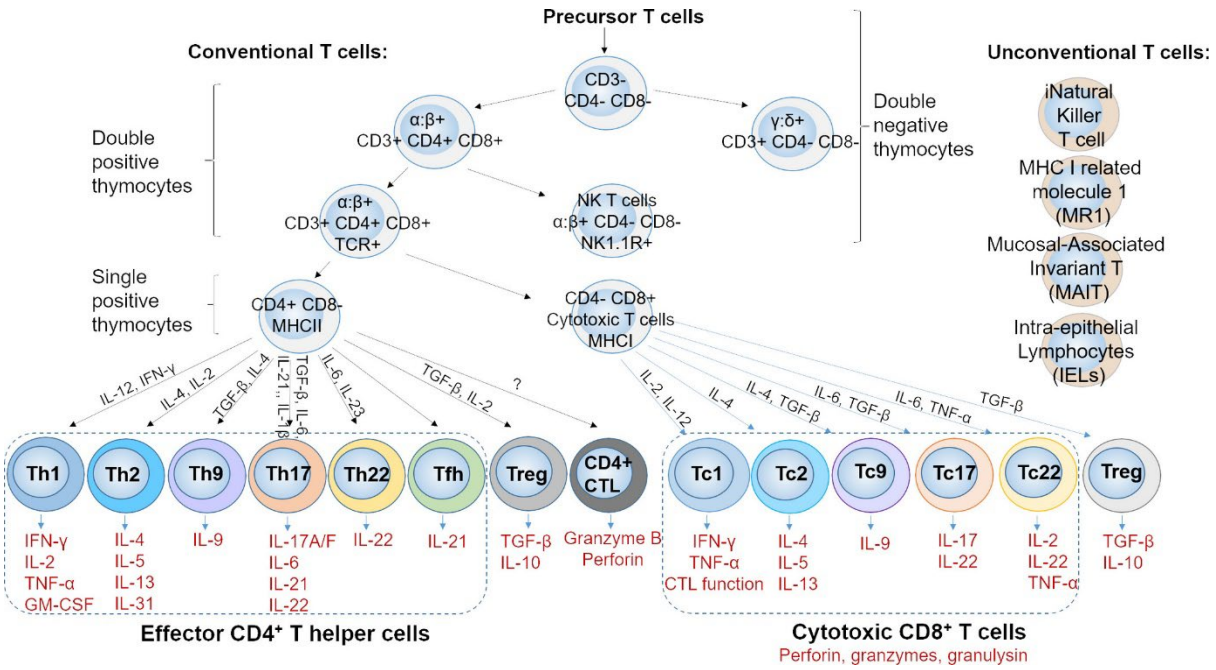

Figure 2: Differentiation pathways of T lymphocytes (Kortekaas Krohn et al., 2022)

1.3 Th1 and Th2 Cells

Th1 cells are primarily involved in the cellular immunity against intracellular pathogens such as bacteria and viruses. Th1 cells express the transcription factor T-bet and the surface marker CD161 among others (Szabo et al., 2000). Upon activation, these cells produce pro-inflammatory cytokines, including interferon-gamma (IFN-γ) and tumour necrosis factor-alpha (TNF-α), which enhance phagocytosis, promote the activation of macrophages and cytotoxic T cells and stimulate the production of opsonising antibodies. Therefore, Th1 cells are crucial for clearing intracellular pathogens and providing long-lasting immunity (O'Garra & Vieira, 2007).

Th2 cells, on the other hand, are responsible for the humoral immunity and responses against extracellular parasites, allergens and helminths. Th2 cells express the transcription factor GATA3 and they produce the following cytokines: IL-4, IL-5, IL-9 and IL-13 (Zhu et al., 2006). The release of IL-5 and IL-13 induces the production of eosinophils which trigger apoptosis in infected cells. Th2 cells are also crucial for infections or inflammation in the airways, such as asthma (Nakayama et al., 2017).

1.4 Treg Cells

T regulatory (Treg) cells are another crucial subset of CD4+ T lymphocytes. These cells are essential for maintaining homeostasis by supressing and regulating other T effector cells, such as Th1, Th2 and Th17 cells (Shevyrev & Tereshchenko, 2020). Treg cells express the transcription factor FOXP3 and are characterised by the production of the anti-inflammatory cytokine IL-10 and TGF-β (Ohkura et al., 2012; Palomares et al., 2014). The cytokine IL-10 exhibits the ability to suppress Th17 and Th1 directly in the kidney and gut, respectively (Ostmann et al., 2013; Wadwa et al., 2016).

Another subtype of Treg cells are T regulatory type 1 (Tr1) cells. These cells produce IL-10, the signature cytokine of Treg cells but lack the expression of FOXP3. The interleukin, IL-27 has been identified as an inducer of Tr1 cells *in vitro* (Awasthi et al., 2007; Pot et al., 2009).

1.5 Th17 Cells

Th17 cells were first identified in 2005 (Harrington et al., 2005). These cells were initially characterised by their induction through IL-23 and their role in infection and inflammation (Park et al., 2005). Since then, their master transcription factor has been identified as RORγT (Ivanov et al., 2006). Their main drivers were discovered to be TGF-β and IL-6, which induce non-pathogenic Th17 cells (Veldhoen et al., 2006). RORγT is essential for IL-17A production and is also expressed by other IL-17A producing cells such as γδ T cells. Another important

transcription factor for Th17 cells is RORα, which is also expressed in other lymphoid and myeloid cells (Yang et al., 2008).

However, studies also discovered pathogenic Th17 cells in various autoimmune diseases, such as rheumatoid arthritis, which were induced by IL-6, IL-1β and IL-23 (Ghoreschi et al., 2010; McGeachy et al., 2007).

1.5.1 Th17 plasticity

T cell plasticity refers to the ability of T cells to transdifferentiate and adapt their functions based on environmental triggers such as cytokine signalling. This ability enables T cells to respond effectively to various pathogens and ensure immune homeostasis. However, in the context of autoimmune disease, dysregulated T cell plasticity may lead to pathological immune responses (Lee et al., 2009).

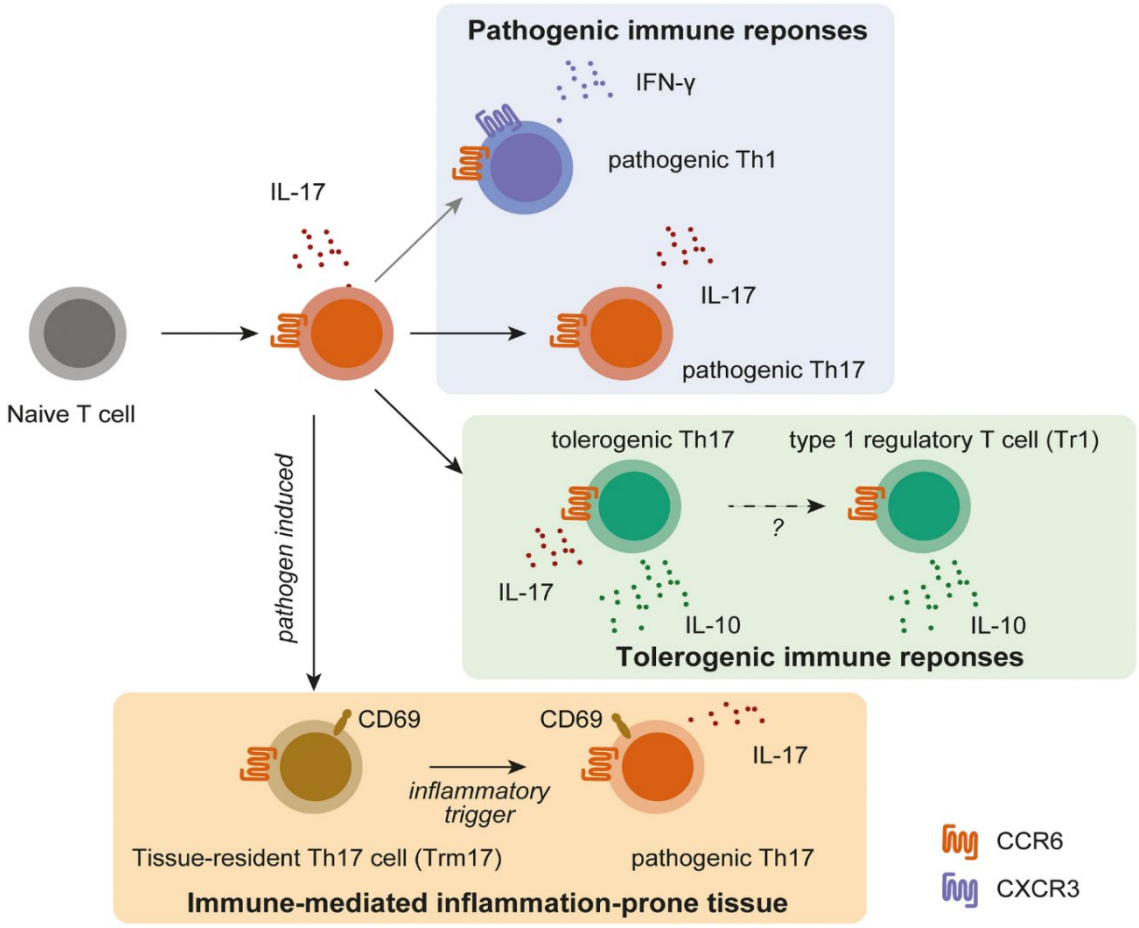

Figure 3: Th17 plasticity (Soukou et al., 2021)

Th17 cells have also been shown to exhibit plasticity in different organs with various different factors capable of inducing these changes (Hirota et al., 2011). One of the primary factors influencing this Th17 plasticity is the cytokine milieu. The presence of TGF-β and IL-6 is essential for the initial differentiation and development of Th17 cells. However, exposure to the cytokines IL-12 and IFN-γ can induce a shift towards a Th1-like phenotype (Mukasa et al., 2010). The co-expression of CCR6 and CXCR3 is an indicator of Th1-like ex-Th17 cells (Figure 3), which have been shown to be pathogenic (Acosta-Rodriguez et al., 2007). These cells are characterised by the production of IFN-γ on top of IL-17A. Conversely, the presence of IL-4 can drive Th17 cells towards a Th2-like phenotype. These Th2-like ex-Th17 cells are characterised by the production of IL-13 and IL-4 (Bhaumik & Basu, 2017; Dardalhon et al., 2008).

Metabolic signals and the microenvironment can also trigger a change in the Th17 cell phenotype. Some factors that can affect the function and stability of Th17 cells are nutrient availability, hypoxia and the presence of microbial metabolites. For example, short-chain fatty acids produced by gut microbiota can promote the expansion and function of Treg cells from Th17 cells (Chen & Tang, 2021; Sun et al., 2017).

This plasticity of Th17 cells can have various implications. Even though this ability is remarkable and allows for a robust immune response, it can also promote inflammatory diseases, for example, in multiple sclerosis or rheumatoid arthritis (Schnell et al., 2023). The transition of Th17 cells into Th1-like cells can enhance the clearance of intracellular pathogens by inducing macrophage activation and production of IFN-γ (Harbour et al., 2015).

Studies have shown that Th17 cells can also contribute to the pathogenesis of inflammatory diseases because their plastic nature enables them to acquire pathogenic properties under certain conditions. In multiple sclerosis, Th17 cells produce GM-CSF which exacerbates neuroinflammation and tissue damage (Rasouli et al., 2015). Similarly, in rheumatoid arthritis Th17 cells produce both IL-17 and IFN-γ which contributes to inflammation and destruction (de Wit et al., 2016). In renal autoimmune disease Th17 cells acquire a Th1-like phenotype,

contributing to renal tissue damage (Enk et al., 2024; Krebs et al., 2016). This tissue adaptation ability of Th17 cells in the kidney will be the focus of this study.

1.6 Autoimmune kidney disease

The kidney is a paired organ located on the bilaterally in the retroperitoneal space. The organ is separated into the following regions: filtering units and glomeruli in the kidney cortex as well as a tubular system that entails the cortex and medulla which is responsible for the regulation of fluid, salt and metabolite reabsorption. The kidney is comprised of approximately 1 million nephrons. These nephrons consist of blood vessels, tubules, collecting ducts and glomeruli (Figure 4). Each nephron contains one glomerulus. The glomerulus consists of a cluster of many blood vessels that filter the blood. Glomeruli have thin walls that allow waste and water to pass into the tubule and leave the body via urine (Kurts et al., 2025).

The kidney has a wide range of functions, but its main function is the excretion of toxic waste products from the blood through urine. Other functions of the kidney include the maintenance of the body's water and electrolyte level as well as the base-acid balance in the whole body (Hamm et al., 2015). The kidney also releases the hormones erythropoietin and renin, to regulate erythropoiesis as well as bone integrity and blood pressure respectively (Crowley et al., 2024; Jelkmann, 2011). Additionally, the kidneys convert Vitamin D into calcitriol which is essential for calcium absorption and bone health (Ginsberg & Ix, 2024).

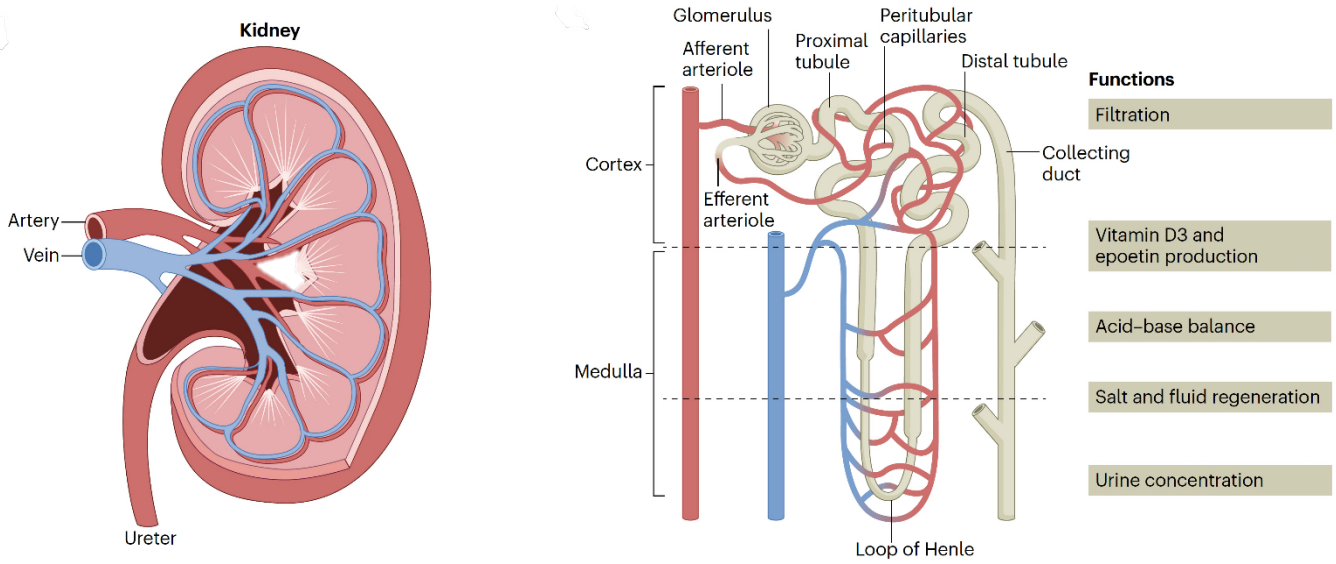

Figure 4: The kidney and the physiology of the nephron (Kurts et al., 2025)

Chronic kidney diseases affect approximately 10-12% of the world population (Levin et al., 2017). One of those renal diseases is rapidly progressive glomerulonephritis (RPGN), which is characterised by a rapid loss of kidney function. RPGN can be categorised into three main types (Couser, 1988). Anti-glomerular basement membrane (GBM) glomerulonephritis is categorised as Type I RPGN and is driven by autoantibodies against type IV collagen in the GBM. Type II RPGN, also known as immune complex RPGN, can be recognised by the formation of immune complexes which are deposited in the kidney and cause cell infiltration. Type III RPGN is known as pauci-immune RPGN which makes up approximately 50% of all RPGN cases worldwide. It is characterised by a lack of prominent complement or immune complex depositions in the kidney but is associated with increased anti-neutrophil cytoplasmic antibodies (ANCA) in the peripheral blood (Mohamed et al., 2024). The histopathology of RPGN is characterised by glomeruli with a crescentic shape. This phenomenon is called crescentic glomerulonephritis (cGN). Crescentic GN is an acute immune-mediated disease, often resulting in chronic remission due to inflammation and injury, and in severe cases leading to irreversible kidney failure (Al Mushafi et al., 2021).

1.7 The role of Th17 in the kidney and intestine

As immune cells, Th17 cells fulfil their role in the kidney by protecting against infections and maintaining tissue integrity. The two main protective functions of Th17 cells in the kidney are IL-17 mediated recruitment of neutrophils and induction of antimicrobial peptide production (Schmidt et al., 2018). However, the pathological potential of Th17 cells in the kidney is more prominent. In autoimmune diseases such as anti-GBM glomerulonephritis and lupus nephritis, Th17 cells exacerbate inflammation and tissue injury. Th17 cells secrete IL-17A and IL-17F, which trigger the recruitment of inflammatory cells, including neutrophils and macrophages, to the kidney, further driving tissue damage (Riedel et al., 2016; Schmidt et al., 2021). Studies have also revealed elevated levels of IL-17 in lupus nephritis patients, correlating with disease severity (Paquissi & Abensur, 2021). Other studies conducted with mice models have revealed that the blockade of IL-17 or its receptors in the kidney can ameliorate tissue damage in the kidney (Odobasic et al., 2011).

In the intestine, Th17 cells are essential for maintaining homeostasis and mounting immune responses against enteric pathogens (Rossi & Bot, 2013). Th17 cells produce IL-17 and IL-22 which enhance epithelial barrier function by triggering the production of antimicrobial peptides, promoting epithelial cell proliferation and repair. The release of these cytokines also strengthens the barrier against pathogens via mucus stimulation by goblet cells (Valeri & Raffatellu, 2016).

However, the dysregulation of Th17 cells in the gut has been implicated in inflammatory bowel diseases (IBD) such as Crohn's disease and ulcerative colitis (Perez et al., 2020). The excessive production of IL-17 and IL-22 contributes to inflammation in IBD, leading to epithelial cell damage and disruption of the intestinal barrier (Cătană et al., 2015). Elevated levels of Th17 and Th17-related cytokines were detected in patients with IBD, correlating with disease severity (Jiang et al., 2014).

The implications of Th17 cells in both the kidney and gut prompts further research into their roles in inflammation and any novel therapeutic approaches that counteract their pathogenic effects.

1.8 Tcf7

Tcf7 is a gene that encodes for the T cell specific transcription factor TCF-1 (T cell factor-1). *Tcf7* is an essential component of early T cell development, proliferation and survival. TCF-1 is a member of the TCF/LEF (T cell factor-1/lymphoid enhancer) family, which is involved in the WNT signalling pathway. *Tcf7* plays a role in the WNT signalling pathway due to its interaction with β-catenin which is a key component of the signalling pathway (Ma et al., 2012). This interaction is responsible for the activation or repression of target gene expression. This transcriptional activity influences various cellular processes in T lymphocytes (Gounari & Khazaie, 2022).

Tcf7 also plays a role in immune responses by regulating the expression of genes involved in T cell effector functions. Studies have shown that *Tcf7*-deficiency in T cells results in impaired proliferation and cytokine production upon antigen stimulation (Zhu et al., 2015). Additionally, *Tcf7* has been revealed to be involved in regulating the balance between effector and memory T cell differentiation in CD8+ T cells (Yu et al., 2017).

Changes in *Tcf7* expression can contribute to aberrant T cell activation and dysregulated immune responses which can exacerbate various diseases such as cancer, infectious diseases and autoimmune disorders (Arnovitz et al., 2022).

1.9 *Tcf7* and Th17 cells

As previously mentioned, *Tcf7* plays a key role in T cell development and its effector functions. Therefore, it also affects the development of Th17 cells as well as their ability to produce cytokines, such as IL-17A and IL-22. Studies have shown that *Tcf7* can act as a negative regulator of Th17 cells in early developmental stages by inhibiting the expression of RORγT

and IL-17. This ensures a balance between the production of other T helper cell subtypes, including Tregs to ensure immune tolerance and prevent autoimmunity (Van Loosdregt & Coffer, 2018). During later stages, *Tcf7* has the ability to promote Th17 differentiation by facilitating the expression of genes necessary for Th17 cell function.

Th17 cells with stemness associated features have been identified in the spleen. A study revealed two different subsets of Th17 cells which are characterised by their expression of CD27 or the lack thereof. The cells that are $CD27^{+}$ express a lot of markers associated with plasticity or stemness. These particular cells very highly express TCF-1 whereas the $CD27^{-}$ Th17 cells displayed low expression of TCF-1 (Karmaus et al., 2019). This suggests that the cells exhibiting tissue adaptation qualities highly express TCF-1, indicating that this transcription factor is a key regulator of Th17 cell state.

A recent study has also revealed TCF-1 to be a key regulator of Th17 cell states, determining whether they remain in their homeostatic condition or adopt pro-inflammatory functions. This study suggests that TCF-1 binds to the key transcription factor of Th17 cells, RORγT. This binding suppresses the pro-inflammatory function of Th17 cells and allows them to remain in their homeostatic condition (Mangani et al., 2024).

Since elevated levels of Th17 cells were detected in various autoimmune diseases, targeting *Tcf7* could be a potential therapeutic approach for modulating Th17-mediated immune responses and alleviating disease symptoms. This approach could potentially reduce the number of Th17 cells in the affected tissue and thus restore the balance between Th17 and Treg cells, thereby reducing inflammation and preventing tissue damage.

1.10 Hypothesis and aim

Th17 cells in the kidney are known to be pathogenic and seem to be stable. However, it is also a known fact that Th17 cells have the ability to exhibit plasticity. Studies suggest that Th17 cells could also exhibit this plasticity in the kidney, however the drivers of this phenomenon are still to be uncovered. This study aims to gain a deeper understanding of the role of the transcription factor, TCF-1, in the plasticity and tissue adaptation ability of Th17 cells in renal autoimmune diseases.

We hypothesise that *Tcf7* plays a negative regulatory role in the stability of Th17 cells, causing them to become more pathogenic. This will be investigated by generating a transgenic mouse line with a *Tcf7* knock-out within the Th17 cells and assessing the disease outcome.

2 Materials and Methods

2.1 Materials

2.1.1 Mice

Line Name	Genetic Feature	Background	Supplier
Wildtype	-	C57BL/6	The Jackson Laboratory, Maine, USA
IL17A Fate Reporter	$IL17A^{cre}$ x $R26^{eYFP}$	C57BL/6	The Jackson Laboratory, Maine, USA
Tcf7 Knock-out	$Tcf7^{fl/fl}$ x $IL17A^{cre}$ x $R26^{eYFP}$	C57BL/6	The Jackson Laboratory, Maine, USA

2.1.2 Primers for Genotyping

Primer name	Nucleotide sequence	Length (nucleotides)
17AyfpF	CAA GTG CAC CCA GCA CCA GCT GAT C	25
17AyfpRwt	CTT AGT GGG TTA GTT TCA TCA CAG C	25
17AyfpiCreR	GCA GCA GGG TGT TGT AGG CAA TGC	24
Rosa26 Seq1	AAA GTC GCT CTG AGT TGT TAT	21
Rosa26 Seq2	GCG AAG AGT TTG TCC TCA ACC	21
Rosa26 Seq3	GGA GCG GGA GAA ATG GAT ATG	21
Tcf7 Seq1	GCC TGG GCT ACA AAA CAA GAT C	22
Tcf7 Seq2	GAG TCA GCA GGT TTC CCA CA	20

2.1.3 Antibodies

Antibody	Clone	Supplier
Goat anti-Mouse Albumin Antibody Affinity Purified	Polyclonal	Bethyl Laboratories Inc. Cat. No. A90-134A
Goat anti-Mouse Albumin Antibody HRP Conjugated	Polyclonal	Bethyl Laboratories Inc. Cat. No. A90-134P

2.1.4 FACS Antibodies

Antibody	Conjugate	Isotype	Clone	Supplier	Antibody dilution
CD3	BV421/V450	Syrian Hamster IgG2, κ	500A2	BD Cat: 740014	1 : 100
CD3	PE	Armenian Hamster IgG	145-2C11	BioLegend Cat: 100307	1 : 100
CD4	BV650	Rat IgG2a, κ	RM4-5	BioLegend Cat: 100545	1 : 100
CD45	PerCP	Rat IgG2b, κ	30-F11	BioLegend Cat: 103130	1 : 200
IFN-g	BV711	Rat IgG1, κ	XMG1.2	BioLegend Cat: 505836	1:100
IL-10	PE-Cy7	Rat IgG2b, κ	JES5-16E3	BioLegend Cat: 505026	1:100
IL-17A	BV605	Rat IgG1, κ	TC11-18H10.1	BioLegend Cat: 506927	1:100
RORγt	APC	Mouse IgG2a, κ	Q31-378	BD Cat: 562682	1:100
Tcf7	PE	Rabbit IgG	C63D9	Cell Signalling Technologies Cat: 14456	1:100

2.1.4 Buffers, Solutions and Media

Buffer	Composition
Coating buffer (albumin ELISA)	Content of one carbonate-bicarbonate buffer capsule in 100 ml aqua dest.
Digestion medium (kidney)	500 ml RPMI-supplemented with 10% FCS, 1% HEPES, 1% penicillin/streptomycin
DTT solution	50 ml 10X Hanks balanced salt solution (HBSS), 50 ml 10X HEPES-bicarbonate buffer, 50 ml 10% FBS (heat-inactivated), 350 ml H_2O, 15.4 mg dithioerythritol (DTT; Calbiochem) per 100 ml of buffer (1 mM final).
Erythrocyte lysis buffer	NH_4Cl 160 mM :Tris-HCL 170 mM (9:1 v/v), pH= 7,6
IEL Buffer	500 ml PBS, 50 ml FCS, 5.5 ml 100X Sodium Pyruvate, 11ml HEPES, 11 ml EDTA, 5.5 ml Penicillin/Streptomycin, 110 µl Polymyxin B
Paraformaldehyde (PFA) 4%	89 ml Sörensen buffer, 11 ml 37% Paraformaldehyde
Percoll gradient solution	106 ml H_2O, 74 ml Percoll PLUS, 20 ml 10x PBS
1X Perm Wash	1 part 10X Permeabilization Buffer and 9 parts aqua dest. under the hood
pPostcoat solution (albumin ELISA)	1 package 50mM Tris buffered saline in 1L distilled water, 1% BSA, pH 8,0
Sample / conjugate diluent (albumin ELISA)	200 ml of Postcoat solution, 1 ml 10% Tween20
Sörensen buffer	3,03g $NaHPO_4$ + 14,14g Na_2HPO_4 add to 1L with bi dest. H_2O, pH= 7,2-7,4
Stimulation medium	1 ml X-vivo, 1 µl β-Mercaptoethanol, 0.05 µl PMA, 1 µl Ionomycin, 2 µl Brefeldin A
Wash solution (albumin ELISA)	1L aqua dest., content of one package 50mM Tris buffered saline, 0,05% Tween20, pH 8,0

2.1.5 Chemicals and consumables

Product	Supplier	Cat. no.
Creatinine, 10g	Sigma Aldrich, St. Louis, Missouri, USA	C4255 – 10G
Dulbecco´s Phosphate Buffered Saline (DPBS(1x))	Thermo Fisher Scientific, Waltham, Massachusetts, USA	14190-094
Fetal calf serum (FCS)	Thermo Fisher Scientific, Waltham, Massachusetts, USA	10500-064
eBioscience™ Permeabilization Buffer (10X)	Thermo Fisher Scientific, Waltham, Massachusetts, USA	00-8333
Hanks´ Balanced Salt Solution	Thermo Fisher Scientific, Waltham, Massachusetts, USA	14170-088
Tris buffered saline, with BSA, pH 8,0	Sigma Aldrich, St. Louis, Missouri, USA	T6789
Tris buffered saline, with Tween20, pH 8,0	Sigma Aldrich, St. Louis, Missouri, USA	T9039
Tween20	Bethyl Laboratories Inc., Montgomery, Texas, USA	E108
Carbonate-Bicarbonate Buffer Capsules	Sigma Aldrich, St. Louis, Missouri, USA	C3041
Ionomycin, Free acid, (f. Streptomyces conglobatus)	Sigma Aldrich, St. Louis, Missouri, USA	407950-1MG
Phorbol 12-Myristate 13-Acetate (PMA)	Sigma Aldrich, St. Louis, Missouri, USA	P1585
RPMI-1640 medium	Thermo Fisher Scientific, Waltham, Massachusetts, USA	21875-034

2.1.6 Plasticware

Product	Supplier	Cat. no.
C tube	Miltenyi Biotech, Bergisch Gladbach, Germany	130-093-37
Cell culture micro plate, 96-well, u-bottom	Greiner Bio-One Holding, Kremsmünster, Austria	650180
Cell culture micro plate, 96-well, v-bottom	Greiner Bio-One Holding, Kremsmünster, Austria	651160
Cell counting slides	Bio-Rad Laboratories Inc., Hercules, California, USA	145.0015
Falcon Round-Bottom Polypropylene Tubes, 5 ml, with cap	Stemcell Technologies, Vancouver, Canada	38057
Falcon Round-Bottom Polypropylene Tubes, 5 ml, without cap	Stemcell Technologies, Vancouver, Canada	38056
Falcon tubes, 15 ml	Greiner Bio-One Holding, Kremsmünster, Austria	188271
Falcon tubes, 50 ml	Greiner Bio-One Holding, Kremsmünster, Austria	227261
Micro tube, 1.5 ml	Sarstedt, Nümbrecht, Germany	72.690.001
Micro tube 1.5 ml with cap	Sarstedt, Nümbrecht, Germany	72.692
Micro tube, 1.3 ml (filled with K3 EDTA)	Sarstedt, Nümbrecht, Germany	41.1504.015
Micro tube 0.5 ml, PP	Sarstedt, Nümbrecht, Germany	72.699
Filter Tip, 10 µl	Sarstedt, Nümbrecht, Germany	70.1130.410
Filter Tip, 100 µl	Sarstedt, Nümbrecht, Germany	70.760.12
Filter Tip, 200 µl	Sarstedt, Nümbrecht, Germany	70.760.211
Filter Tip, 1000 µl	Sarstedt, Nümbrecht, Germany	70.762.411
Serological pipettes, 50 ml	Sarstedt, Nümbrecht, Germany	86.1256.001
Serological pipettes, 25 ml	Sarstedt, Nümbrecht, Germany	86.1685.001
Serological pipettes, 10 ml	Sarstedt, Nümbrecht, Germany	86.1254.001

Serological pipettes, 5 ml	Sarstedt, Nümbrecht, Germany	86.1253.001
T175 Cell culture flask	Sarstedt, Nümbrecht, Germany	83.3912

2.1.7 Kits

Product	Supplier	Cat. no.
XNAT2 Extract-N-Amp Tissue PCR Kit	Sigma Aldrich, St. Louis, Missouri USA	XNAT2
BD Cytofix/Cytoperm™ Fixation/Permeabilization Solution Kit	BD (Becton, Dickinson and Company), Franklin Lakes, New Jersey, USA	554714
LIVE/DEAD Fixable Near-IR Dead cell staining Kit	Thermo Fisher Scientific, Waltham, Massachusetts, USA	L34975
Creatinin Jaffe Kinetic Fluid (5+1)	Hengler Analytik, Steinbach, Germany	114444

2.1.8 Equipment

Equipment	Supplier
BD Symphony A3	BD (Becton, Dickinson and Company), Franklin Lakes, New Jersey, USA
BD FACS Aria Fusion	BD (Becton, Dickinson and Company), Franklin Lakes, New Jersey, USA
BD FACS Aria IIIu	BD (Becton, Dickinson and Company), Franklin Lakes, New Jersey, USA
Biological safety cabinet Nuaire KS12	Thermo Scientific / Heraeus, Waltham, Massachusetts, USA
C1000 Touch Thermal Cycler	Bio-Rad Laboratories Inc., Hercules, California, USA
Centrifuge 5417R	Eppendorf, Hamburg, Germany
Centrifuge C1008-B my Fuge mini centrifuge	Greiner Bio-One, Kemsmunster, Austria
Citadel Tissue Processor Shandon 1000	Thermo Fisher Scientific, Waltham, Massachusetts, USA

CO2-Incubator HERAcell 240	Thermo Scientific / Heraeus, Waltham, Massachusetts, USA
CO2-Incubator, B 5042	Thermo Scientific / Heraeus, Waltham, Massachusetts, USA
Freezer (-20°C)	Liebherr, Bulle, Switzerland
Fridge, CP 43 CPel 4313-20	Liebherr, Bulle, Switzerland
GentleMACS Dissociator	Miltenyi Biotech, Bergisch Gladbach, Germany
Siemens Multistix 10 SG	Siemens Healthcare Diagnostics Inc., Tarrytown, New York, USA
Counting chamber Neubauer	Carl Roth, Karlsruhe, Germany
Cutfix one-use scalpel	B. Braun, Melsungen, Germany
Pipet Boy	INTEGRA Biosciences AG, Zizers, Switzerland
Syringe Omnifix-F	B. Braun, Melsungen, Germany
Syringe Injekt-F	B. Braun, Melsungen, Germany
Syringe needle, Sterican 23G	B. Braun, Melsungen, Germany
Syringe needle, Sterican G20	B. Braun, Melsungen, Germany
Surgical instruments (Scissors, clambs, tweezers, sharp spoon)	Carl Roth, Karlsruhe, Germany
Vortexer MS 3 Basic	IKA, Staufen, Breisgau, Germany
Vortexer mini EU Version	Greiner Group AG, Kremsmünster, Austria
Water bath incubator, Typ 1012	Gesellschaft fur Labortechnik, GFL, Burgwedel, Germany
Zeiss light microscope IM35	Carl Zeiss AG, Jena/ Oberkochen, Germany

2.1.9 Software

Software	Developer
Adobe Illustrator 2023 version 28.5	Adobe Inc., San Jose, California, USA
BD FACS Diva software; version 8.0.1	BD Biosciences, Franklin Lakes, New Jersey, USA
FlowJo; version 10.5.3	Tree Star, Ashland, Oregon, USA
GraphPad Prism; versions 6, 7, 8 and 9	GraphPad Software Inc., La Jolla, California, USA
T-Base; version 14.3	4D SAS, 60 Rue d`Alsace, 92110 Clichy, France
Mircrosoft Office 2016	Microsoft, Redmond, Washington, USA

2.2 Methods

2.2.1 Genotyping of transgenic mice

The genotype of all transgenic mice used in experiments was validated by PCR (polymerase chain reaction) (Table 2) and gel electrophoresis. Small biopsies were taken of the mice tails by trained professionals. DNA was extracted from these biopsies using the XNAT Extract-N-Amp Tissue PCR kit according to the manufacturer's protocol, which is as follows:

100 µl of extraction solution and 25 µl of tissue preparation solution were added to each tail biopsy. The tail biopsy in the solution was incubated at 55°C for 15 minutes in a thermal cycler. After the incubation, the extraction was stopped by adding 100 µl of neutralising solution.

Different PCR mixes were made using the extracted DNA containing different primers (listed in material section) (Table 1). These different primers were used to detect the various genes of interest.

Gene	Reagent/Primer	Volume(µl) x1
Tcf7flox	10X DreamTaq MasterMix	2.5
	dNTPs (10mM)	0.5
	DreamTaq Polymerase	0.2
	Tcf7flox Primer 1	0.125
	Tcf7flox Primer 2	0.125
	Nuclease free water	18.55
IL17Acre	10X DreamTaq MasterMix	1.5
	dNTPs (10mM)	1.5
	DreamTaq Polymerase	0.11
	IL17Acre Primer 1	0.45
	IL17Acre Primer 2	0.45
	IL17Acre Primer 3	0.45
	Nuclease free water	8.54
R26eYFP	10X DreamTaq MasterMix	1.5
	dNTPs (10mM)	1.5
	DreamTaq Polymerase	0.11
	R26eYFP Primer 1	0.45
	R26eYFP Primer 2/3	0.45
	Nuclease free water	8.09

Table 1: PCR master mixes

Gene	Step	Temperature (°C)	Time
IL17Acre	1	94	00:03:00
R26eYFP	2	94	00:00:40
	3	65	00:00:40 ΔT= -0,3 °C
	4	72	00:00:45
	5	Go to step 2 x30	
	6	72	00:05:00
	7	15	∞
Tcf7flox	1	94	00:05:00
	2	94	00:00:40
	3	65	00:00:40 ΔT=-0.3°C
	4	72	00:00:55
	5	Go to step 2 39X	
	6	72	00:05:00
	7	4	∞

Table 2: Genotyping PCR steps

2.2.1.1 Gel electrophoresis

A 1.5% agarose gel was prepared with ethidium bromide. A casting tray was filled with 200 ml of the agarose gel and left to cool down for 20 minutes with two well combs. Once the gel was hardened the combs were removed and the casting tray was placed in an electrophoresis chamber with the gel. The chamber was filled with TAE buffer until the gel completely emerged. Every gel contained a well with water, as a negative control, a Bl6 wildtype sample, as a positive control and a 1000 bp ladder. A voltage of 120 mV and a current of 400 mA were applied to the gel for 37 minutes in order to form an electrical field in the chamber. This electrical field allows the negatively charged DNA to be pulled towards the positive charge. Depending on the size of the fragment the DNA migrates through the gel at different speeds and distances, thus separating the DNA according to the fragment size. Once this was done, the gel was removed a picture of the fragments was taken in a UV photo chamber.

2.2.2 Histological tissue preparation

All histological slices taken from murine tissue were stored in 4% PFA overnight at 4°C. These were washed in 1x PBS three times in a shaker with each washing step lasting 30 minutes. These tissues were then transferred to paraffin cassettes and processed in a histological citadel. This citadel was pre-loaded with a series of ethanol solutions ranging from 60% to 100% volume/volume (v/v), alongside paraffin and xylene, and subjected to varying temperatures in immersion baths over a duration of 15 hours. Following embedding in paraffin, the tissue specimens were cooled to -15°C and sectioned using a microtome to achieve slices with a thickness ranging between 0.5 to 1.0 µm.

2.2.2.1 PAS Staining

In order to determine renal damage a periodic acid-schiff (PAS) staining was conducted on the renal histological slices. The tissue slices were deparaffinised and hydrated for the PAS staining (Table 3).

Step	Reagent	Concentration (%)	Duration (mins)
1	Xylene	100	5
2	Xylene	100	5
3	Xylene	100	5
4	ETOH	100	5
5	ETOH	100	5
6	ETOH	100	5
7	ETOH	96	5
8	ETOH	96	5
9	ETOH	70	5
10	ETOH	70	5
11	Aqua dest.		5
12	Aqua dest.		5
13	Aqua dest		5

Table 3: PAS rehydration and deparaffinisation

Step	Reagent	Concentration (%)	Duration (mins)
1	ETOH	70	2
2	ETOH	96	2
3	ETOH	96	2
4	ETOH	96	2
5	ETOH	100	2
6	ETOH	100	5
7	ETOH	100	10
8	Xylene	100	5
9	Xylene	100	5
10	Xylene	100	5

Table 4: PAS dehydration

Following rehydration and deparaffinization, the tissue specimens underwent oxidation using a 0.5% v/v periodic acid solution for 15 minutes at room temperature (RT). Subsequently, the samples were rinsed with running tap water for 2-3 minutes, followed by a wash with distilled water (aqua dest). The tissue sections were then treated with Schiff's reagent at RT for 40 minutes, after which they were washed with warm running tap water for 7 minutes, followed by a rinse with distilled water. During the incubation with Schiff's reagent, the sections exhibited a light pink hue.

The staining of cellular nuclei, mitochondria, elastin, myelin, and collagen fibres was achieved by exposing the tissue sections to a ready-to-use haematoxylin solution (Bohmer, 1865) at RT for 1-2 minutes, resulting in an immediate dark pink colouration. After periodic acid-Schiff (PAS) staining, the histological samples were examined for adequabohmte staining and could be subjected to additional staining if necessary. Following this, all samples underwent a brief treatment with hydrochloric acid (HCl)/ethanol solution by briefly immersing each sample into the solution 2-3 times.

The samples were then washed again under cold running water for 2 minutes, followed by a rinse with distilled water. Finally, the PAS-stained tissue sections were dehydrated (Table 4) and a cover slip was applied using a mounting medium (Eukitt).

2.2.2.2 Light microscopy of kidney

The tissue slices were placed onto a microscope slide holder for subsequent microscopic examination and crescent counting. The assessment employed an objective lens with a 20-fold magnification, resulting in an overall microscopic magnification of 200-fold.

To assess renal damage based on the microscopic tissue slices, a total of 30 glomeruli were counted, and the proportion of pathogenic glomeruli was calculated. This resulted in the “percentage of crescentic glomeruli”.

To quantify the “tubulointerstitial score”, four images of each kidney, sourced from diverse renal cortical sections, were obtained. These images were subsequently overlaid onto a template comprising a total 40 reference dots. The number of dots residing within the interstitium was tallied, and the mean count from all four images was determined.

2.2.2.3 H&E Staining

For the “hematoxylin-eosin” staining, hematoxylin undergoes oxidation to form haematein. In this context, the alkaline haemalum dye stains structures that are acidic or basophilic in nature blue. These structures predominantly encompass the ribosome-rich endoplasmic reticulum and the DNA-containing cell nuclei. This staining was used to dye the duodenum tissue samples.

Following rehydration and deparaffinization, the tissue specimens were exposed to haemalum for a duration of 2 minutes. Subsequently, the samples underwent an 8-minute rinse under running tap water followed by distilled water (aqua dest). The tissues were then immersed in eosin solution (0.5% v/v) for 15 seconds and rinsed with distilled water. Following this step, the tissues were sequentially washed with 96% ethanol and then twice with 100% ethanol. Finally, the tissue samples underwent two washes with xylene before being embedded with “Eukitt” mounting medium.

2.2.2.4 Light microscopy of duodenum

A simplified scoring system ranging from 0 – 3 was established based on previous published findings (Becker et al., 2006). The scoring was conducted by a trained professional for four different categories: chronic inflammatory infiltration, lamina propria neutrophils and eosinophils, neutrophils in epithelium and crypt destruction.

2.2.3 Induction of nephrotoxic nephritis (NTN)

Mice were injected intraperitoneally on day 0 with 150µl of sheep anti-mouse glomerular membrane antibodies which was prediluted 1:1 with PBS. The mice spent day 0 – 3 in a heated

cabinet accompanied with soft food to aid any initial symptoms of disease. Following the first three days the albuminuria of the mice was checked using Siemens Multistix to ensure successful induction of disease. (A proteinuria level above “++” was deemed successful, see Table 5). Urine was then collected on day 9 and stored at -20°C for later measurements of the albuminuria and creatinine. On day 10 the mice were sacrificed and their kidneys were harvested for cells extraction and a small slice of a kidney was stored in 4% PFA (see 2.2.2).

2.2.3 Urine sample collection and proteinuria determination

Metabolic cages were fabricated for the collection of urine samples by affixing the lid of a pipette tip box onto a 96-well plate using adhesive tape. The perforations in the lid facilitated adequate ventilation within the cage. Six wells were filled with water to ensure hydration for the animals. Mice were confined to these metabolic cages for approximately 4 hours before being returned to their standard housing cages. Urine specimens were extracted from the 96-well plate using a 1000 µl pipette for subsequent analysis. The urine samples were stored at -20°C.

2.2.4 Isolation of cells from murine kidneys

During organ extraction, the renal capsule was excised to facilitate tissue digestion. After a cross-section of the mid-section of the kidney was removed, the organ was minced in a petri dish using a scalpel and subsequently transferred into a C tube (for a GentleMACS dissociator) containing 5 ml of digestion medium (see section 2.1.4). Collagenase D (20 µl) and DNase I (10 µl) were added to the C tube, thoroughly mixed, and then incubated in a water bath at 37°C for 40 minutes.

Following digestion, the C tubes were placed onto the GentleMACS dissociator, and the "mSpleen 1.01" followed by "mLung 2.01" programs were executed to further process the tissue. Following centrifugation of the cell suspension (300 g, 8 minutes, 4°C), the supernatant was discarded.

To enrich for leukocytes, a density gradient separation was performed to eliminate fat and other tissue debris. The cell pellet was resuspended in 37% Percoll in a 15 ml tube (see section 2.1.4) and centrifuged at 500 g for 15 minutes at room temperature (RT). The supernatant was then discarded, and the tube was inverted and placed in a tube stand to drain residual Percoll. The cells were washed once more and transferred into FACS tubes in a suitable medium for subsequent staining or stimulation. If cells were not stimulated and processed for cell sorting, an erythrocyte lysis (as described in section 2.2.4.1) was performed.

2.2.4.1 Erythrocyte lysis of renal samples

Depending on the severity of bleeding encountered during organ removal, significant quantities of erythrocytes may be present in the cell pellet during lymphocyte purification. These erythrocytes have the potential to interfere with the detection of lymphocytes in FACS analysis.

An erythrocyte lysis buffer was prepared by combining 9 parts NH_4Cl with one part Tris-(hydroxymethyl)-aminomethane hydrochloride (Tris-HCl) (refer to section 2.1.4). The cell pellet was then resuspended in 1 ml of erythrocyte lysis buffer and incubated at room temperature for 3-5 minutes, depending on the extent of erythrocyte presence in the cell pellet. The lysis process was halted by adding 5 ml of PBS (4°C). Subsequently, the cells were centrifuged at 350 g for 5 minutes at 4°C and washed twice with 2 ml of PBS.

2.2.5 ELISA of renal albumin

The enzyme-linked immunosorbent assay (ELISA) technique was employed to indirectly quantify the concentration of albumin. This assay was conducted on a 96-well plate, which had been pre-coated with an anti-murine, anti-albumin antibody.

The horseradish peroxidase (HRP) coupled to the murine albumin antibody (detection antibody) catalysed the reaction with the 3,3',5,5'-tetramethylbenzidine (TMB) substrate solution. During this process, hydrogen peroxide (H_2O_2) was reduced to water (H_2O), leading

to a colour change in the solution to blue, with an absorption maximum of 650nm. The reaction was terminated by the addition of sulfuric acid (H_2SO_4) to prevent the precipitation of oxidized TMB, which could affect measurements. Stopping the reaction with H_2SO_4 resulted in another colour change towards yellow at a wavelength of 450nm due to electron transfers(Martin et al., 1984). The degree of colour change was directly proportional to the amount of detection antibody bound, and hence, to the concentration of albumin in the sample.

The buffers necessary for the albumin ELISA were prepared one day prior to the experiment (refer to section 2.1.4). Murine urine samples were collected according to the procedure described in 2.2.3, and albuminuria was quantified using urine sticks.

The albumin ELISA was conducted over a period of two days. On the first day, a solution of 100µl anti-murine albumin antibody diluted in 9900µl coating buffer (1:100 dilution) was prepared. Using a multichannel pipette, 100µl of the diluted antibody was added to each well of a high-binding 96-well plate. The plate was then refrigerated at 4°C overnight to allow for coating.

On the second day, each well of the plate was washed three times with 200µl washing buffer. Following each wash, the plate was tapped on tissues laid out on the laboratory bench to remove excess buffer, ensuring accurate pre-sample dilutions.

Subsequently, 200µl of post-coating solution per well was added and incubated for 30 minutes at room temperature to block unspecific binding sites. Sample dilutions and standard dilutions were prepared as outlined in Table 5 and Table 6, with sample dilutions derived from proteinuria quantification using urine sticks (see section 2.2.3).

After another round of washing, 100µl of either diluted sample or standard was pipetted into a 96-well plate. The plate was then incubated for 1 hour at RT, during which the albumin in the samples and standards bound to the anti-murine albumin antibody. Following incubation, each well was washed five times with 200µl washing buffer.

A 1µl HRP-coupled detection antibody was diluted in 50 ml of sample diluent (1:50,000 dilution) and thoroughly mixed. 100µl of the diluted HRP-coupled detection antibody was then added to each well of the plate. The plate was covered and incubated for 1 hour at RT. The detection antibody bound to the albumin previously bound by the anti-murine albumin antibody.

After another washing step, 100µl of substrate solution (TMBE) was added to each well, and the plate was incubated in the dark for 15 minutes at RT. Concurrently, the photometer was activated, and the layout of the plate with sample and standard dilutions was entered. The addition of 100µl 2M H_2SO_4 per well under the hood halted the substrate reaction.

Following termination of the reaction, the plate was immediately measured in the photometer at 450nm, and the concentrations of albumin in the murine urine samples were determined.

Proteinuira (Urine Multistix)	Dilution factor
Trace	1 : 1000
+	1 : 1000
++	1 : 20 000
+++	1 : 50 000
++++	1 : 100 000

Table 5: ELISA dilution determination

	Dilution	Standard + Diluent
S0	10 000 ng/ml	2 µl stock solution in 198 µl sample diluent
S1	1000 ng/ml	100 µl S0 in 900 µl sample diluent
S2	500 ng/ml	300 µl S1 in 300 µl sample diluent
S3	250 ng/ml	300 µl S2 in 300 µl sample diluent
S4	125 ng/ml	300 µl S3 in 300 µl sample diluent
S5	62.5 ng/ml	300 µl S4 in 300 µl sample diluent
S6	31.25 ng/ml	300 µl S5 in 300 µl sample diluent
S7	15.625 ng/ml	300 µl S6 in 300 µl sample diluent
S8	7.8125 ng/ml	300 µl S7 in 300 µl sample diluent

Table 6: ELISA standard concentrations

2.2.6 Determination of renal creatinine

For the determination of creatinine from urine, the Creatinine-Kit Jaffee Kit (2.1.7) was utilized. Standards S1-S5 were prepared according to the specifications outlined in Table 7. The reagent was prepared by combining one part picric acid with five parts alkaline buffer, as directed by the manufacturer. Subsequently, 10 µl of either NaCl (as a negative control), standard, or urine sample was pipetted into the wells of a 96-well plate. Following this, 50 µl of the reagent was added to each well using a multichannel pipette. After an incubation period of 1 minute at room temperature (RT), the plate was read in a plate reader at 430nm, and the absorbance values were recorded. The plate was then read again after a further 5 minute incubation period to allow for colour development.

	Dilution	Standard + Diluent
S0	1 g/l in NaCl	-
S1	0.5 g/l	500 µl S0 +500 µl NaCl
S2	0.4 g/l	300 µl S0 +300 µl NaCl
S3	0.3 g/l	350 µl S0 + 350 µl NaCl
S4	0.2 g/l	100 µl S0 + 400 µl NaCl
S5	0.1 g/l	50 µl S0 + 450 µl NaCl

Table 7: Creatinine standard concentrations

2.2.7 Quantification of blood urea nitrogen

During the organ extraction, a heart puncture was performed to extract blood from the mice. The blood was stored in a tube containing EDTA to avoid coagulation. The tubes were centrifuged for 10 minutes at max speed. After centrifugation, the serum was removed and stored in a 1.5 Eppendorf tube at -20°C. The blood urea nitrogen (BUN) level of the serum was determined using a Cobas analyser by trained professionals.

2.2.8 Induction of anti-CD3 induced duodenitis

To induce anti-CD3 duodenitis, mice were intraperitoneally injected with 15µg of an anti-CDε antibody dissolved in PBS with a final volume of 150 µl using a 1 ml syringe. These injections were given on day 0, day 2 and on day 4 four hours prior to organ extraction.

2.2.9 Isolation of cells from murine duodenum

The duodenum was removed from sacrificed mice. A small section of the duodenum was taken for histological analysis. After this, the tissue was cut horizontally. The duodenum was then washed twice in cold PBS in a petri dish. This was transferred into a 50 ml falcon tube, containing 20 ml PBS with 2 mM DTT, which was rigorously shaken by hand. The tissue was then blotted on a tissue for drying and transferred into a 50 ml falcon tube containing 20 ml

IEL buffer with 2 mM DTT. This tube was placed in a shaker for 30 minutes at 37°C and 200 rpm at a 45° angle. Once this was done, the tube was centrifuged at 360g and 4° for 7 minutes. The supernatant was discarded through a 100 µm strainer (with extra holes manually added with a tweezer), the tissue was removed from the strainer using tweezers and blotted dry on a tissue. This was then put in a 50 ml falcon tube, containing 20 ml PBS++ and rigorously shaken by hand. Once this was done, the PBS++ was discarded and the tissue was transferred to C-tubes containing 5 ml of digestion medium with 10 µl DNase I and 20 µl collagenase D. The C-tubes were attached to a Miltenyi GentleMACS and the programs "37_m_LPDK_1" and "m_intestine" were run back to back. After this procedure, the resulting solution was run through a 70 µm strainer and the tissue in the strainer was mashed using the end of a syringe and washed three times with 10 ml RPMI medium. The cells were then centrifuged as previously described and resuspended in 1 ml PBS. The cells were now ready for consecutive FACS staining.

2.2.10 Staining for FACS analysis

Cells that were used for intracellular staining (to identify cytokine expression) were stimulated for 3 hours in an incubator at 37°C with 5% CO_2 in stimulation medium (refer to section 2.1.4). After the stimulation, 2 ml of MACS buffer was added to the cells and these were centrifuged at 350g for 7 minutes at 4°C, then resuspended in 1 ml PBS. These cells were now ready for FACS staining.

For extracellular staining, the cells were first resuspended in 1 ml of 1:1000 (in PBS) NiR for the live/dead staining and incubated for 10 minutes at RT in the dark. 2 ml of MACS was then added to the FACS tubes to stop the staining procedure and the cells were centrifuged as previously described. After this, the supernatant was discarded and 5 µl of mouse serum was added to the cells, to ensure blocking of any unspecific binding, and incubated for 5 minutes at RT. During the incubation the antibody master mix prepared (Table 8) and 50 µl of the antibody master mix was added and incubated at 20 minutes at RT in the dark.

	Fluorescence	Dilution	x1 (µl) (V=100)
CD4	BV650	1:100	1
CD45	PerCP	1:200	0.5
CD3	V450/BV421	1:100	1
MACS-Buffer			47.5

Table 8: FACS antibody staining panel for extracellular staining

Once the extracellular staining was complete, 2 ml of PBS was added to each sample and the cells were again centrifuged and 200 µl of 3.7% PFA (in MACS) was added to each sample to fixate the cells. This was incubated for 20 minutes at RT. Once this was complete, the cells were ready for intracellular and intranuclear staining.

For this particular staining procedure, it is important that that the cells are permeabilised to ensure the entry of the staining antibodies into the cells and nucleus. For ths 2 ml of permeabilisation wash buffer (PermWash) was added to the cells once the fixation incubation was over. These cells were centrifuged and resuspended in 2 ml PermWash and incubated for 20 minutes at RT.

The cells were then centrifuged, the supernatant discarded and 50 µl of the antibody master mix (Table 9) for intracellular and intranuclear staining was added to the cells and incubated overnight at 4°C in the dark.

	Fluorescence	Dilution	x1 (µl) (V=100)
IL-17A	BV605	1:100	1
IFNγ	BV711	1:100	1
IL-10	Pe-Cy7	1:100	1
Tcf7	PE	1:50	2
RORgT	APC	1:100	1
PW-Buffer			44

Table 9: FACS antibody staining panel for intracellular and intranuclear staining

The next day, the cells were washed twice with 2 ml PermWash. Then the cells were resuspended in 250 µl PBS. The cells were then analysed using the BD Symphony A3.

2.2.11 Flow cytometric cell sorting

For the sorting of lymphocytes from the kidney, cells were extracted (as described in 2.1.9) and the extracellular staining was conducted (as described in 2.1.10). The antibody master mix was made according to the table below:

	Fluorescence	Dilution	x1 (µl) (V=100)
CD45	PerCp	1:100	1
CD3	PE	1:100	1
CD4	APC	1:100	1
MACS			47

Table 10: FACS antibody staining panel for cell sorting

2.2.10 Whole kidney tissue dissociation

To extract single cell suspensions from the whole murine kidneys, Miltenyi Biotec Multi Dissociation Kit 2 was used, and all steps were done according to the protocol. The kit extracts the single cell suspensions by enzymatically degrading the extracellular matrix, which maintains the structural integrity of tissues. After this dissociation, the suspension is filtered to remove any remaining larger particles. The cells were then processed immediately for single cell sequencing.

2.2.12 Single Cell Sequencing

All libraries were generated using the kits from 10X Genomics. The technology from 10X Genomics creates single cell suspensions with oil droplets containing single cells along with barcoded gel beads, these supensions are called GEMs (gel

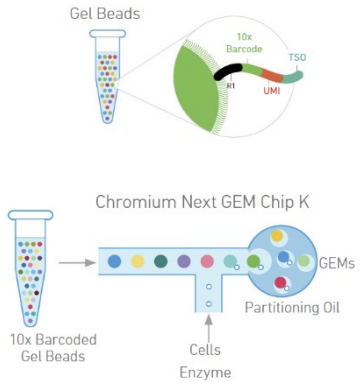

Figure 5: GEM generation in chip (from 10X Genomics protocol)

beads in emulsions) (Figure 5). In order to generate these GEMs, single cell gel beads, a master mix with cells and partitioning oil are loaded onto a chip and inserted into the chromium controller which creates these GEMs. As soon as the GEMs are generated, the cells undergo a PCR. Here the gel beads are dissolved and any co-partitioned cells are lysed. An illumina R1 sequence, a 10X barcode, a UMI (unique molecular identifier and template oligo switch (TSO) are released following the lysis and mixed together with the lysed cells. This mixture also contains previously added reverse transcriptase (RT) and poly(dT) RT primers. The incubation in the thermal cycler for the PCR produces 10X Barcoded, full-length cDNA form poly-adenylated mRNA (Figure 6).

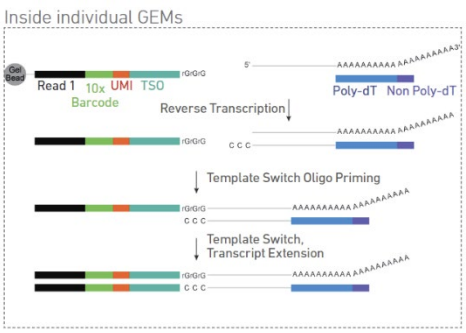

Figure 6: Generation of cDNA from GEMs (from 10X Genomics protocol)

Once the cDNA has been generated, the cDNA strands are purified in the post GEM-RT clean-up and the cDNA is amplified via PCR using primers against common 5' and 3' ends. This amplification produces sufficient cDNA for subsequent library construction.

The cDNA can now be used to generate a 5' gene expression library. Prior the generation of the library, the amplicon size of the cDNA is optimised using enzymatic fragmentation and size selection. Then P5, P7, i5 and i7 sample indexes as well as illumina R2 sequences are added to the cDNA via end repair, A-tailing, adaptor ligation and sample index PCR (Figure 7).

Once the libraries were generated, all samples were sequenced with Novogene using Illumina sequencing. For the gene expression libraries, 50 000 reads per cell were sequenced for an in-depth analysis.

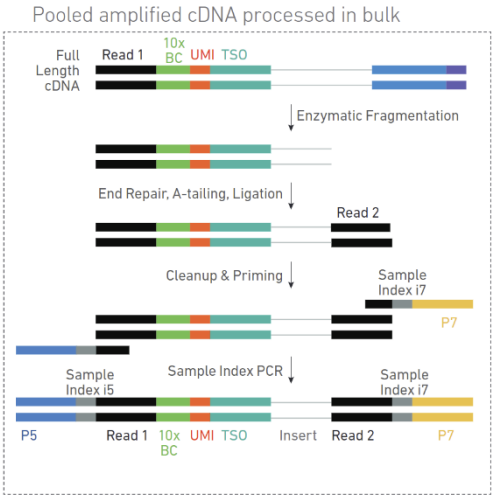

Figure 7: Generation of gene expression library (from 10X Genomics protocol)

2.2.12.1 Single cell sequencing of sorted cells and whole kidney

All single cell libraries were made using the 10X Genomics 5' v2 Kit and the protocol (CG000330) was followed step by step.

2.2.12.1 Single nuclei sequence for ATAC

Nuclei from murine kidney tissue was isolated using the 10X Genomics protocol CG000124. Once the nuclei were isolated, GEMs and gene expression libraries were produced according to protocol CG000496. Prior to loading the cells in the chip, the nuclei suspensions are incubated in a transposition mix which includes the enzyme, transposase. This enzyme enters the nuclei and fragments the DNA in open regions of the chromatin. This protocol follows the same chemistry as described in 2.2.12. to produce the GEMs (Figure 8). Then the gene expression library is produced according to the protocol.

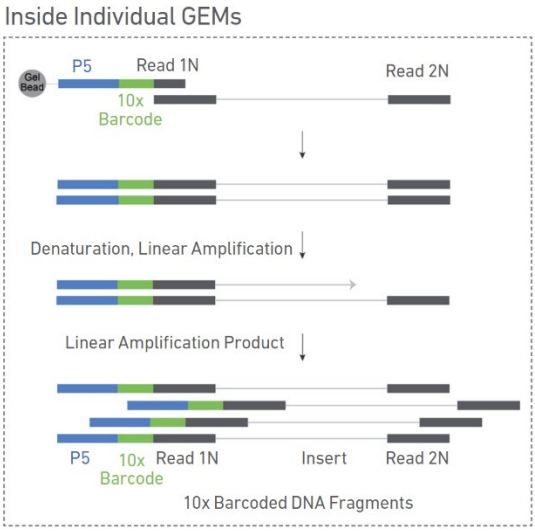

Figure 8: GEMs of ATAC protocol (from 10X Genomics protocol)

2.2.13 Bioinformatical analysis

All bioinformatic analyses were conducted in R. Single cell RNA-seq datasets were processed and analysed using the Seurat pipeline, following established protocols for data integration and clustering (Butler et al., 2018; Satija et al., 2015). Single-nuclei datasets were analysed with the Signac pipeline, which is tailored for single-cell chromatin accessibility data (Stuart et al., 2021).

3 Results

3.1 Single cell & single nuclei sequencing data

Different datasets using different 10X Genomics platforms was generated to obtain a deeper understanding of the renal cells from mice. All libraries prepared were sequenced using Illumina platforms. The data from scRNA-seq is much more detailed than that of bulk sequencing since it captures molecular information from each individual cell that is entered into the microfluidics system that produces the GEMs. The final data that is captured and analysed consists of transcripts which are RNA molecules post-transcription (Kolodziejczyk et al., 2015).

Similar to the scRNA-seq data, snATAC-seq data captures the information of each individual nuclei from the dataset. During the pre-processing of the nuclei, the Tn5 transposase enzyme is used to tag the accessible regions of chromatin. The chromatin is a part of the chromosomes found in the nuclei of cells that is highly condensed and contains DNA, RNA and proteins. Accessible regions of the chromatin are the regions that are open and allow the insertions of the enzyme. These accessible regions are tagged and the resulting data from sequencing contains fragments of accessible DNA (Yekelchyk et al., 2024). This allows the uncovering if transcription factor activities in certain cell types. This section will show the analyses conducted and the resulting data.

3.1.1 Renal leukocytes from cGN induced and control mice

Leukocytes from cGN induced and control kidneys were sorted using FACS. For both groups the $CD45^+$ and $CD3^+CD4^+$ cells were sorted and the YFP^+ cells were additionally sorted for the cGN group (Figure 9A). Even in inflammatory conditions, Th17 cells are not very abundant in the kidney, so only approximately 6000 YFP^+ cells were sorted.

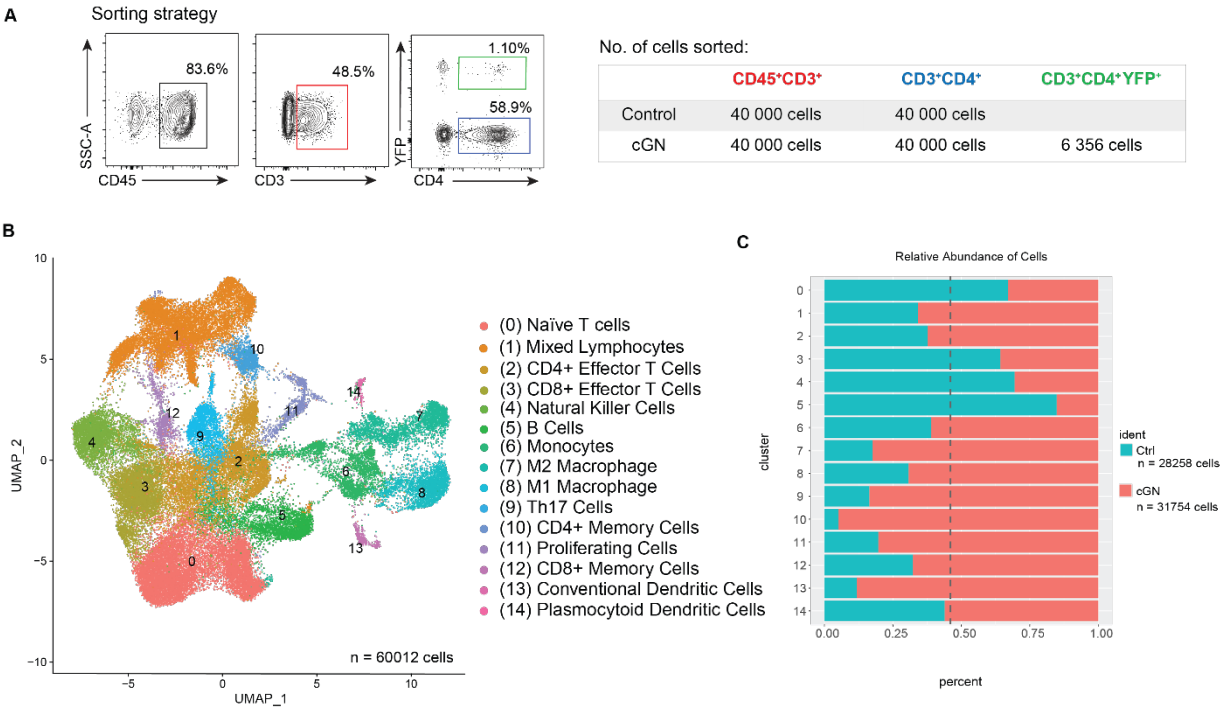

Figure 9: Overview of cell sorting, clustering and cell group distribution analysis of leukocytes from the cGN model.
A) Sorting strategy and cell counts for each group, detailing the number of cells sorted from the experimental cGN and control groups. **B)** Clustering analysis of all cells following data merging and integration, displaying cell populations as distinct clusters based on shared transcriptional profiles. **C)** Composition of each identified cluster, represented as percentages, showing the relative contributions of cells from the cGN and control groups within each cluster.

All cells were then merged and integrated using the Seurat pipeline (Butler et al., 2018). Cells were clustered based on shared transcriptional profiles and visualised as distinct populations using UMAP. Each cluster was identified and labelled based on differentially expressed genes characteristic of the cluster (Figure 9B). Most clusters had a distinct population of cells. However, one cluster had both $CD4^+$ and $CD8^+$ cells. This cluster was labelled as “Mixed Lymphocytes”. The cluster labelled as “Th17 cells” predominantly comprised of the YFP^+ sorted cells. However, due to the integration process, a small proportion of YFP^- cells were included in this cluster, and some YFP^+ cells were distributed among other clusters. The Th17 cells were closely associated with and intermingled with the $CD4^+$ Effector Cells cluster, reflecting shared transcriptional characteristics and functional overlap, supporting the data's validity. Interestingly, there was so distinct cluster identifying T regulatory cells who are the

main producers of the anti-inflammatory cytokine IL-10. This is a vary intriguing finding that showcases the anti-inflammatory response of the immune cells to the cGN induction.

The relative number of cells in each cluster that came from either the control or the cGN group was calculated and displayed using a stacked graph (Figure 9C). Most of the cells in the Naïve T cells cluster and B cells cluster come from the control group under healthy conditions rather than from the cGN induced mice. The two clusters with the majority of cells coming from cGN induced mice are the $CD4^+$ Memory Cells and Conventional Dendritic Cells clusters. When looking at the Th17 cells cluster, most cells come from the cGN induced mice. A very small percentage of cells in the Th17 cluster appear to derive from the control group. While this was not an expected result, could reflect a low baseline presence of Th17-like cells in the control group. Alternatively, this could be due to the integration process, which can introduce minor spillover of cells between clusters (Tran et al., 2020).

To investigate the differential expression of key markers in cGN and control groups, the expression levels of *YFP, Il17a*, and *Tcf7* were analysed and visualised using feature plots and violin plots (Figure 10). The feature plots display the spatial distribution of RNA expression across all cells present in the UMAP, whereas violin plots provide a comparative view of expression levels between the cGN and control group.

The *YFP* expression (Figure 10A) was predominantly observed in cells from the cGN induced mice, as expected, confirming the successful identification of YFP^+ cells associated with the disease model. Most of the YFP^+ cells are found in the Th17 cell cluster, whilst some are also detected in the $CD4^+$ memory cells cluster and proliferating cells cluster.

Similarly, *Il17a* expression (Figure 10B) was enriched in the cGN group compared to the control, which reflects the pro-inflammatory role of Th17 cells in cGN pathology. Most of the cells highly expressing *Il17a* are found in the Th17 cell cluster and mostly align with the *YFP* expression on the UMAP. However, there seem to be more *YFP* expressing cells in cGN conditions than *Il17a* expressing cells. This suggests that not all the YFP^+ cells produce IL-

17A anymore. Since these cells are YFP^+ it is evident that these cells once produced IL-17A, suggesting that these cells stopped the expression or could have transdifferentiated into another cell type.

In contrast, *Tcf7* expression (Figure 10C) showed a distinct distribution, with higher expression levels in cells from the control group compared to the cGN group, especially in naïve cells. Interestingly, high *Tcf7* expression was also detected in the Th17 cells cluster. This finding is consistent with the potential regulatory role of TCF-1 in Th17 cell differentiation and its potential involvement in disease suppression.

These data underline the differential expression of critical markers and validate the association of *YFP* and *Il17a* with disease progression. They also highlight the inverse relationship of Tcf7 expression in the context of cGN when compared to the control group.

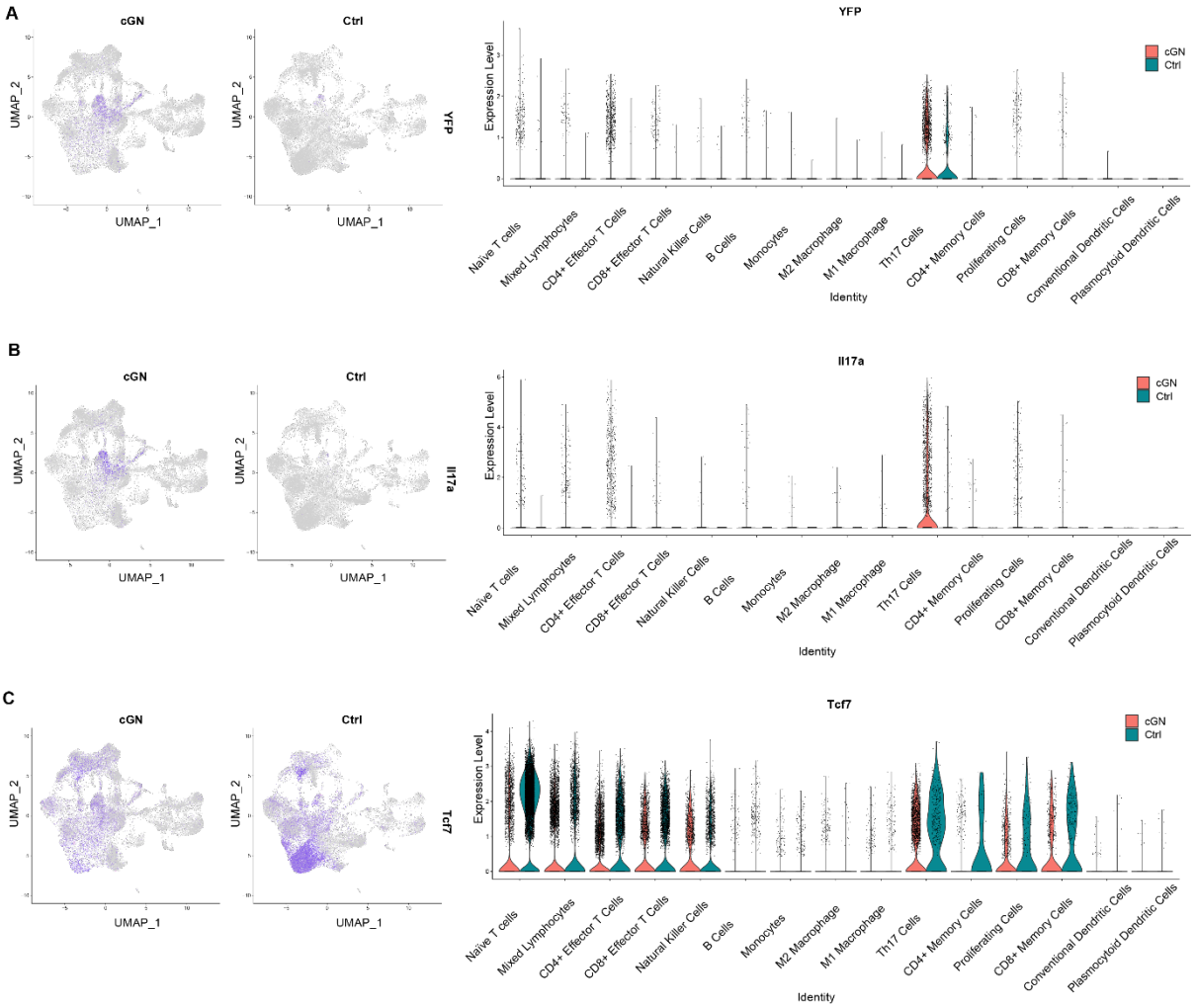

Figure 10:Differential expression of key markers in cGN and control groups.
Feature plots and corresponding violin plots illustrating RNA expression levels of *YFP*, *Il17a*, and *Tcf7*. **A)** Expression patterns of *YFP*, **B)** *Il17a*, and **C)** *Tcf7*, with feature plots displaying spatial distribution across all cells and violin plots comparing expression levels between the cGN and control groups. The violin plots highlight the differential expression of each gene, showing distinct expression patterns between the two groups.

3.1.2 Th17 cells from cGN induced and control mice

To further characterise and study the Th17 cells in the kidney, Th17 cell cluster from the leukocyte dataset (Figure 9B) was further subclustered. Based on their transcriptional profiles, distinct subpopulations within the Th17 cell cluster were identified (Figure 11A). The six different clusters identified withing the Th17 cell cluster are as follows: classic Th17 cells, Th1-like ex-Th17 cells, Lyz2^{high}Cd74^{high} expressing cells, γδ T cells, Tcf7^{high}Ccr6^{high} expressing cells and Tox^{high} expressing cells. These diverse subpopulations within the Th17 cell cluster suggest functional specialisation or differentiation states within Th17 cells.

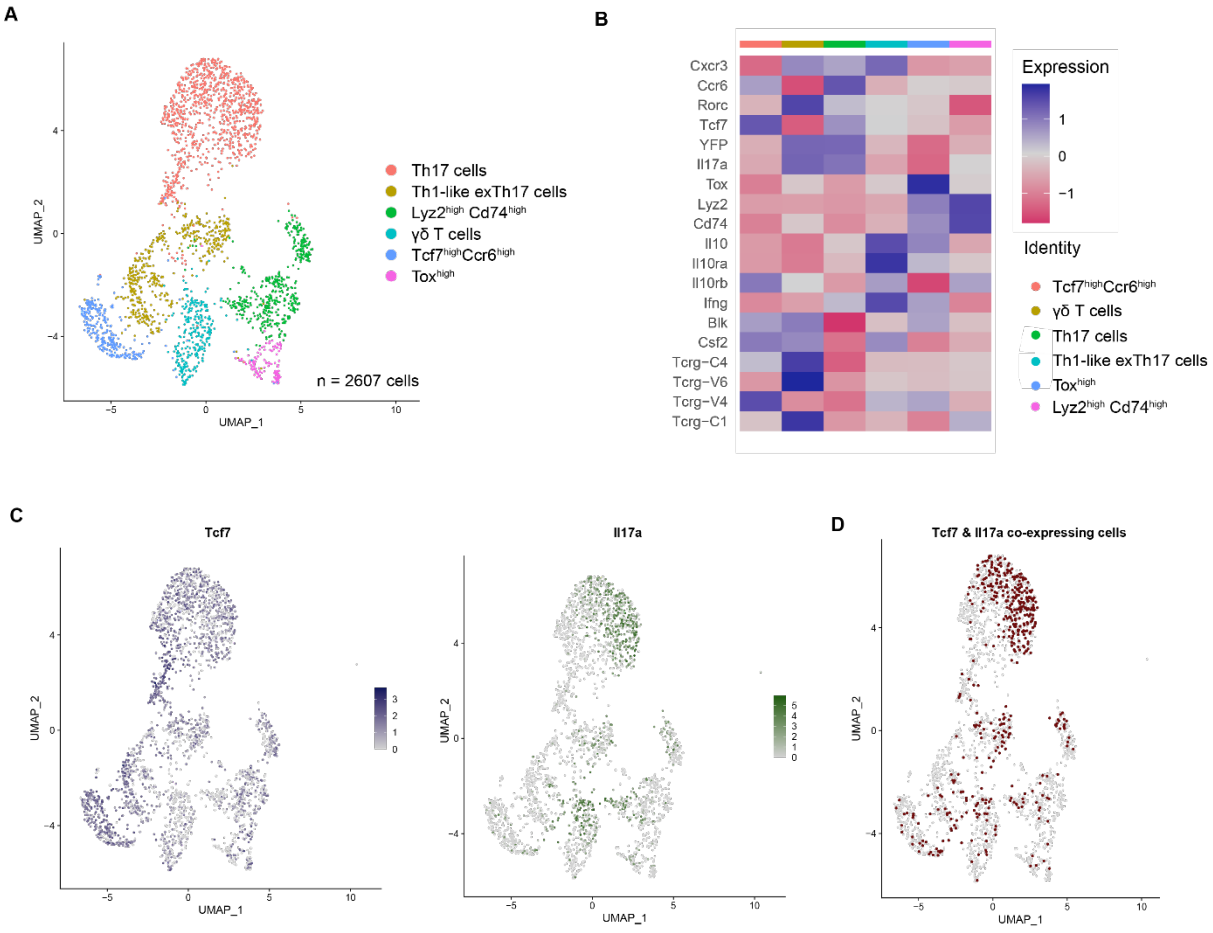

Figure 11:Analysis of Th17 cluster within the cGN leukocyte dataset
A) Subclustering of the Th17 cell population, revealing distinct subpopulations based on transcriptional profiles within the broader Th17 cluster. **B)** Heatmap displaying the average differential expression of marker genes used to identify each Th17 subcluster. **C)** Feature plots illustrating RNA expression patterns of *Tcf7* and *Il17a* within the Th17 subclusters. **D)** UMAP visualisation highlighting cells co-expressing *Tcf7* and *Il17,* emphasising their spatial localisation within the Th17 subcluster.

The marker genes used to identify these distinct subclusters were visualised by implementing a pseudo bulk analysis and using a heatmap which displays the average expression of these specific markers across the different subclusters (Figure 11B). The distinct patterns of marker gene expressions allowed the identification of the diversity within the Th17 cell cluster, which also suggests functional differences among Th17 cells in the kidney in cGN conditions. The cluster identified as Th17 cells contains the traditional Th17 cells, which highly express *Ccr6*, *Il17a*, *Rorc* and *YFP*. Notably, these cells are highly expressing *Tcf7*. The Th1-like ex-Th17 cells were identified by the high expression of *Cxcr3* but the lack of *Ccr6* expression. These cells also display a lower expression of *Tcf7*, suggesting that the transcription factor triggers a transdifferentiation process in Th17 cells resulting in them becoming Th1-like ex-Th17 cells. Additionally, these cells show a high expression of IFNγ, IL-10 and IL-10 receptors, suggesting that they could be related to the significantly higher IL-10 expression in cGN detected in the FACS analysis (Figure 19). The $Lyz2^{high}Cd74^{high}$ expressing cells also exhibit elevated *Il10* expression but a significantly lower expression of *Rorc*. The γδ T cells were identified by their high expression of *Tcrg-C4*, *Tcrg-V4* and *Tcrg-C1* which are classic markers for the T cell receptor gamma chain. These cells also have the ability to produce IL-17A, which is why they are also highly expressing *Il17a* and *YFP*. The $Tcf7^{high}Ccr6^{high}$ expressing cells are characterised by their lack of *Cxcr3* but high expression of *Il10rb*. The Tox^{high} expressing cells show expression of *Lyz2*, *Cd74*, *Il10* but show a significantly lower expression of *Il10rb*.

To further investigate the relationship between Tcf7 and IL-17A expression within the Th17 subclusters, the RNA expression of these genes was displayed using a feature plot (Figure 11C). Differential expression of *Tcf7* and *Il17a* was observed across the subclusters. The gene for the transcription factor TCF-1 seems to be expressed by cells across all subclusters of Th17 cells. Whereas the *Il17a* expression seems to be spatially localised on the UMAP to the Th17 cells cluster and the γδ T cells cluster.

The cells that co-express both *Tcf7* and *Il17a* were highlighted to visualise and localise the cells within the different subclusters (Figure 11D). Most of the cells expressing both genes are

found in the classic Th17 cell cluster and the Tcf7^{high}Ccr6^{high} expressing cell cluster. This finding suggests that specific subpopulations of Th17 cells, defined by high *Tcf7* and *Il17a* expression, may play distinct roles in the context of cGN. However, even though these cells are not very abundant in the Th17 subcluster, they seem to be mostly spatially spread across the UMAP.

Overall, these results illustrate the transcriptional complexity of the Th17 cluster and provide evidence of functional and phenotypic heterogeneity within this population in cGN.

3.1.3 Pseudotime analysis of Th17 cells

To investigate the expression of key markers within the Th17 cell subcluster, the previously generated UMAP (Figure 11A) was integrated into the Monocle3 pipeline (Cao et al., 2019). Monocle3 is a bioinformatical tool that enables the analysis of scRNA-seq data in order to uncover trajectories and reconstruct developmental lineages. The integration process slightly changed the shape of the previously generated UMAP (Figure 12A). The key markers that were plotted are *Rorc*, *Il17a*, *YFP*, *Tcf7*, *Ccr6* and Cd74. These chosen markers were previously used to identify the clusters in the previously generated UMAP (Figure 11B).

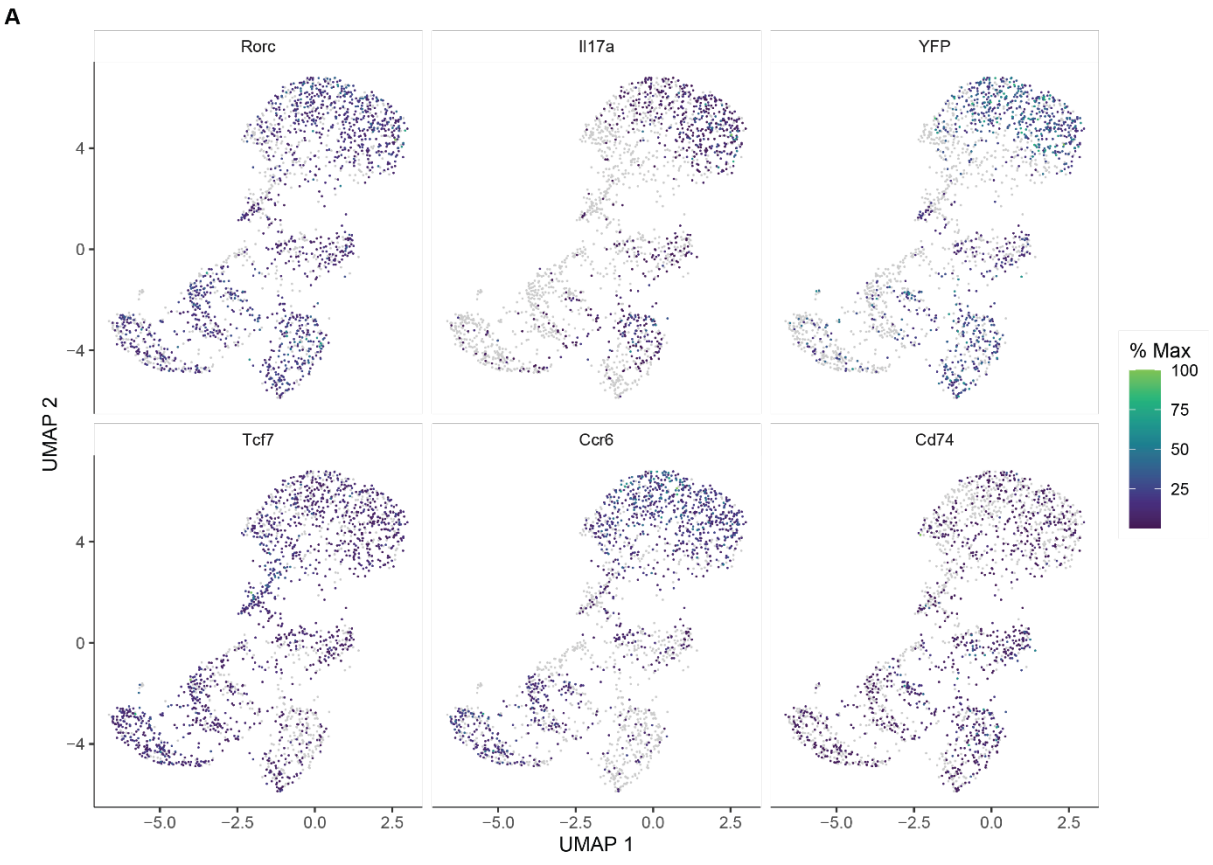

Figure 12: Visualization of Gene Expression on UMAP Integrated into the Monocle3 Pipeline.
A) Feature plots depicting the expression levels of key genes associated with Th17 cells. The markers include *Rorc, YFP, Tcf7, Ccr6* and *Cd74*. Gene expression is projected on a UMAP generated with Seurat and incorporated into the Monocle3 trajectory analysis pipeline.

The UMAP visulisation of the Th17 cells using the Monocle3 pipeline shows a sucessful integration into the pipeline since to co-localisation of the key markers align with the previously generated UMAP and the localised expression of the gene markers (Figure 11B).

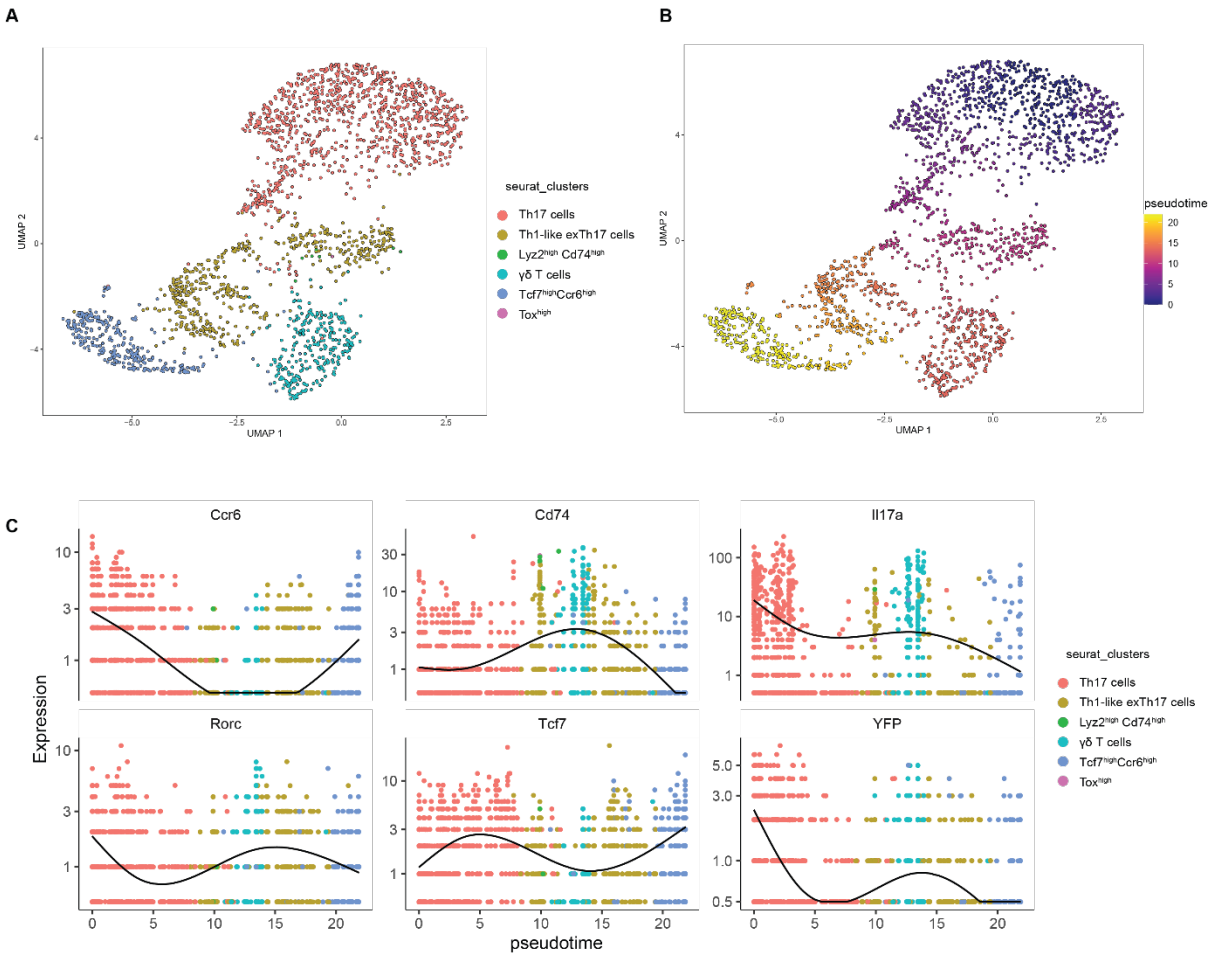

Figure 13: Analysis of Th17 Cell Differentiation Using Seurat and Monocle3.
A) UMAP visualisation generated using the Seurat pipeline and integrated into the Monocle3 trajectory analysis framework showing clusters of Th17 cells and related populations. B) Pseudotime plot illustrating the differentiation trajectory across the UMAP, starting from the classic Th17 cell cluster. C) Expression of key marker genes (*Ccr6, Cd74, Il17a, Rorc, Tcf7* and *YFP)* displayed along the pseudotime trajectory. Cells are coloured according to their respective Seurat-identified clusters.

Furthermore, the Seurat clusters previously calculated (Figure 11A) were visualised in the Monocle3 integrated dataset using a UMAP (Figure 13A). The clustering and UMAP have altered slightly, however the overall UMAP aligns with the previously calculated UMAP. Next, the Monocle3 pseudotime trajectory was calculated on the UMAP by choosing the classical

Th17 cell cluster as the starting point (Figure 13B). The highest pseudotime score is observed in the Tcf7^{high}Ccr6^{high} cluster, suggesting these specific Th17 cells are found further along the differentiation trajectory calculated by Monocle3.

In order to further investigate the different markers determining Th17 cell fate, the selected key gene markers were visualised along the pseudotime trajectory in each cluster starting from the classical Th17 cluster (Figure 13C). The expression of *Ccr6* peaked very early in the trajectory in the classical Th17 cluster, but shows a drastic decline within the cluster along the pseudotime axis. Then a sudden increase of the *Ccr6* expression is observed in the Th1-like ex-Th17 cells cluster, this increase continues into the Tcf7^{high}Ccr6^{high} cluster. The expression of *Cd74* is very constant in the classical Th17 cell cluster and shows and increase in the Th1-like ex-Th17 cells and γδ T cell clusters, where it peaks. However, the expression of *Cd74* decreases within the Th1-like ex-Th17 cells cluster and continues to decline within the Tcf7^{high}Ccr6^{high} cluster. A fairly constant expression of *Il17a* is observed across all clusters, but the lowest expression is seen in the Tcf7^{high}Ccr6^{high} cluster. The expression of *Rorc* peaks in the classical Th17 cell cluster but also reaches the lowest level of expression within the same cluster. The expression of the transcription factor, RORγT, increases again in the γδ T cell and Th1-like ex-Th17 cells cluster and decreases in expression in the Tcf7^{high}Ccr6^{high} cluster which is the furthest cluster along the pseudotime axis. The expression of the transcription factor TCF-1 along the pseudotime axis shows an inverse relationship to the expression of RORγT along the pseudotime. The expression of *Tcf7* increases along the pseudotime within the classical Th17 cell cluster but also starts to decrease within the same cluster. This decrease follows into the Th1-like ex-Th17 cells and γδ T cell clusters where it reaches its lowest expression. The expression of the transcription factor, TCF-1, increases again within the Th1-like ex-Th17 cells and Tcf7^{high}Ccr6^{high} cells cluster where it reaches its peak in expression. The expression of YFP peaks within the classical Th17 cells cluster but also plummets within the same cluster along the pseudotime. The expression remains low, except a small increase

within the γδ T cell cluster and reaches and expression level of 0.5 again within the Th1-like ex-Th17 cells cluster. This expression level remains constant along the pseudotime.

In summary, these results reveal an interesting inverse relationship between the expression of the transcription factors RORγT and TCF-1 along the pseudotime. The increased expression of TCF-1 in the later stages of the pseudotime suggest some transcriptioncal activities of this transcription factor within Th17 cells that determine the final fate of these cells.

3.1.4 ATAC-seq data from cGN induced mice

In order to gain a deeper understanding of the activity of the transcription factors in Th17 cells and their chromatic accessibility landscape, ATAC-seq was conducted using sorted $CD4^+$ and YFP^+ cells from *Il17A^{cre} x R26^{eYFP}* mice. The cells were gated on $CD45^+$ and $CD3^+$ before gating on the desired cells (Figure 14A) ensuring a better and purer sort. Once all the YFP^+ cells were sorted, the nuclei from these cells were isolated and processed for further sequencing. Since the number of Th17 cells in the kidney is relatively low, all the YFP^+ from a pool of 15 mice were sorted. Therefore, a lot more $CD4^+$ cells were obtained, compared to YFP^+ cells. From the sorted cells, all 30 000 YFP^+ cells were used for the nuclei isolation, whilst only approximately half of 50 000 cells, from the total $CD4^+$ sorted cells were utilised.

The processed nuclei were then bioinformatically analysed using the Signac Pipeline (Stuart et al., 2021). The two datasets, $CD4^+$ and YFP^+ nuclei, were merged and integrated. This dataset was visualised using UMAP, which revealed distinct clusters representing transcriptionally diverse subpopulations (Figure 14B). These clusters most likely represent specific functional states or lineages of $CD4^+$ and YFP^+ cells in the kidney in cGN conditions.

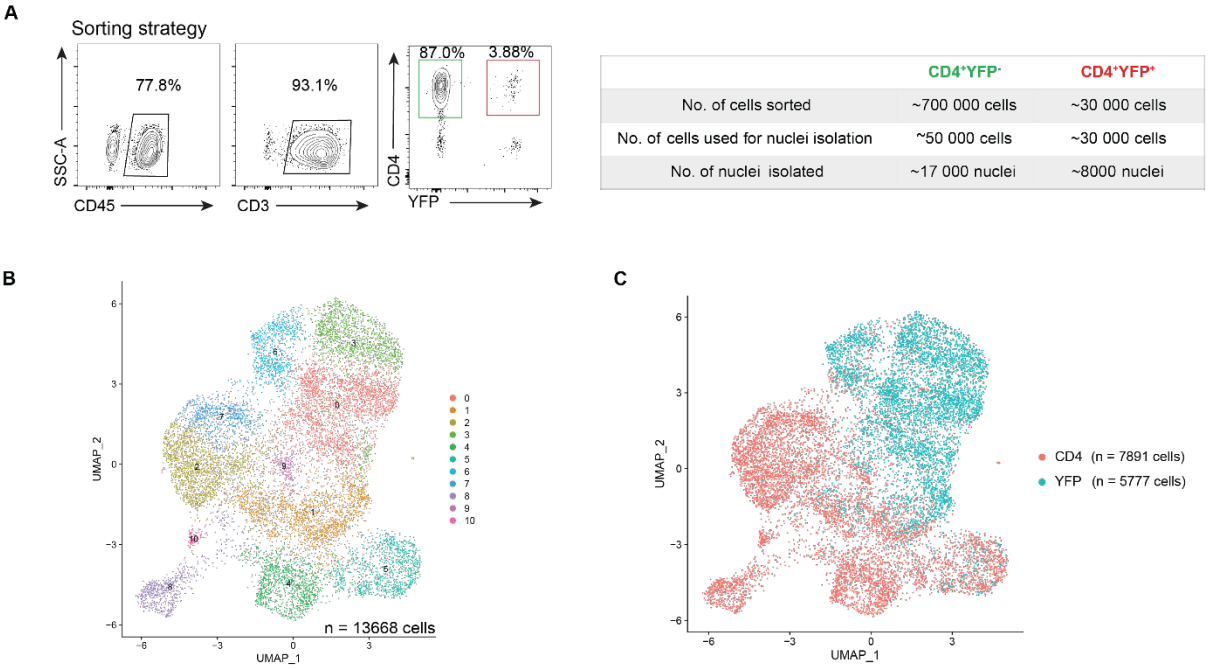

	CD4⁺YFP⁻	CD4⁺YFP⁺
No. of cells sorted	~700 000 cells	~30 000 cells
No. of cells used for nuclei isolation	~50 000 cells	~30 000 cells
No. of nuclei isolated	~17 000 nuclei	~8000 nuclei

Figure 14: Overview of cell sorting, clustering and integration of ATAC-seq data of cGN induced mice

A) Sorting strategy for isolating CD4⁺ and YFP⁺ cells, accompanied by a table summarising the number of cells sorted, cells processed for nuclei isolated and the final number of nuclei isolated. B) UMAP illustrating the different clusters of nuclei from the dataset. C) UMAP illustrating the distribution of nuclei derived from the two sorting populations, highlighting their localisation across clusters.

To visualise the distribution of CD4⁺ and YFP⁺ cells across the UMAP, another UMAP was created displaying the origin of the cells based on the sorting strategy (Figure 14C). This visualisation revealed that the two populations are largely localised to opposite sides of the UMAP, with limited interspersion. A small region of overlap was observed in the central area of the UMAP, suggesting the presence of a transitional or shared population of nuclei between the two sorts. This distinct distribution indicates that the chromatin accessibility profiles of the CD4⁺ and YFP⁺ nuclei differ significantly, reflecting potential functional or developmental differences between these populations in cGN.

Further analysis of the ATAC-seq data was performed to identify and annotate the clusters. To achieve this, a separate UMAP was generated using the previously shown scRNA-seq data from cGN mice (Figure 9). For this reference UMAP, CD4⁺ and YFP⁺ cells were filtered out from the dataset and new clusters were calculated. These clusters were then identified using

their differentially expressed genes, allowing the identification of distinct T lymphocyte cell types (Figure 15A).

Using the Signac pipeline, the scRNA-seq data was integrated with the ATAC-seq data to transfer cluster annotations via label transfer anchors. This method enabled the labelling and identification of the ATAC-seq UMAP clusters based on the transcriptional profiles identified in the reference UMAP (Figure 15B). This integration process caused substantial changes in the initial clustering of the ATAC data UMAP. This could be due to the fact that chromatin accessibility data reflects regulatory potential which does not always correlate with the transcriptional activity captured by scRNA-seq. Thus, the integration process probably prioritised aligning chromatin accessibility patterns with their closest transcriptional counterparts, leading to a reorganisation of the clusters. These changes emphasise the complexity of integrating multimodal datasets and highlight the differences between regulatory landscapes and gene expression profiles.

Motif enrichment analysis was performed by integrating the JASPAR database into the dataset. This analysis uses the database to scan the open chromatin regions in each individual cell and assigns a motif presence score to each open chromatin regions. The frequency of each motif occurrence is compared to a background set, determining the motif enrichment in each cell. This motif enrichment analysis was conducted for *Tcf7* and *Rorc* (Figure 15C). These two transcription factors are essential for the differentiation and function of Th17 cells. The motif enrichment for TCF-1 was very high in naïve T cells which is to be expected since the transcription factor is essential for early T cell development. However, high chromatic accessibility of TCF-1 was also observed in both Th17 cell clusters. This suggests that the transcription factor is active in these cells and plays a potential functional role. The motif of the transcription factor RORγT was also highly enriched in the Th17 cell clusters. However, high chromatin accessibility was also observed in the Th1 cell clusters. This finding could reflect shared or overlapping networks between Th1 and Th17 cells, suggesting potential crosstalk or plasticity between these cells.

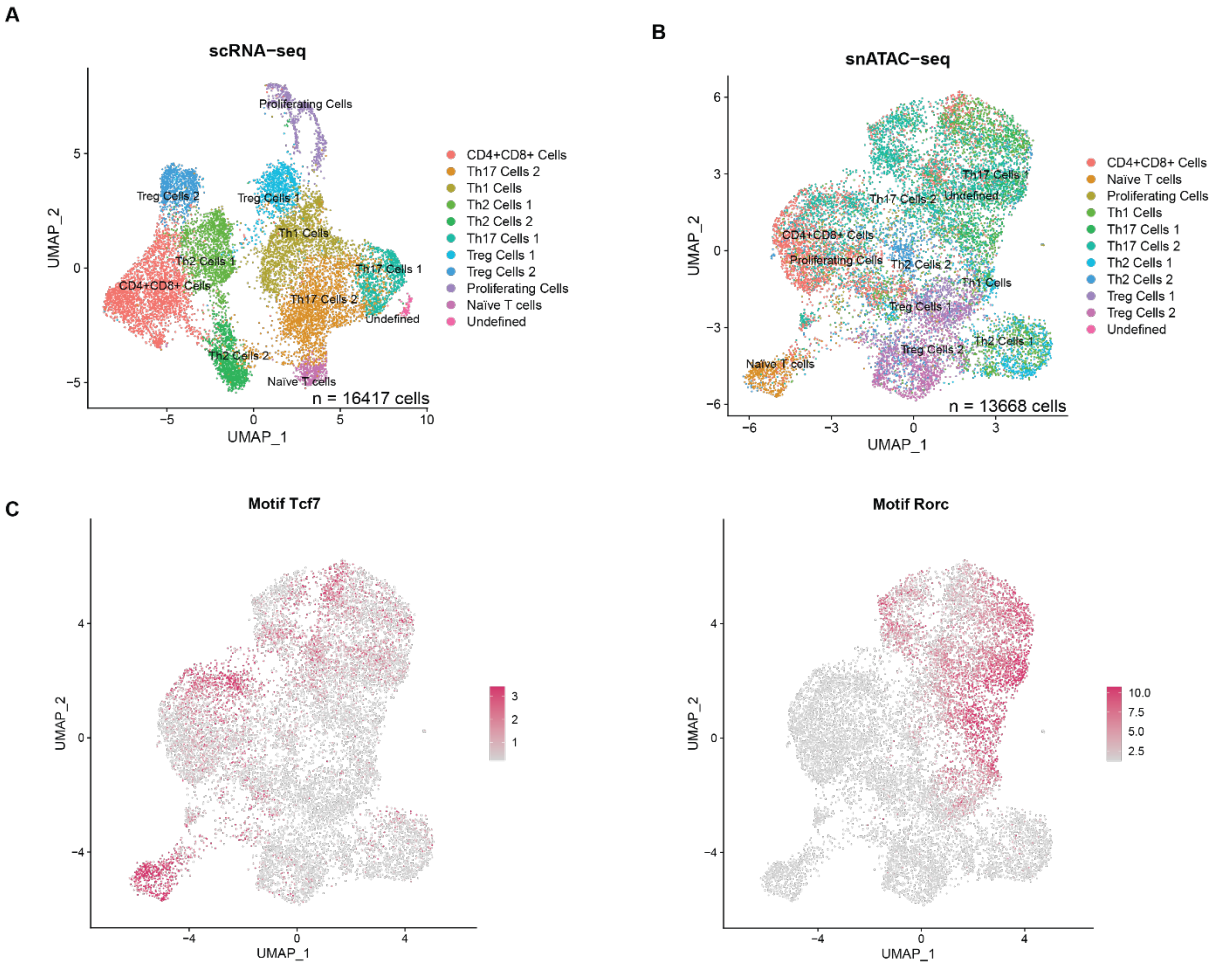

Figure 15: Integration and analysis scRNA-seq and ATAC-seq data
A) Reference UMAP generated from an existing single-cell leukocyte dataset, filtered to include CD4^{+} and YFP^{+} cells. **B)** Transfer of labelling anchors from the reference dataset onto the ATAC-seq UMAP, resulting in the finalised labelling of nuclei. **C)** Motif enrichment analysis plots for *Tcf7* and *Rorc*, highlighting regulatory element activity associated with these transcription factors.

3.2 Functional *in vivo* FACS data

To investigate the role of TCF-1 in Th17 cells in the kidney, a mouse line with the gene, *Tcf7*, knocked out within Th17 cells was generated and these mice were induced with cGN. In order to compare whether this effect is specific to the kidney, a duodenitis inducing model was used to investigate Th17 cells in the intestine.

3.2.1. Establishment of transgenic mice for experimental purposes

In order to study Th17 cells *in vivo* fate mapping mice were used. The control group consisted of *Il17A*^{cre} *x R26*^{eYFP} mice, whilst the experimental group was comprised of *Tcf7*^{flox} x *Il17A*^{cre} *x R26*^{eYFP} mice (Figure 16A). In the control group, all IL-17A-producing cell were tagged with an eYFP gene to ensure later identification in FACS and single cell datasets. These mice were then crossed with mice that had the *Tcf7* gene flanked with loxP sites (Figure 16A). The resulting mouse line had the gene, *Tcf7*, knocked-out in all IL-17A-producing cells that were still tagged by the eYFP gene. This deletion method allows the T cells to develop without any disruptions since TCF-1 is an essential transcription factor for early T cell development (Wang et al., 2021). Thus, the full development of Th17 cells is ensured since the TCF-1 gene is deleted only once the cells start producing the cytokine IL-17A. This means that any effects observed in the experimental mouse line will be due to the role of TCF-1 in fully developed Th17 cells. Therefore, these two mouse lines would allow a successful investigation of Th17 cells as well as the effect on Th17 cells in the absence of the transcription factor TCF-1.

FACS analysis was used to validate the experimental group (Figure 16B). The data shows high Tcf7 expression within the YFP^{+} cells in the control group but the expression is significantly reduced, approaching negligible levels, within the experimental group. These findings indicate successful genetic modification in the experimental group.

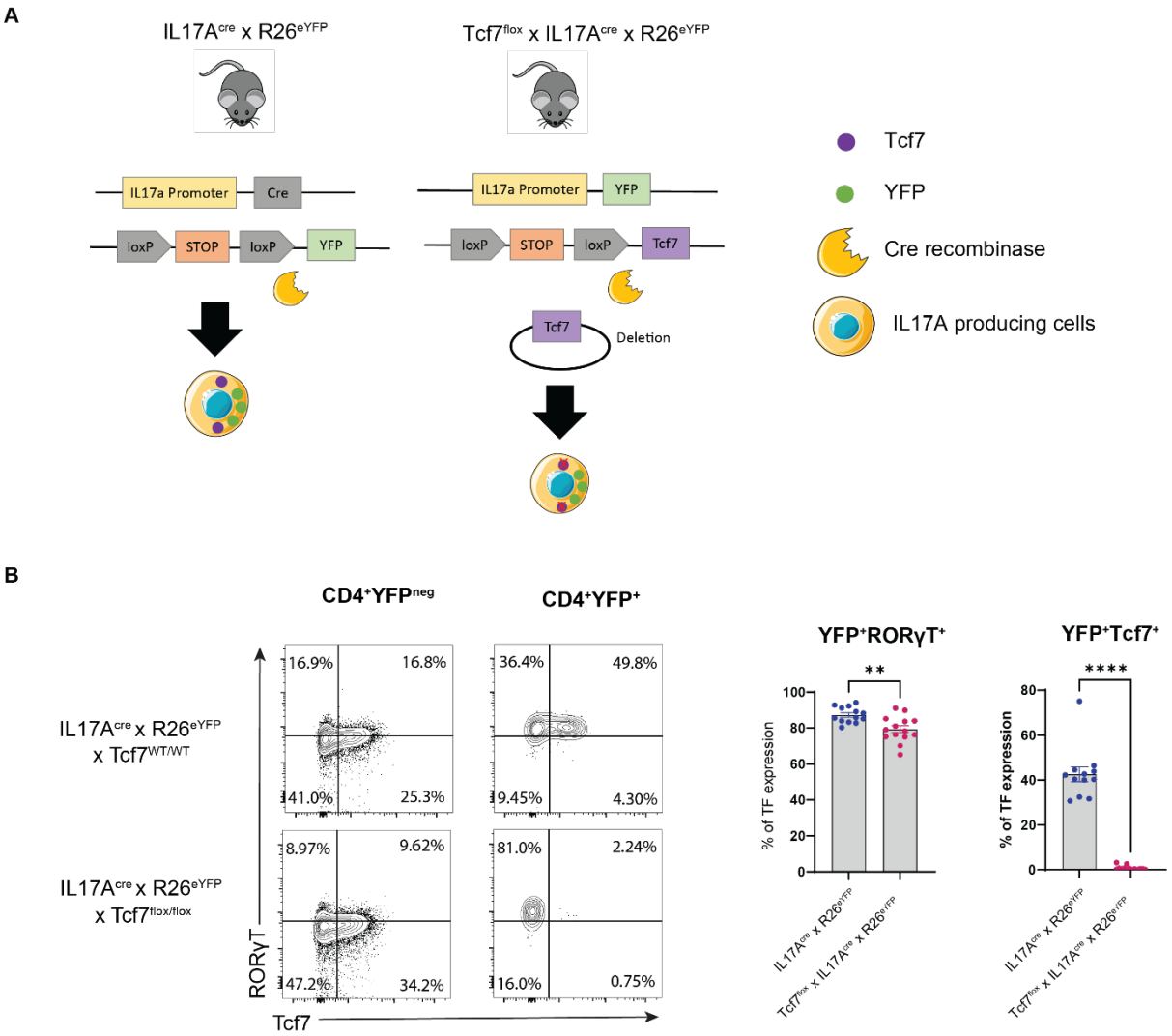

Figure 16: Genetic modification and validation of experimental mouse lines.
A) Schematic representation of the genetic modifications in the control and experimental mouse lines. The control line tags IL-17A-producing cells with *eYFP* for identification. In the experimental line, the *Tcf7* gene is flanked by loxP sites, enabling targeted knockout of *Tcf7* specifically in IL-17A-producing cells. **B)** FACS analysis confirms the successful knockout of the *Tcf7* transcription factor in IL-17A-producing cells in the experimental line, as evidenced by the absence of *Tcf7* expression compared to the control line.

3.2.2 *In vivo* FACS analysis in crescentic glomerulonephritis

Both groups of mice were treated with NTN serum to induce cGN. On day 3 after induction, a U-Stix was used to check for proteinuria and ensure the mice were sick (see 2.2.3). On day 9 the mice were put in metabolic cages to collect urine samples to test for clinical parameters such as albuminuria/creatinine index. The next day the mice were sacrificed for organ harvest (Figure 17A).

On the day of organ harvest, small slices of the kidney were taken for histological analyses. The histological images show cell infiltration in both the control and experimental mouse line induced with cGN which stems from the deposition of immune complexes. Additionally, the glomeruli of the cGN induced mice also showed cell infiltration, swelling and crescent formations when compared to the healthy kidneys (Figure 17B). These results validate the successful induction of cGN in the mice. When comparing the healthy kidneys, no changes were observed. This ensures that the deletion of the transcription factor TCF-1 has no effect on the kidney in healthy conditions, meaning any differences seen in the data is only present in inflammatory conditions.

The quantification of the disease severity in the two mouse lines revealed no significant changes in the albumin/creatinine index when comparing the two mouse lines. This means that in the context of clinical parameters, the disease severity in both groups is the same. However, the histological analysis shows a significantly reduced percentage of glomerular crescents, indicating a reduced disease severity in the *Tcf7* knock-out group (Figure 17C). Since glomerular crescents are a strong indicator of kidney injury stemming from inflammation, this is a very reliable assessment of disease severity (Figure 17B+C).

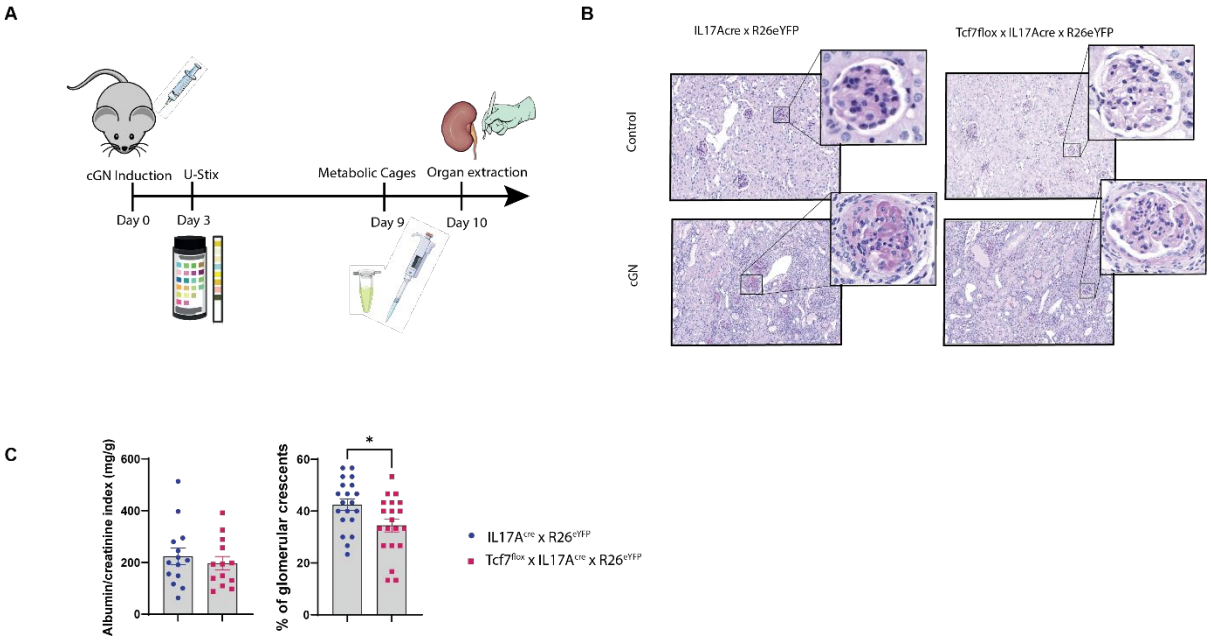

Figure 17: Experimental crescentic glomerulonephritis model and disease severity assessment.

A) Timeline of the cGN disease induction protocol in mice, illustrating the progression from initial induction to endpoint assessments. **B)** Representative histological images of kidney sections from both control and cGN-induced mice across the two mouse lines, showing characteristic pathological changes in response to disease induction. **C)** Quantification of disease severity across two metrics, albumin/creatinine index and percentage of glomerular crescents. These measurements provide a comprehensive assessment of kidney injury and inflammation associated with the cGN model.

Next, the proportion of YFP$^+$ cells was quantified (Figure 18A). As Th17 cells are known for their pathogenic and pro-inflammatory roles, their presence serves as another indicator of disease severity. The FACS data revealed a significantly reduced number of Th17 cells in the kidney in the *Tcf7* knock-out mouse line. However, the amount of YFP$^+$ cells is generally low in the kidney. Nevertheless, the amount of renal Th17 cells in the experimental mouse line was astonishingly low. Given the established pathogenic role of Th17 cells in cGN, this finding correlates with the earlier disease severity assessment, further supporting a reduced disease outcome in the *Tcf7* knock-out group.

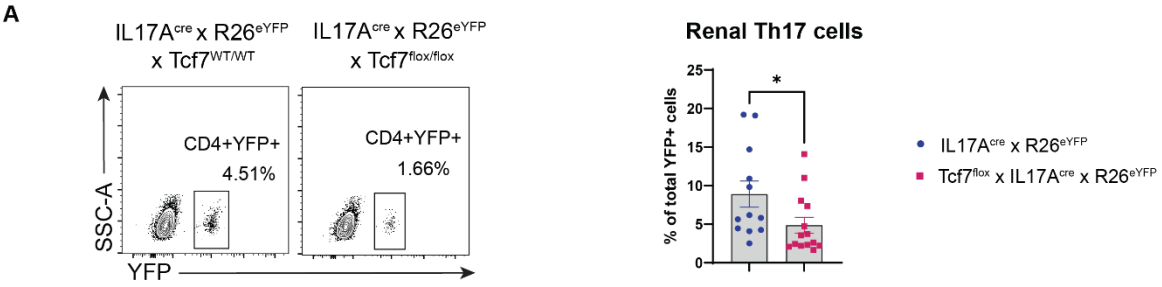

Figure 18: Quantification of YFP$^+$ cells in cGN.
A) FACS plots showing the gating strategy used to identify YFP$^+$ cells and quantify their prevalence in both mouse lines under cGN conditions. The percentage of total YFP$^+$ cells is significantly higher in the control group compared to the experimental group, indicating differential YFP$^+$ cell populations between the two groups.

To further investigate the functional roles of CD4$^+$ T cells in cGN, the cytokine production of different populations within the dataset was analysed using FACS (Figure 19). The expression levels of the key cytokines, IL-17A, IFNγ and IL-10, were quantified. Within the overall CD3$^+$CD4$^+$ population, no significant changes were detected in the expression of any of the cytokines (Figure 19A). The same result was observed when analysing the cytokine expression in the CD4$^+$YFP$^-$ population (Figure 19B). In contrast, the CD4$^+$YFP$^+$ population showed a significantly higher expression of the anti-inflammatory cytokine, IL-10, was observed in the *Tcf7* knock-out group (Figure 19C). This suggests that Th17 cells may adopt an anti-inflammatory phenotype in the absence of the transcription factor TCF-1. The

expression of IFNγ was also much lower when compared to the other two cell populations analysed. This is most likely due to the fact that Th17 cells are not known for their IFNγ expression under normal conditions. Additionally, though not significant, there seems to be a trend showing more IFNγ expression in the *Tcf7* knock-out group.

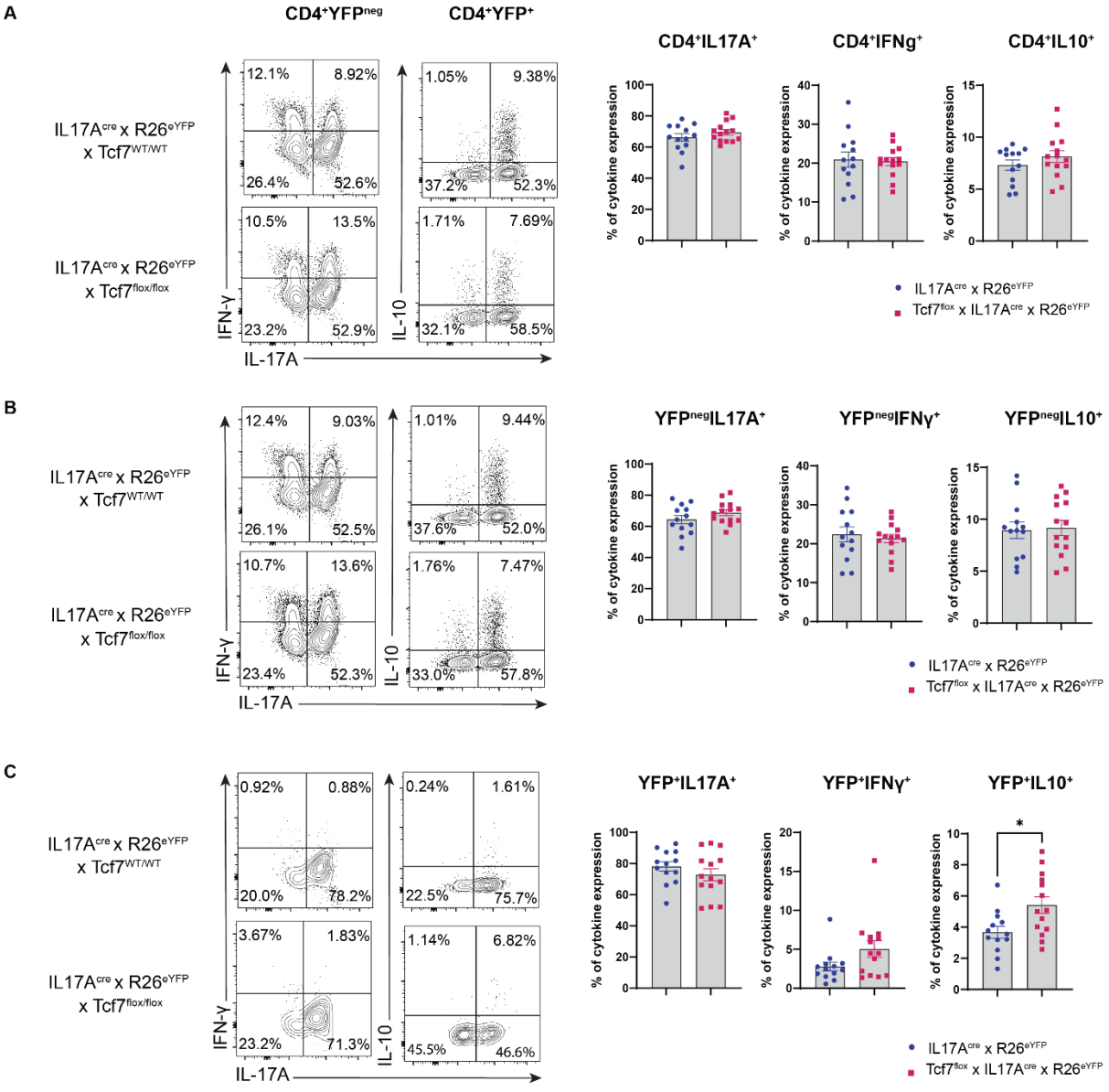

Figure 19*:* Cytokine expression profiles in cGN across CD4⁺ T cell subsets.
FACS analysis of cytokine production, showing gating strategy and quantification of *Il17a, Ifnγ*, and *Il10* expression within CD4⁺ T cell subsets. **A)** Expression of cytokines within the CD3⁺CD4⁺ T cell population. **B)** Cytokine expression in CD4⁺YFP⁻ cells, and **C)** Cytokine expression in CD4⁺YFP⁺ cells. These data illustrate the differential cytokine production profiles across distinct CD4⁺ T cell subsets within the cGN model.

3.2.3 *In vivo* FACS analysis in anti-CD3 induced duodenitis

To evaluate whether the findings from the functional FACS analysis were specific to the kidney or could also observed in other organs, the same analyses were conducted using a different autoimmune model: anti-CD3 induced duodenitis. This model triggers inflammation in the duodenum, allowing assessment of the immune responses in the intestinal system.

Both the control and experimental mouse lines were injected with an anti-CD3 antibody to induce duodenitis. The mice were given three injections over a period of 4 days: on day 0, day 2 and on day 4, they were injected 4 hours prior to the organ harvest (Figure 20A).

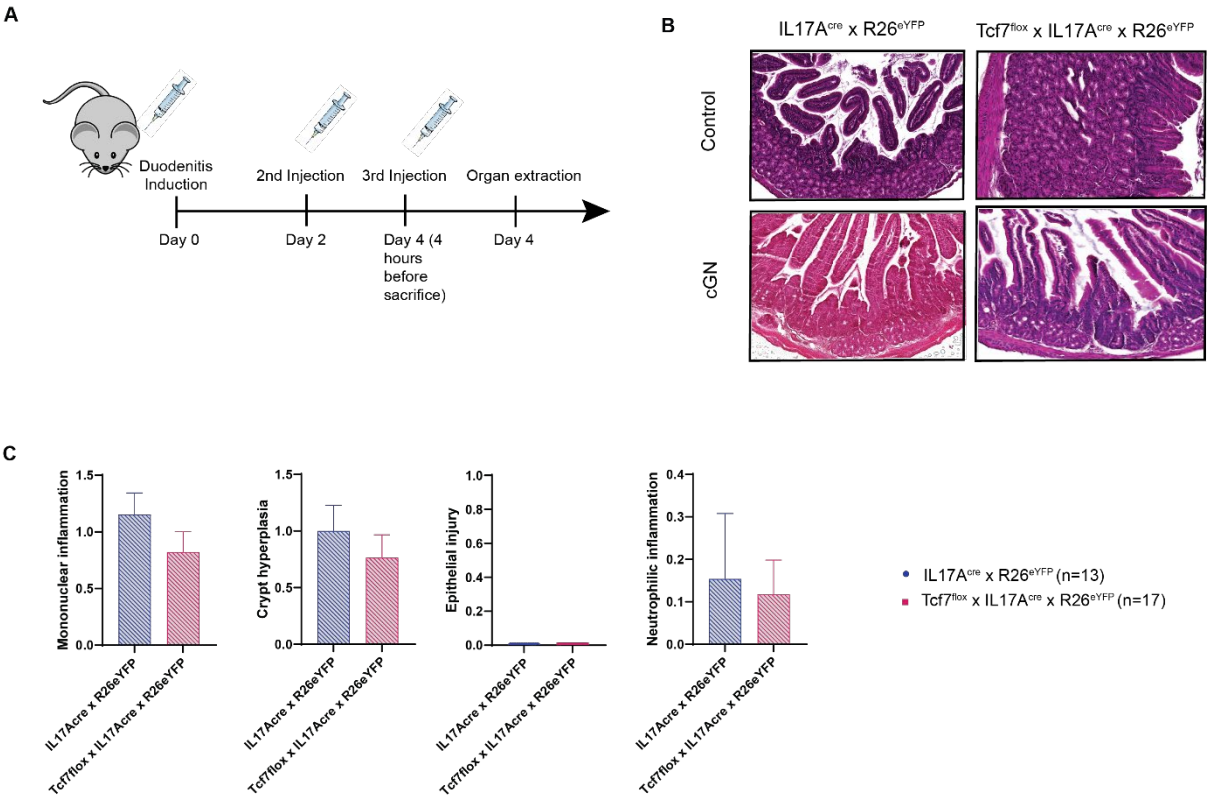

Figure 20: Anti-CD3 induced duodenitis model and disease severity assessment.
A) Timeline of the duodenitis disease induction protocol in mice, illustrating the progression from initial induction to endpoint assessments. **B)** Representative histological images of duodenum sections from both control and anti-CD3 treated mice across the two mouse lines, showing characteristic pathological changes in response to disease induction. **C)** Quantification of disease severity across multiple metrics, including mononuclear inflammation, cryptic hyperplasia, epithelial injury, and neutrophilic inflammation. These measurements provide a comprehensive assessment of duodenum injury and inflammation associated with the duodenitis model.

Small slices of the duodenum were taken from each mouse for histological analyses (Figure 20B). The histological images were analysed to see whether there is a difference under healthy conditions between the *Il17A*^{cre} *x R26*^{eYFP} and *Tcf7*^{flox} x *Il17A*^{cre} *x R26*^{eYFP} mouse lines. No differences were observed, this assures that the deletion of the transcription factor in Th17 cells also has no effect in the duodenum under healthy conditions. This means that any differences in the data revealed, will be due to the inflammatory conditions. The quantification of the disease severity using multiple parameters, mononuclear inflammation, crypt hyperplasia, epithelial injury and neutrophilic inflammation showed no significant changes between the two mouse lines in inflammatory conditions. When looking at the histological images, there were also no obvious differences observed.

Next, the proportion of YFP$^+$ cells in the duodenum was quantified (Figure 21A). As Th17 cells are known for their pathogenic and pro-inflammatory roles, their presence serves as another indicator of disease severity. The FACS data revealed a significantly increased number of Th17 cells in the duodenum. This data indicates that the reduced number of Th17 cells in the *Tcf7* knock-out group in inflammatory conditions is specific to the kidney. However, since no difference in the disease severity was observed in the two groups, the effect of the increased number of Th17 cells in the duodenum remains unknown.

A

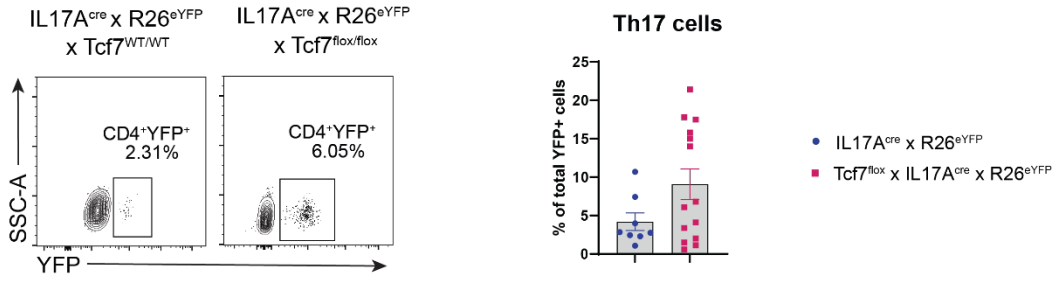

Figure 21: Quantification of YFP$^+$ cells in anti-CD3 induced duodenitis.
A) FACS plots showing the gating strategy used to identify YFP$^+$ cells and quantify their prevalence in both mouse lines under duodenitis conditions. The percentage of total YFP$^+$ cells is significantly higher in the control group compared to the experimental group, indicating differential YFP$^+$ cell populations between the two groups.

Similar to the cGN experiments, the functional roles of $CD4^+$ T cells in duodenitis were also investigated by analysing the cytokine production of different populations within the dataset using FACS (Figure 22). The expression levels of the key cytokines, IL17a, IFNγ and IL-10, were quantified. Within the overall $CD3^+CD4^+$ population there was a significantly higher expression of IL-17A in the *Tcf7* knock-out group when compared to the control group. When looking at the IL-10 expression, there is a significant reduction in the presence of the cytokine in the YFP^+ cells in the *Tcf7* knock-out group when compared to the control mouse line. The same results for the IL-17A and IL-10 expression as the $CD3^+CD4^+$ population was also revealed in the $CD4^+YFP^-$ population in the *Tcf7* knock-out group. In both of these populations there was no change detected in the IFNγ expression (Figure 22A + B). The $CD4^+YFP^+$ population also showed no significant changes in the IFNγ expression in both groups. However, there was a significantly reduced expression of the anti-inflammatory cytokine, IL-10, in the *Tcf7* knock-out group, whereas no changes were detected in the IL-17A expression (Figure 22C). This result is very different from the results observed in the $CD4^+YFP^+$ population in cGN. This indicates that the anti-inflammatory phenotype adopted by the Th17 cells in the absence of the transcription factor, TCF-1, is specific to the kidney and the absence of TCF-1 has a completely different impact in the gut, indicating a different regulatory for the transcription factor in the duodenum.

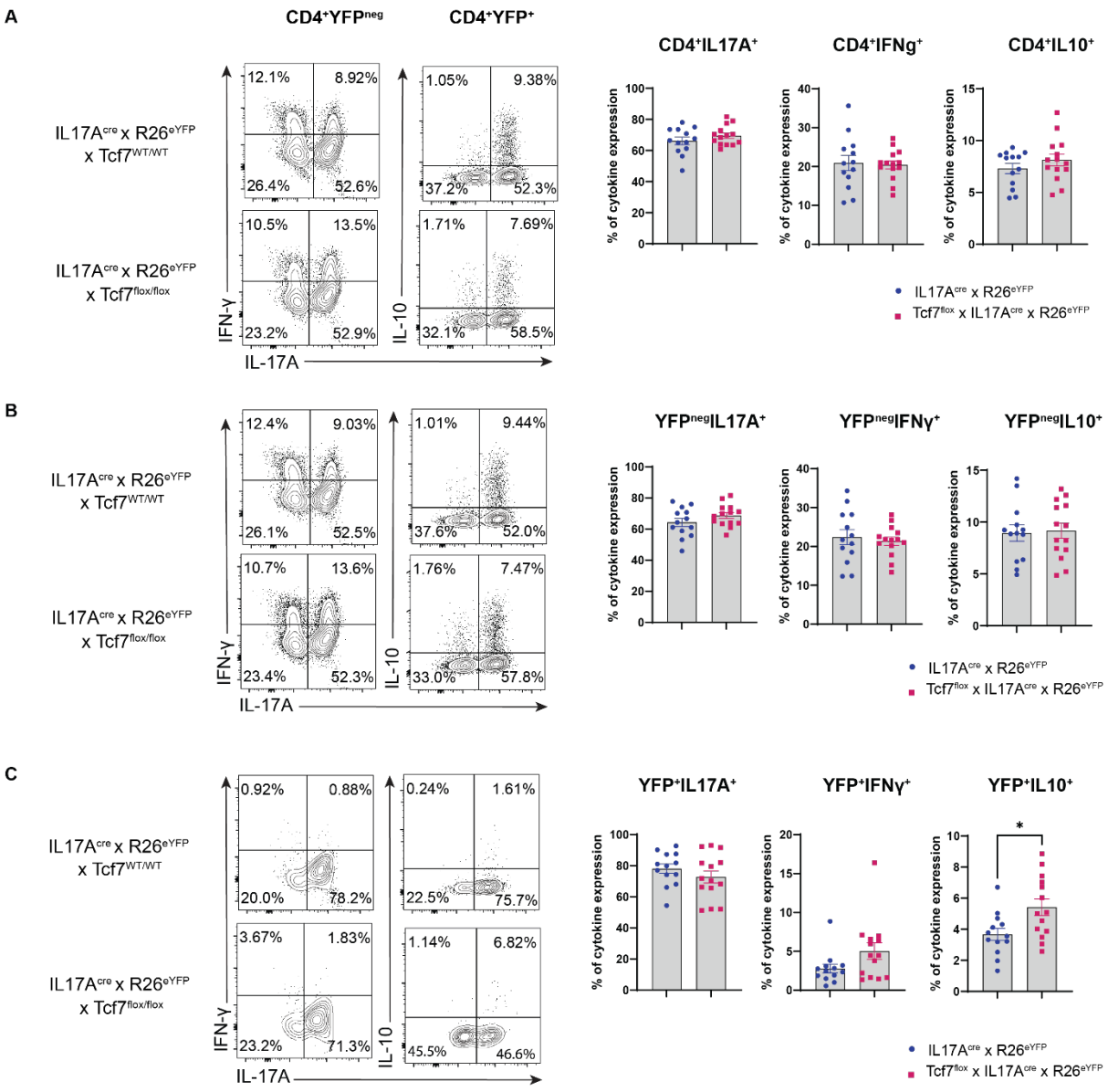

Figure 22: Cytokine expression profiles in anti-CD3 induced duodenitis across CD4⁺ T cell subsets.

FACS analysis of cytokine production, showing gating strategy and quantification of *Il17a*, *Ifnγ*, and Il10 expression within CD4⁺ T cell subsets. **A)** Expression of cytokines within the CD3⁺CD4⁺ T cell population. **B)** Cytokine expression in CD4⁺YFP⁻ cells, and **C)** Cytokine expression in CD4⁺YFP⁺ cells. These data illustrate the differential cytokine production profiles across distinct CD4⁺ T cell subsets within the duodenitis model.

3.3 Whole kidney analysis

3.3.1 scRNA-seq of the whole kidney from control and cGN induced mice

To obtain a deeper understanding of the functional role of Th17 cells, single cell sequencing was performed on the whole kidney of control and cGN induced *Il17A*^{cre} *x R26*^{eYFP} mice. The kidneys obtained from the mice were processed with a tissue dissociation kit to obtain a single cell suspension. This suspension was then used to generate single cell libraries for snRNA-seq. After sequencing, the cells were filtered out to ensure only the presence of high quality cells in the dataset for further processing. Following data merging and integration, clustering analysis was conducted to identify distinct cell populations based on shared transcriptional profiles. The results were visualized using UMAP, which revealed multiple well-defined clusters corresponding to specific cell types and functional states within the kidney (Figure 23A). These clusters reflect the cellular heterogeneity present in both cGN and control conditions.

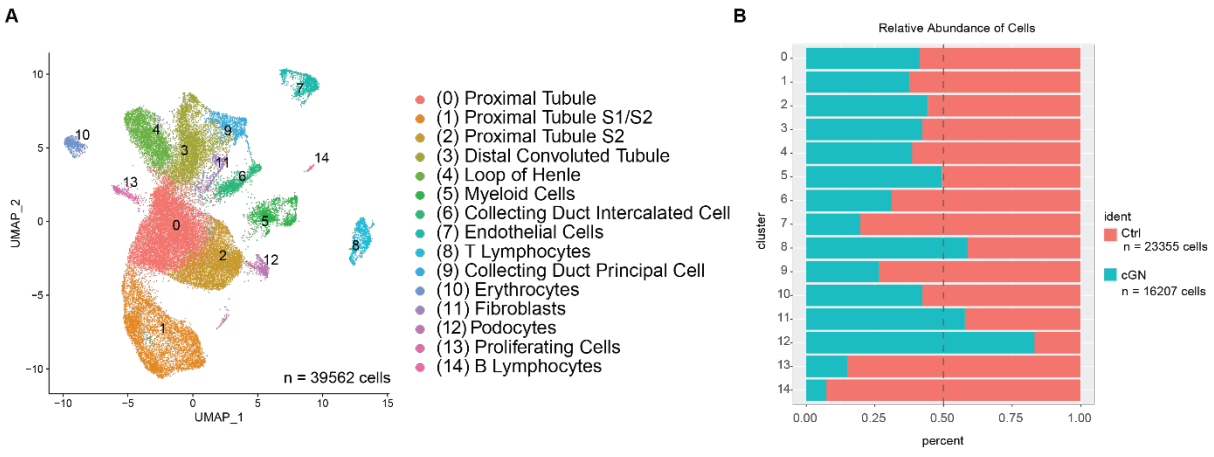

Figure 23: Clustering analysis of single cell RNA-seq data from the whole kidney.
A) UMAP visualisation of single cell RNA-sequencing data, showing distinct clusters of cells identified based on shared transcriptional profiles after data merging and integration. **B)** Proportional representation of cells from the cGN and control group within each identified cluster, highlighting differences in cluster composition between experimental conditions.

To compare the effects of cGN on the proportional representation of different cell types, the composition of each cluster was assessed across the cGN and control groups by calculating the relative abundance of cells in each cluster (Figure 23B). Certain clusters displayed a considerable shift in their proportional representation between the experimental conditions. For example, T lymphocytes and myeloid cells showed an increased representation in the cGN group, consistent with the inflammatory environment associated with the disease. Conversely, clusters corresponding to homeostatic or non-immune cell populations, such as tubular epithelial cells, showed a reduced proportional representation in cGN. Additionally, a significant increase in the relative abundance of podocytes was observed in the cGN group. This phenomenon could be resulting from reactive changes in podocyte transcriptional profiles or recruitment of podocyte-like cells in response to glomerular injury.

To investigate intercellular communication in the kidney, the data was bioinformatically analysed using CellChat (Jin et al., 2021). An outgoing signalling pathway analysis was conducted. This analysis uses databases such as CellChatDB which specifies known ligand-receptor interactions. For each cluster, the ligands that are highly expressed are identified and matched to cells that express the associated receptors of that ligand. Using this information, the outgoing interaction strength of a cell cluster is calculated. The individual ligand-cell interactions are grouped into predefined pathways from the available databases. The strength of the outgoing signalling pathways is quantified based on the cumulative signalling contributions from the ligands expressed in each cell cluster.

This outgoing signalling pathway analysis was performed on the T lymphocytes cluster (Figure 24A). The analysis revealed a network of pathways involved in immune modulation and inflammation, highlighting their central role in orchestrating kidney immune responses during cGN, especially their close interplay with B cells. These pathways are most likely both pro-inflammatory and regulatory signals, revealing the dual roles of T cells in promoting inflammation while potentially contributing to resolution mechanisms.

The same outgoing signalling pathway analysis was conducted on endothelial cells since these cells play an important role in the kidney under inflammatory conditions (Figure 24B). The analysis revealed strong outgoing signalling pathways to proliferating cells, myeloid cells, B lymphocytes and T lymphocytes. This finding is consistent with the role of endothelial cells as key mediators of immune cell trafficking and tissue injury in cGN.

To further explore regulatory signalling, the RNA expression of Il10ra and Il10rb, encoding the IL-10 receptor subunits, was examined across the kidney dataset (Figure 24C). The feature plots showed that *Il10ra* is highly expressed in myeloid cells and T lymphocytes, whereas *Il10rb* is expressed across multiple cell populations. This widespread expression indicates that IL-10 signalling may play a critical anti-inflammatory role in modulating the immune response and limiting tissue damage in cGN.

A noteworthy finding is that *Il10rb* is very highly expressed in endothelial cells, whilst *Il10ra* shows very low expression in endothelial cells. This suggests that endothelial cells may be responsive to IL-10 through the IL-10 receptor beta subunit, potentially contributing to the regulation of inflammation and tissue repair processes in cGN.

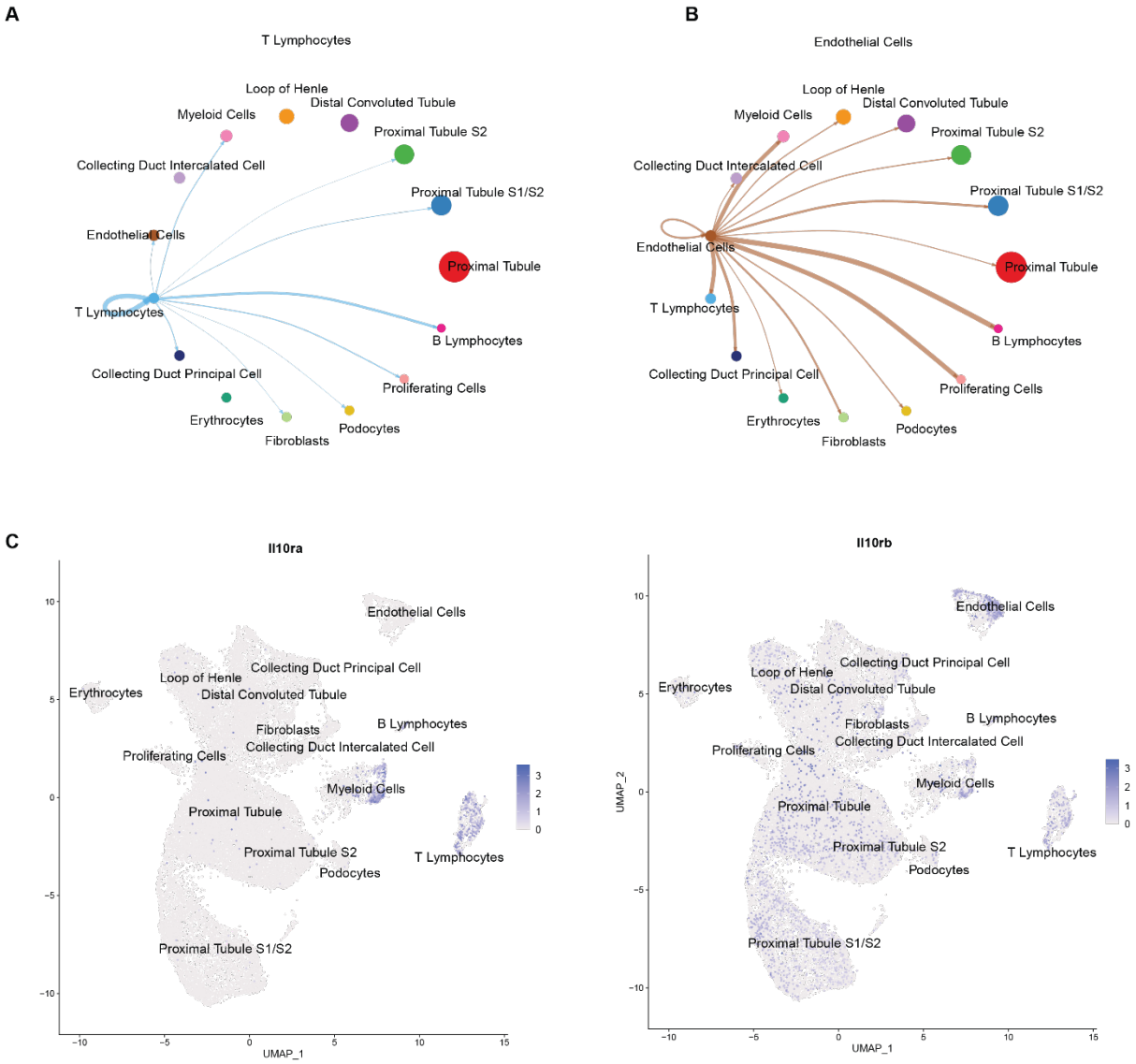

Figure 24: Analysis of signalling pathways and IL-10 receptor expression in the whole kidney **A)** Outgoing signalling pathway analysis from T lymphocytes in the whole kidney, visualised using CellChat. **B)** Outgoing signalling pathway analysis from endothelial cells in the whole kidney, also generated using CellChat. **C)** Feature plots displaying the RNA expression of *Il10ra* and *Il10rb*.

4 Discussion

This study identified the transcription factor TCF-1 as a negative regulator of Th17 cell plasticity playing an important role in the disease outcome of cGN. Various approaches were used in this study to investigate the functional role of TCF-1 on Th17 cells. By integrating histological, cellular, and functional analyses, this study demonstrates that the loss of Tcf7 in Th17 cells results in significant alterations in disease severity, immune cell phenotypes, and cytokine profiles, highlighting Tcf7 as a key regulator of Th17 cell-mediated inflammation in the kidney. This section will discuss and analyse the results obtained and reveal future implications.

4.1 Single cell sequencing analysis

4.1.1 High expression of TCF-1 in Th17 cells from murine kidneys

The scRNA-seq of renal leukocytes provided valuable insights into the cellular heterogeneity of immune cells in the kidney under a healthy homeostatic condition as well as inflammatory conditions. Most YFP^+ cells were found in the Th17 cell cluster, validating the correct identification of the cells. However, there are some YFP^+ that appear in other clusters such as naive T cells, $CD4^+$ effector cells and proliferating cells. Since Th17 cells are also $CD4^+$ effector cells, it would make sense that in the integration process, some cells end up in that cluster. This also emphasises the functional plasticity and diverse roles of T cell subsets under inflammatory conditions. Additionally, some YFP^+ cells might have been sorted together with the $CD4^+YFP^-$ or $CD45^+$ sort since the purity from FACS sorting is not always 100% (Basu et al., 2010). Furthermore, there are other cells that produce IL-17A, such as $CD8^+$ T cells, ILCs and myeloid cells (Mills, 2023). Therefore, it is plausible that not all YFP+ cells are Th17 cells, which explains the presence of the *YFP* gene in other cell clusters.

The lack of a distinct T regulatory cell cluster is another very interesting finding and suggests that they may be mixed in with other T cell clusters in the dataset due to a close transcriptional relationship or there could simply be a low abundance of Treg cells in the dataset. If the resolution is increased in calculating the UMAP, there could be a distinct Treg cluster found. However, increasing the resolution would cause smaller clusters to form that would be a part of a bigger cluster. The current resolution was picked carefully and was deemed to be the most appropriate. While this approach was used in this work, another possibility would be to perform overclustering and in a second step merge similar clusters. However, since more IL-10 production was observed in the *Tcf7* knock-out, perhaps a Treg cluster could be found in the single cell dataset of the *Tcf7* knock-out group. However, no such dataset exists as of yet.

The higher expression of *Il17a* in the cGN induced mice when compared to the control mice highlights the pro-inflammatory role of IL-17A and Th17 cells in cGN (Chebotareva et al., 2020). The *Il17a* expression is localised in the Th17 cell cluster on the UMAP, suggesting that in cGN Th17 cells are the main producers of the cytokine IL-17A in the kidney.

The expression of *Tcf7* further highlighted its potential regulatory role in cGN. While *Tcf7* expression was predominantly observed in naïve T cells under control conditions, it is also observed in the Th17 cell cluster in cGN induced renal immune cells. This suggests that TCF-1 may modulate Th17 cell differentiation and function, determining their pro- or anti-inflammatory role (Ma et al., 2011). The functional analysis revealed that the absence of TCF-1 in the Th17 cells results in the cells adopting an anti-inflammatory role. The presence of the transcription factor in the Th17 cells of the cGN induced mice which show a high expression of *Il17a* under inflammatory conditions supports the hypothesis that that TCF-1 could be a key regulatory factor in the pathogenic role of Th17 cells in the kidney. To explore this further, a single cell dataset from the *Tcf7* knock-out mice under cGN conditions would be necessary to check for the expression of both *Il17a* and *Il10* to confirm an increase or decrease of these cytokines. Additionally a functional validation by the *Tcf7* knock-out mice or other genetic perturbation would also be useful to confirm the role of TCF-1 on the IL-10 expression.

4.1.2 Differential expression of distinct sub-clusters revealed within renal murine Th17 cells

To further characterise the Th17 cells in the kidney, the heterogeneity of these cells was investigated by sub-clustering the Th17 cells only from the scRNA-seq dataset (Figure 9B). The sub-clustering process revealed six distinct clusters when the most appropriate resolution of the UMAP was determined (Figure 11A). This significant transcriptional heterogeneity of the Th17 cells in the kidney indicates that they are not in one constant state, but rather undergo tissue adaptation into specialised subsets that may contribute differently to disease progression or resolution.

The presence of the classically defined Th17 cells supports the already established role of these cells in promoting inflammation, especially through the production of IL-17A. However, the identification of Th1-like ex-Th17 cells found within the Th17 subcluster suggests a plasticity or a form of tissue adaptation of these cells, as previously described, in chronic inflammatory conditions (Kamali et al., 2019). In these conditions, Th17 cells sometimes acquire Th1-like properties whilst losing the expression of IL-17A and increasing the IFNγ production, acquiring an anti-inflammatory role.

The $Lyz2^{high}Cd74^{high}$ expressing cells could represent antigen-presenting Th17 cells or a population of Th17 cells that display enhanced interactions with antigen-presenting cells. The surface marker CD74 is a key marker for MHCII complexes, suggesting that the Th17 cells could also be potentially involved in antigen processing, modulating the adaptive immune responses (Su et al., 2017). The *Lyz2* gene enables lysosome activity which induces macrophage activation in murine tissues (Keshav et al., 1991). This correlates with the already established role of Th17 cells releasing pro-inflammatory cytokines that promote the activation of macrophages (Paust et al., 2023). Additionally, $Lyz2^{high}Cd74^{high}$ expressing cells were also previously identified in the analysis of brain immune cells as having a pro-inflammatory and

antigen presenting profile suggesting a dual role in both the innate response and adaptive response activation (Golomb et al., 2020).

Given that γδ T cells are known to produce IL-17 and contribute to tissue inflammation, the subset of these cells found within Th17 cells could reflect a distinct but functionally related population within the broader Th17 cell spectrum (Coulter et al., 2017).

The $Tcf7^{high}Ccr6^{high}$ expressing cell cluster highlights a population with high expression of TCF-1 which is not a usual marker of Th17 cells and Ccr6 which is known to be one of the main markers of these cells. The concurrent expression of Ccr6, which is a key chemokine receptor associated with Th17 migration, suggests that these cells may represent a precursor or less-differentiated Th17 subset with enhanced migratory capacity. The enrichment of Tcf7 in this subset correlates with its established role in maintaining T cell plasticity, suggesting that these cells could serve as a reservoir for further differentiation into either pathogenic or regulatory Th17-like cells.

Lastly, the identification of a Tox^{high} expressing cells cluster suggests a population with potential regulatory or exhausted characteristics. The *Tox* gene is frequently associated with T cell exhaustion, particularly in chronic inflammatory conditions (Khan et al., 2019). The functional significance of this subcluster still remains unknown, but its presence raises the possibility of a self-limiting mechanism within the Th17 response that may be relevant in disease resolution or immune homeostasis.

4.1.3. Inverse expression of RORγT and TCF-1 within the Th17 cell pseudotime trajectory

To gain a deeper insight into the transcriptional dynamics and potential lineage relationships within the Th17 cell population, the previously identified UMAP based clustering (Figure 11A) was successfully integrated into the Monocle3 trajectory analysis framework (Figure 12A). This approach enabled the inference of developmental progression and differentiation trajectories within the Th17 subcluster, leveraging the power of unsupervised single-cell analysis tools (Cao et al., 2019; Qiu et al., 2017). However, some minor alterations in the UMAP structure were observed following the integration, these changes are most likely attributable to differences in the dimensionality reduction algorithms and normalization approaches used by Monocle3 as opposed to Seurat. But despite these methodological differences, the spatial organization of the major subclusters remained preserved, validating the robustness of the initial clustering strategy.

The consistent and co-localized expression of key Th17-associated markers after the Monocle3 integration process provides further confirmation of the biological accuracy of the clustering and reinforces the identities assigned to each subpopulation (Figure 12). The overlapping presence of the Th17 effector cells marker genes, *Rorc* and *Il17a*, supports their association with the classic Th17 cell phenotype. The *YFP* gene expression is largely mirrored by the *Il17a* expression, but shows a broader distribution. This suggests a degree of functional plasticity, a previously active Th17 phenotype in cells that may have since downregulated their IL-17A expression or newly differentiated Th17 cells that don't possess the reporter gene. In contrast, the expression of *Tcf7* was very distinctly localised on the UMAP, highlighting a subpopulation of Th17 cells with potentially less differentiated or stem-like characteristics.

The use of Monocle3 trajectory analysis to investigate the differentiation states of kidney-infiltrating Th17 cells has revealed substantial transcriptional heterogeneity within this population and provided new insights into their potential lineage progression during

inflammation. By implementing the pseudotime analysis and defining the classical Th17 cell cluster as the trajectory root, distinct transcriptional programs were uncovered along the inferred differentiation axis calculated by the algorithm (Figure 13).

One of the key observations was the inverse expression pattern of the lineage-defining transcription factors RORγT and TCF-1 along the pseudotime axis. *Rorc* expression, which peaked early in the trajectory, declined steadily as cells progressed toward the terminal Tcf7^{high}Ccr6^{high} expressing cells cluster. In contrast, *Tcf7* expression was initially low, increased transiently and then increased sharply in the terminal states. This inverse trend suggests a potential switch in transcriptional control, where TCF-1 may begin to dominate regulatory influence in later stages of Th17 cell differentiation affecting their final fate. These findings support a model in which Th17 cells may transition from a pro-inflammatory phenotype towards a less classic or rather more regulatory state, possibly through TCF-1–mediated mechanisms. Given previous evidence that TCF-1 can antagonise effector T cell programs and promote self-renewal or quiescence (Escobar et al., 2020), its reappearance at later pseudotime points could potentially point to a key checkpoint that shapes the long-term fate or plasticity of Th17 cells in the kidney.

The dynamic expression of other genes such as *Ccr6*, *Cd74*, and *Il17a* also reflects the functional transitions occurring within the Th17 cell clusters. The chemokine receptor CCR6, which is associated with Th17 cell migration, showed a biphasic pattern, declining early before reappearing in the Tcf7^{high}Ccr6^{high} expressing cells cluster. This may indicate changes in migratory potential or tissue adaptation over time. The surface marker CD74 which is involved in MHC class II antigen presentation (Basha et al., 2012), exhibited a gradual increase through intermediate clusters before declining in terminal states, potentially pointing to transient antigen-presenting capabilities among Th17 or γδ T cells during inflammation (Akitsu & Iwakura, 2018). Interestingly, *Il17a* expression remained relatively stable, yet the reduction in expression of this cytokine in the Tcf7^{high}Ccr6^{high} expressing cells cluster suggests a reduced effector function in these cells. This aligns with the notion that not all YFP^{+} cells continue to

express the cytokine, possibly due to transdifferentiation or acquisition of alternative phenotypes, pointing towards tissue adaptation characteristics within Th17 cells (Agalioti et al., 2023).

The heterogeneous expression of *YFP* further supports this idea. Although initially exhibiting a high abundance in expression in classical Th17 cells, its expression sharply declined along the pseudotime axis and remained low in later clusters. Given that YFP expression marks cells that have previously expressed *Il17a*, this decline highlights a potential decoupling of historical IL-17A expression from current function, reinforcing the concept of Th17 plasticity and tissue adaptation.

In summary, these findings emphasise the complexity of Th17 cell differentiation within the kidney during crescentic glomerulonephritis. The identification of a $Tcf7^{high}$ cell cluster subset in the end of the chosen trajectory suggests that TCF-1 may not only act as a negative regulator of classical Th17 functions but may also define a distinct transcriptional state with altered effector potential. This suggests alternate possibilities regarding the role of TCF-1 in promoting Th17 cell persistence, reprogramming, or resolution of inflammation. Future functional studies would be required to determine whether these $Tcf7^{high}$ cells possess regulatory properties or represent a state of transition towards exhaustion, memory, or alternative T helper lineages.

4.1.4 High RORγT chromatin accessibility in Th17 and Th1 cells

To elucidate the regulatory landscape of Th17 cells in the kidney under inflammatory conditions, snATAC-seq was used, focusing on sorted $CD4^+$ and YFP^+ cells from murine kidneys. This technique provided insights into chromatin accessibility profiles and allowed for the inference of transcriptional regulatory programs active in Th17 cells during cGN (Preissl et al., 2018). The bioinformatic integration and analysis of the $CD4^+$ and YFP^+ datasets using the Signac pipeline revealed distinct chromatin accessibility profiles (Shi et al., 2022). The UMAP visualization demonstrated that $CD4^+$ and YFP^+ nuclei formed largely separate clusters, with only a small overlap seen in the central region. This spatial segregation within the UMAP strongly suggests that the transcriptional regulatory characteristics of these two populations differs significantly. The small area of overlap could potentially reflect a transitional state, indicative of Th17-derived cells that are undergoing phenotypic plasticity or are in the process of undergoing tissue adaptation.

The observed differences in chromatin accessibility probably represent divergent enhancer landscapes and transcription factor binding patterns, which underline the specialised functions of $CD4^+$ T cells and Th17 cells in the context of cGN (Linke et al., 2022). The distinct clustering of the YFP^+ nuclei implies the existence of a Th17-specific regulatory signature that is different from the broader $CD4^+$ population. Moreover, the partial overlap between YFP^+ and $CD4^+$ clusters may suggest epigenetic trajectories associated with Th17 cell differentiation or potential transdifferentiation pathways into non-classical effector subsets, which have been previously reported in other autoimmune models (Gagliani et al., 2015; Krebs & Panzer, 2018).

Additionally, the motif analysis that was conducted further elucidates the regulatory potential within the individual clusters of the Th17 cells. The *Tcf7* motif enrichment was highest in naïve T cells, consistent with its established role in early T cell lineage commitment (Weber et al., 2011). However, unexpectedly high accessibility was also observed in Th17 clusters, indicating that TCF-1 may retain a functional role beyond the initial lineage commitment,

possibly influencing Th17 cell maintenance or plasticity in inflammatory environments. This observation is particularly intriguing considering the previously observed inverse relationship between *Tcf7* and *Rorc* expression along the pseudotime trajectory. This suggests a dynamic interplay between the two transcription factors during Th17 cell differentiation and fate determination.

In contrast, the *Rorc* motif was strongly enriched within the Th17 cell cluster, confirming its already established role as the master transcription factor of Th17 cells (Hall et al., 2022). However, the motif accessibility of RORγT was also high in the Th1 cluster, hinting at transcriptional plasticity or a shared developmental pathway between Th1 and Th17 cells (Bhaumik & Basu, 2017). This finding correlates with the established role that T helper cells have the ability to exhibit plasticity in inflammatory conditions where they adapt to their environment and acquire characteristics of another cell type (Huber et al., 2017). The presence of RORγT motifs in Th1-like populations supports this model of Th17-to-Th1 transition and/or vice versa, which has been documented in various autoimmune and inflammatory disease contexts (Kamali et al., 2019).

In summary, these data support a model in which Th17 cells in the kidney possess a distinct regulatory identity, which may be affected by the local microenvironment or be driven by sustained exposure to antigens in the inflamed kidney. Furthermore, the findings suggest that the transcription factors RORγT and TCF-1 may not act alone, but as a part of a complex network wherein they affect Th17 cell function and fate together in an environment dependent manner.

4.2 Functional *in vivo* analysis

4.2.1 Increased expression of IL-10 in Th17 cells of cGN induced mice

Using a Th17-specific *Tcf7* knock-out mouse model the role of TCF-1 in maintaining the Th17 cell population was revealed through the reduced numbers of YFP^+ cells in the *Tcf7* knock-out group (Figure 18). The pathogenic role of Th17 cells in autoimmune kidney diseases had already been established (Krebs et al., 2020). Therefore, the significant reduction in renal Th17 cells, suggests that TCF-1 plays an important role in maintaining Th17 cell populations at sites of inflammation. This observation is further strengthened with the finding that the *Tcf7* knock-out group had a reduced disease severity when compared to the control group (Figure 17). Previous studies have shown that TCF-1 inhibits IL-17 gene expression and therefore controls the function of Th17 cells (Zhang et al., 2018). This would explain the reduced disease severity in the knock-out group.

Effector functions of Th17 cells are mainly mediated by the production of the pro-inflammatory cytokine IL-17 (Yasuda et al., 2019). While this is the main cytokine produced by Th17 cells, the YFP^+ cells in the *Tcf7* knock-out mice exhibited a significant increase in the expression of the anti-inflammatory cytokine IL-10 (Figure 19). This finding implies that in the absence of TCF-1, Th17 cells may undergo a phenotypic switch toward an anti-inflammatory or regulatory role. Such a shift could directly contribute to the observed attenuation of cGN pathology, as IL-10 is known to suppress inflammation and mediate tissue repair (Ip et al., 2017).

In contrast to the distinct changes within the $CD4^+YFP^+$ population, the overall cytokine expression profiles in the total $CD4^+$ and $CD4^+YFP^-$ populations did not exhibit significant differences between experimental groups (Figure 19). This indicates that the effects seen in the disease severity are a result of the *Tcf7* deletion in the IL17A-producing cells, stem from the Th17 cell population in the kidney. The specificity of these changes suggests a pivotal role of TCF-1 in modulating Th17 cell phenotype and function in cGN.

While no significant changes were observed in the albumin/creatinine ratio, the histological reduction in glomerular crescents provides a more sensitive measure of disease severity in the cGN model. This discrepancy between clinical and histological parameters is a limiting factor that may suggest a potential involvement of non-Th17-mediated mechanisms in the disease process. Nevertheless, the histological evidence aligns with the immunological findings, supporting a protective role for *Tcf7* deletion in the context of cGN.

The observed reduction in Th17 cells and their shift toward an IL-10-producing phenotype suggests a dual role for TCF-1 in promoting both the maintenance and pathogenicity of Th17 cells. This aligns with previous studies indicating that TCF-1 is essential for the development of effector T cell subsets (Gounari & Khazaie, 2022).

In summary, the functional analyses conducted using FACS identify TCF-1 as a critical regulator of Th17 cell function in the kidney, with its absence resulting in reduced Th17 cell numbers and a shift toward an anti-inflammatory phenotype.

4.2.2 Reduced expression of IL-10 in Th17 cells in duodenitis induced mice

In order to understand whether the functional role of TCF-1 is organ-specific, the same analyses conducted in the kidney were also conducted in the gut using the anti-CD3 induced duodenitis model.

In the anti-CD3-induced duodenitis model, no significant differences in disease severity were observed between the *Tcf7* knock-out and control groups across multiple histological parameters (Figure 20). This is a contrast compared to the findings in the kidney under inflammatory conditions (Figure 17), suggesting a kidney-specific role for *Tcf7* in modulating inflammation.

Another contrasting observation in the gut, is the significantly increased number of Th17 cells in the *Tcf7* knock-out mouse line in the gut (Figure 21). This indicates that the regulatory role TCF-1 plays in Th17 cells is dependent on the tissue microenvironment. However, no

correlation was seen between the disease severity and the increased number of Th17 cells, indicating that the Th17 cells may not be as involved in inflammation in the duodenum when compared to the kidney, even though studies have shown that Th17 cells are pathogenic in the gut in inflammatory conditions (Cao et al., 2023).

Cytokine analysis from the duodenum (Figure 22) further highlighted tissue-specific differences in Th17 cell function. Contradictory to the cGN model, where the deletion of *Tcf7* led to increased IL-10 production within the Th17 cell population, the duodenitis model displayed a significantly reduced IL-10 expression in this population. This finding indicates that Th17 cells in the duodenum fail to adopt an anti-inflammatory phenotype in the absence of TCF-1. This reduction in IL-10 expression along with the increased IL-17A expression within the total $CD4^+$ population, may be a contributing factor to the unchanged disease severity despite the increased Th17 cell numbers.

While *Tcf7* deficiency promotes a shift to an anti-inflammatory Th17 phenotype in the kidney, this regulatory shift is absent in the duodenum. Instead, Th17 cells in the *Tcf7* knock-out group in duodenitis appear to retain a predominantly pro-inflammatory phenotype, characterised by increased IL17A and reduced IL-10 expression.

Factors such as local cytokine milieu, antigenic stimuli, and tissue-resident cell interactions could be responsible for the different functional conditions of Th17 cells (Lee et al., 2012; Stockinger & Omenetti, 2017). In the kidney, where inflammation is driven by factors such as immune complex deposition and complement activation (Kesarwani et al., 2024), the absence of the transcription factor TCF-1 seems to limit Th17 cell pathogenicity and promote an anti-inflammatory phenotype. In contrast, the intestine's immune system, which is influenced by other factors such as continuous exposure to commensal microbes or dietary antigens (Light & Nagler, 2024), may regulate Th17 cell responses in a TCF-1 independent manner, maintaining their pro-inflammatory phenotype even in the absence of TCF-1.

4.3 Whole kidney scRNA-seq analysis

4.3.1 High expression of IL-10 receptors in endothelial cells

Having observed the IL-10 cytokine expression in renal leukocytes of the transgenic mice, a whole kidney scRNA-seq analysis was conducted to look for any interactions of the leukocytes with other cell types in the kidney. The proportional shifts seen in certain immune and structural cell types between control and cGN mice reflects the hallmark pathological features of cGN (Figure 23B) (Jennette & Thomas, 2001). The increased number of T cells and myeloid cells reflects the established roles of immune cells in driving inflammation and tissue injury in cGN. In contrary, the reduced amount of some structural cells such as tubular epithelial cells is most likely caused by the tissue damage and loss of functional units associated with cGN (Fujita et al., 2015). The increase in the amount of podocytes in the cGN group is noteworthy. During cGN conditions a loss or reduced number of podocytes would be expected. However, the increase in podocytes could suggest another function of these cells. A study using transgenic mice has observed an enrichment of progenitor-like or parietal epithelial cells in renal injury models that exhibit podocyte-like phenotypes (Lasagni et al., 2015). This study points towards the occurrence of podocyte regeneration through podocyte-like cells to counteract the tissue damage caused during inflammation.

Using CellChat DB (Jin et al., 2021) the intracellular signalling networks based on the ligand-receptor expression profiles were reconstructed. The concept of the highly complexly coordinated adaptive immune responses in cGN were revealed in the outgoing signalling pathway analysis of T lymphocytes (Figure 24A), for example the outgoing signalling pathway was enriched with B cells and other pathways associated with immune activation and lymphocyte crosstalk. However, the outgoing signalling pathways point towards both pro-inflammatory and regulatory functions. This suggests that the role of T cells may both cause the inflammation and aid in the resolution. The aid in resolution could be associate with the tissue adaptation characteristics of T cells wherein the pathogenic T cells may

transdifferentiate into cells with anti-inflammatory roles to ameliorate the disease outcome (Gagliani et al., 2015).

Endothelial cells have an established role in leukocytes adhesion and transmigration action as central mediators of immune cell recruitment and activation (Amersfoort et al., 2022). Therefore, the outgoing signalling pathways of endothelial cells were investigated (Figure 24B). The analysis revealed a broad range of outgoing pathways towards proliferating and myeloid cells as well as both T and B cells, reinforcing the role of endothelial cells in the immune response (Shao et al., 2020). The outgoing pathways analysis could also hint towards an immunomodulatory function of the endothelial cells in cGN conditions, for example by contributing to cytokine production which could either aid the inflammation or the resolution of the disease in the kidney.

Another noteworthy observation is the expression of IL-10 receptor subuntis in the kidney (Figure 24C). Since the functional analysis revealed a higher expression of IL-10 and YFP^+ cells in cGN conditions (Figure 19C) the expression of IL-10 receptors was investigated. The *Il10ra* gene, which encodes the ligand-binding alpha chain of the IL-10 receptor, was mainly highly expressed in T cells and myeloid cells. These cell types are usually targeted by an IL-10 driven anti-inflammatory immune response (Maynard & Weaver, 2008). This suggests that these cell populations respond to an IL-10 driven anti-inflammatory response under cGN conditions, which limits tissue damage thus ameliorating the disease outcome.

In contrast, the gene that encodes the beta chain of the IL-10 receptor subunits, *Il10rb*, is expressed more widely across all renal cell types but shows very high expression in endothelial cells. The gene *Il10rb* is not only associated with the IL-10 receptor family but also with other class II cytokine receptors such as IL-22R and IL-26R (Donnelly et al., 2004). This suggests that the renal endothelial cells interact or respond with multiple cytokines under cGN conditions, potentially aiding in an anti-inflammatory response. However, the low expression level of *Il10ra* observed in endothelial cells suggests an absence or limitation of the IL-10 signalling mechanism within these cells since both the *Il10ra* and *Il10rb* subunits are required

for an IL-10 driven response (Shouval et al., 2014). Nevertheless, there could be some other unknown mechanisms that might upregulate *Il10ra* in endothelial cells under certain conditions triggering an IL-10 signalling response. On the other hand, the sole presence of *Il10rb* in endothelial cells could point towards an IL-10-independent function of *Il10rb* or to complex heterodimeric signalling pathways involving other cytokines in cGN. The improved disease outcome observed in the *Tcf7* knock-out mice and the increased expression of IL-10 in Th17 cells in these mice could also suggest a blockage or limitation of the IL-10 signalling pathway by the transcription factor TCF-1 in cGN conditions. Alternatively, it could also suggest that the knock-out of TCF-1 in Th17 cells allows more Th17 cells to transdifferentiate into IL-10 producing T cells which could be Th1 or Treg cells. Additionally, the increased presence of *Il10rb* in endothelial cells may suggest that these cells could be targets for an anti-inflammatory response which would aid vascular homeostasis and tissue repair.

Conclusion

In summary, this study shows that the transcription factor TCF-1 plays a negative regulatory role in the plasticity of Th17 cells since the absence of the transcription factor in Th17 cells results in a higher expression of IL-10 of YFP^+ cells in cGN mice. This suggests that in the absence of TCF-1, Th17 cells are able to transdifferentiate into IL-10 producing cells resulting in an anti-inflammatory response improving the disease outcome in mice. However, the exact mechanism of this phenomenon remains to be discovered.

In order to gain a deeper understanding of the role of TCF-1 in the plasticity of Th17 cells and IL-10 cytokine production in cGN. The single cell and single nucleus analyses conducted with the *Il17A*^{cre} *x R26*^{eYFP} mice also need to be conducted with *Tcf7*^{flox} x *Il17A*^{cre} *x R26*^{eYFP} mice as well and the datasets need to be compared for any differences in the differential expressions. Additionally, to confirm whether the higher IL-10 cytokine expression and the improved disease outcome is a result of the TCF-1 knock-out in the mice more *in vivo* experiments need to be conducted. An experiment that could be conducted would be to treat both mice lines, *Il17A*^{cre} *x R26*^{eYFP} and *Tcf7*^{flox} x *Il17A*^{cre} *x R26*^{eYFP}, with anti-IL-10. This experiment would follow the same procedure as the previously conducted trials in this study. If the higher IL-10 cytokine production is responsible for the previously observed improved disease outcome, it would be expected to observe no more difference in the disease outcome. This would confirm that the absence of TCF-1 within Th17 cells improves the disease outcome.

This finding could be used to develop a new therapeutic approach in cGN patients. For example, if further experiments reveal that an increased IL-10 expression leads to a better disease outcome, augmenting the IL-10 signalling in patients could be a viable therapeutic strategy. Additionally, uncovering the mechanism responsible for the tissue adaptation process that enables the transdifferentiation of Th17 cells can also be used to investigate further therapeutic approaches. Even though Th17 cells are known to cause tissue injury under cGN conditions, their plasticity might have the opposite effect. Being able control the plasticity of

Th17 cells could result in a therapeutic strategy that targets Th17 cells by enabling them to transdifferentiate into cells that trigger an anti-inflammatory response in cGN patients.

References

Acosta-Rodriguez, E. V., Rivino, L., Geginat, J., Jarrossay, D., Gattorno, M., Lanzavecchia, A., Sallusto, F., & Napolitani, G. (2007). Surface phenotype and antigenic specificity of human interleukin 17–producing T helper memory cells. *Nature immunology*, *8*(6), 639-646.

Adams, N. M., Grassmann, S., & Sun, J. C. (2020). Clonal expansion of innate and adaptive lymphocytes. *Nature Reviews Immunology*, *20*(11), 694-707.

Agalioti, T., Cortesi, F., & Gagliani, N. (2023). TH17 cell immune adaptation. *Current Opinion in Immunology*, *83*, 102333.

Akitsu, A., & Iwakura, Y. (2018). Interleukin-17-producing γδ T (γδ17) cells in inflammatory diseases. *Immunology*, *155*(4), 418-426.

Al Mushafi, A., Ooi, J. D., & Odobasic, D. (2021). Crescentic glomerulonephritis: pathogenesis and therapeutic potential of human amniotic stem cells. *Frontiers in Physiology*, *12*, 724186.

Amersfoort, J., Eelen, G., & Carmeliet, P. (2022). Immunomodulation by endothelial cells—partnering up with the immune system? *Nature Reviews Immunology*, *22*(9), 576-588.

Andersen, M. H., Schrama, D., Thor Straten, P., & Becker, J. C. (2006). Cytotoxic T cells. *Journal of Investigative Dermatology*, *126*(1), 32-41.

Arnovitz, S., Mathur, P., Tracy, M., Mohsin, A., Mondal, S., Quandt, J., Hernandez, K. M., Khazaie, K., Dose, M., & Emmanuel, A. O. (2022). Tcf-1 promotes genomic instability and T cell transformation in response to aberrant β-catenin activation. *Proceedings of the National Academy of Sciences*, *119*(32), e2201493119.

Arpin, C., Dechanet, J., Van Kooten, C., Merville, P., Grouard, G., Brière, F., Banchereau, J., & Liu, Y.-J. (1995). Generation of memory B cells and plasma cells in vitro. *Science*, *268*(5211), 720-722.

Awasthi, A., Carrier, Y., Peron, J. P., Bettelli, E., Kamanaka, M., Flavell, R. A., Kuchroo, V. K., Oukka, M., & Weiner, H. L. (2007). A dominant function for interleukin 27 in generating interleukin 10–producing anti-inflammatory T cells. *Nature immunology*, *8*(12), 1380-1389.

Basha, G., Omilusik, K., Chavez-Steenbock, A., Reinicke, A. T., Lack, N., Choi, K. B., & Jefferies, W. A. (2012). A CD74-dependent MHC class I endolysosomal cross-presentation pathway. *Nature immunology*, *13*(3), 237-245.

Basu, S., Campbell, H. M., Dittel, B. N., & Ray, A. (2010). Purification of specific cell population by fluorescence activated cell sorting (FACS). *Journal of visualized experiments: JoVE*(41), 1546.

Becker, C., Fantini, M., & Neurath, M. (2006). High resolution colonoscopy in live mice. *Nature protocols*, *1*(6), 2900-2904.

Bhaumik, S., & Basu, R. (2017). Cellular and molecular dynamics of Th17 differentiation and its developmental plasticity in the intestinal immune response. *Frontiers in immunology*, *8*, 241885.

Bohmer, F. (1865). Zur pathologischen, Anatomie der Meningitis cerebromedularis epidemia. *Aerztl. Intelligenzb.(Munchen)*, *12*, 539-550.

Brenner, M. B., McLean, J., Dialynas, D. P., Strominger, J. L., Smith, J. A., Owen, F. L., Seidman, J., Ip, S., Rosen, F., & Krangel, M. S. (1986). Identification of a putative second T-cell receptor. *Nature*, *322*(6075), 145-149.

Butler, A., Hoffman, P., Smibert, P., Papalexi, E., & Satija, R. (2018). Integrating single-cell transcriptomic data across different conditions, technologies, and species. *Nature biotechnology*, *36*(5), 411-420.

Cao, H., Diao, J., Liu, H., Liu, S., Liu, J., Yuan, J., & Lin, J. (2023). The pathogenicity and synergistic action of Th1 and Th17 cells in inflammatory bowel diseases. *Inflammatory Bowel Diseases*, *29*(5), 818-829.

Cao, J., Spielmann, M., Qiu, X., Huang, X., Ibrahim, D. M., Hill, A. J., Zhang, F., Mundlos, S., Christiansen, L., & Steemers, F. J. (2019). The single-cell transcriptional landscape of mammalian organogenesis. *Nature*, *566*(7745), 496-502.

Cătană, C.-S., Neagoe, I. B., Cozma, V., Magdaş, C., Tăbăran, F., & Dumitraşcu, D. L. (2015). Contribution of the IL-17/IL-23 axis to the pathogenesis of inflammatory bowel disease. *World journal of gastroenterology: WJG*, *21*(19), 5823.

Chebotareva, N. V., Vinogradov, A. A., Gindis, A. A., Bobkova, I. N., Cao, W., & Lysenko, L. V. (2020). The balance of proinflammatory cytokines and Treg cells in chronic glomerulonephritis. *Terapevticheskii arkhiv*, *92*(6), 46-52.

Chen, P., & Tang, X. (2021). Gut microbiota as regulators of Th17/Treg balance in patients with myasthenia gravis. *Frontiers in immunology*, *12*, 803101.

Cooper, M. D., Peterson, R. D., South, M. A., & Good, R. A. (1966). The functions of the thymus system and the bursa system in the chicken. *The Journal of experimental medicine*, *123*(1), 75-102.

Coulter, F., Parrish, A., Manning, D., Kampmann, B., Mendy, J., Garand, M., Lewinsohn, D. M., Riley, E. M., & Sutherland, J. S. (2017). IL-17 production from T helper 17, mucosal-associated invariant T, and γδ cells in tuberculosis infection and disease. *Frontiers in immunology*, *8*, 1252.

Couser, W. G. (1988). Rapidly progressive glomerulonephritis: classification, pathogenetic mechanisms, and therapy. *American journal of kidney diseases*, *11*(6), 449-464.

Crowley, S. D., Navar, L. G., Prieto, M. C., Gurley, S. B., & Coffman, T. M. (2024). Kidney Renin–Angiotensin System: Lost in a RAS Cascade. *Hypertension*, *81*(4), 682-686.

Cruvinel, W. d. M., Mesquita Júnior, D., Araújo, J. A. P., Catelan, T. T. T., Souza, A. W. S. d., Silva, N. P. d., & Andrade, L. E. C. (2010). Immune system: Part I. Fundamentals of innate immunity with emphasis on molecular and cellular mechanisms of inflammatory response. *Revista brasileira de reumatologia*, *50*, 434-447.

Dardalhon, V., Awasthi, A., Kwon, H., Galileos, G., Gao, W., Sobel, R. A., Mitsdoerffer, M., Strom, T. B., Elyaman, W., & Ho, I.-C. (2008). Interleukin 4 inhibits TGF-β-induced-Foxp3+ T cells and generates, in combination with TGF-β, Foxp3− effector T cells that produce interleukins 9 and 10. *Nature immunology*, *9*(12), 1347.

de Wit, J., Al-Mossawi, M. H., Hühn, M. H., Arancibia-Cárcamo, C. V., Doig, K., Kendrick, B., Gundle, R., Taylor, P., Mcclanahan, T., & Murphy, E. (2016). RORγt inhibitors suppress TH17 responses in inflammatory arthritis and inflammatory bowel disease. *Journal of Allergy and Clinical Immunology*, *137*(3), 960-963.

Deets, K. A., & Vance, R. E. (2021). Inflammasomes and adaptive immune responses. *Nature immunology*, *22*(4), 412-422.

Delves, P. J., & Roitt, I. M. (2000). The immune system. *New England journal of medicine*, *343*(1), 37-49.

Donnelly, R. P., Sheikh, F., Kotenko, S. V., & Dickensheets, H. (2004). The expanded family of class II cytokines that share the IL-10 receptor-2 (IL-10R2) chain. *Journal of leukocyte biology*, *76*(2), 314-321.

Enk, L. U., Hellmig, M., Riecken, K., Kilian, C., Datlinger, P., Jauch-Speer, S. L., Neben, T., Sultana, Z., Sivayoganathan, V., & Borchers, A. (2024). Targeting T cell plasticity in kidney and gut inflammation by pooled single-cell CRISPR screening. *Science Immunology*, *9*(96), eadd6774.

Escobar, G., Mangani, D., & Anderson, A. C. (2020). T cell factor 1: A master regulator of the T cell response in disease. *Science Immunology*, *5*(53), eabb9726.

Fujita, E., Nagahama, K., Shimizu, A., Aoki, M., Higo, S., Yasuda, F., Mii, A., Fukui, M., Kaneko, T., & Tsuruoka, S. (2015). Glomerular capillary and endothelial cell injury is associated with the formation of necrotizing and crescentic lesions in crescentic glomerulonephritis. *Journal of Nippon Medical School*, *82*(1), 27-35.

Gagliani, N., Vesely, M. C. A., Iseppon, A., Brockmann, L., Xu, H., Palm, N. W., De Zoete, M. R., Licona-Limón, P., Paiva, R. S., & Ching, T. (2015). Th17 cells transdifferentiate into regulatory T cells during resolution of inflammation. *Nature*, *523*(7559), 221-225.

Ghoreschi, K., Laurence, A., Yang, X.-P., Tato, C. M., McGeachy, M. J., Konkel, J. E., Ramos, H. L., Wei, L., Davidson, T. S., & Bouladoux, N. (2010). Generation of pathogenic TH17 cells in the absence of TGF-β signalling. *Nature*, *467*(7318), 967-971.

Ginsberg, C., & Ix, J. H. (2024). New insights into vitamin D metabolism in kidney disease and transplant. *American journal of kidney diseases*, *84*(4), 400-402.

Godfrey, D. I., Uldrich, A. P., McCluskey, J., Rossjohn, J., & Moody, D. B. (2015). The burgeoning family of unconventional T cells. *Nature immunology*, *16*(11), 1114-1123.

Golomb, S. M., Guldner, I. H., Zhao, A., Wang, Q., Palakurthi, B., Aleksandrovic, E. A., Lopez, J. A., Lee, S. W., Yang, K., & Zhang, S. (2020). Multi-modal single-cell analysis reveals brain immune landscape plasticity during aging and gut microbiota dysbiosis. *Cell Reports*, *33*(9).

Gounari, F., & Khazaie, K. (2022). TCF-1: a maverick in T cell development and function. *Nature immunology*, *23*(5), 671-678.

Hall, J. A., Pokrovskii, M., Kroehling, L., Kim, B.-R., Kim, S. Y., Wu, L., Lee, J.-Y., & Littman, D. R. (2022). Transcription factor RORα enforces stability of the Th17 cell effector program by binding to a Rorc cis-regulatory element. *Immunity*, *55*(11), 2027-2043. e2029.

Hamm, L. L., Nakhoul, N., & Hering-Smith, K. S. (2015). Acid-base homeostasis. *Clinical Journal of the American Society of Nephrology*, *10*(12), 2232-2242.

Harbour, S. N., Maynard, C. L., Zindl, C. L., Schoeb, T. R., & Weaver, C. T. (2015). Th17 cells give rise to Th1 cells that are required for the pathogenesis of colitis. *Proc Natl Acad Sci U S A*, *112*(22), 7061-7066. https://doi.org/10.1073/pnas.1415675112

Harrington, L. E., Hatton, R. D., Mangan, P. R., Turner, H., Murphy, T. L., Murphy, K. M., & Weaver, C. T. (2005). Interleukin 17–producing CD4+ effector T cells develop via a lineage distinct from the T helper type 1 and 2 lineages. *Nature immunology*, *6*(11), 1123-1132.

Hirota, K., Duarte, J. H., Veldhoen, M., Hornsby, E., Li, Y., Cua, D. J., Ahlfors, H., Wilhelm, C., Tolaini, M., & Menzel, U. (2011). Fate mapping of IL-17-producing T cells in inflammatory responses. *Nature immunology*, *12*(3), 255-263.

Hoffman, W., Lakkis, F. G., & Chalasani, G. (2016). B cells, antibodies, and more. *Clinical Journal of the American Society of Nephrology*, *11*(1), 137-154.

Huber, S., Gagliani, N., O'Connor Jr, W., Geginat, J., & Caprioli, F. (2017). CD4+ T helper cell plasticity in infection, inflammation, and autoimmunity. *Mediators of Inflammation*, *2017*, 7083153.

Ip, W. E., Hoshi, N., Shouval, D. S., Snapper, S., & Medzhitov, R. (2017). Anti-inflammatory effect of IL-10 mediated by metabolic reprogramming of macrophages. *Science*, *356*(6337), 513-519.

Ivanov, I. I., McKenzie, B. S., Zhou, L., Tadokoro, C. E., Lepelley, A., Lafaille, J. J., Cua, D. J., & Littman, D. R. (2006). The orphan nuclear receptor RORγt directs the differentiation program of proinflammatory IL-17+ T helper cells. *Cell*, *126*(6), 1121-1133.

Jelkmann, W. (2011). Regulation of erythropoietin production. *The Journal of physiology*, *589*(6), 1251-1258.

Jennette, J., & Thomas, D. (2001). Crescentic glomerulonephritis. *Nephrology Dialysis Transplantation*, *16*(suppl_6), 80-82.

Jiang, W., Su, J., Zhang, X., Cheng, X., Zhou, J., Shi, R., & Zhang, H. (2014). Elevated levels of Th17 cells and Th17-related cytokines are associated with disease activity in patients with inflammatory bowel disease. *Inflammation Research*, *63*, 943-950.

Jin, S., Guerrero-Juarez, C. F., Zhang, L., Chang, I., Ramos, R., Kuan, C.-H., Myung, P., Plikus, M. V., & Nie, Q. (2021). Inference and analysis of cell-cell communication using CellChat. *Nature communications*, *12*(1), 1088.

Kamali, A. N., Noorbakhsh, S. M., Hamedifar, H., Jadidi-Niaragh, F., Yazdani, R., Bautista, J. M., & Azizi, G. (2019). A role for Th1-like Th17 cells in the pathogenesis of inflammatory and autoimmune disorders. *Molecular immunology*, *105*, 107-115.

Karmaus, P. W. F., Chen, X., Lim, S. A., Herrada, A. A., Nguyen, T. M., Xu, B., Dhungana, Y., Rankin, S., Chen, W., Rosencrance, C., Yang, K., Fan, Y., Cheng, Y., Easton, J., Neale, G., Vogel, P., & Chi, H. (2019). Metabolic heterogeneity underlies reciprocal fates of T(H)17 cell stemness and plasticity. *Nature*, *565*(7737), 101-105. https://doi.org/10.1038/s41586-018-0806-7

Kesarwani, V., Bukhari, M. H., Kahlenberg, J. M., & Wang, S. (2024). Urinary complement biomarkers in immune-mediated kidney diseases. *Frontiers in immunology*, *15*, 1357869.

Keshav, S., Chung, P., Milon, G., & Gordon, S. (1991). Lysozyme is an inducible marker of macrophage activation in murine tissues as demonstrated by in situ hybridization. *The Journal of experimental medicine*, *174*(5), 1049-1058.

Khan, O., Giles, J. R., McDonald, S., Manne, S., Ngiow, S. F., Patel, K. P., Werner, M. T., Huang, A. C., Alexander, K. A., & Wu, J. E. (2019). TOX transcriptionally and epigenetically programs CD8+ T cell exhaustion. *Nature*, *571*(7764), 211-218.

Kolodziejczyk, A. A., Kim, J. K., Svensson, V., Marioni, J. C., & Teichmann, S. A. (2015). The technology and biology of single-cell RNA sequencing. *Molecular cell*, *58*(4), 610-620.

Kortekaas Krohn, I., Aerts, J. L., Breckpot, K., Goyvaerts, C., Knol, E., Van Wijk, F., & Gutermuth, J. (2022). T-cell subsets in the skin and their role in inflammatory skin disorders. *Allergy*, *77*(3), 827-842.

Krebs, C. F., & Panzer, U. (2018). Plasticity and heterogeneity of Th17 in immune-mediated kidney diseases. *J Autoimmun*, *87*, 61-68. https://doi.org/10.1016/j.jaut.2017.12.005

Krebs, C. F., Reimers, D., Zhao, Y., Paust, H.-J., Bartsch, P., Nuñez, S., Rosemblatt, M. V., Hellmig, M., Kilian, C., & Borchers, A. (2020). Pathogen-induced tissue-resident memory TH17 (TRM17) cells amplify autoimmune kidney disease. *Science Immunology*, *5*(50), eaba4163.

Krebs, C. F., Turner, J. E., Paust, H. J., Kapffer, S., Koyro, T., Krohn, S., Ufer, F., Friese, M. A., Flavell, R. A., Stockinger, B., Steinmetz, O. M., Stahl, R. A., Huber, S., & Panzer, U. (2016). Plasticity of Th17 Cells in Autoimmune Kidney Diseases. *J Immunol*, *197*(2), 449-457. https://doi.org/10.4049/jimmunol.1501831

Kurts, C., von Vietinghoff, S., Krebs, C. F., & Panzer, U. (2025). Kidney immunology from pathophysiology to clinical translation. *Nature Reviews Immunology*, 1-17.

Lasagni, L., Angelotti, M. L., Ronconi, E., Lombardi, D., Nardi, S., Peired, A., Becherucci, F., Mazzinghi, B., Sisti, A., & Romoli, S. (2015). Podocyte regeneration driven by renal progenitors determines glomerular disease remission and can be pharmacologically enhanced. *Stem cell reports*, *5*(2), 248-263.

Lee, Y., Awasthi, A., Yosef, N., Quintana, F. J., Xiao, S., Peters, A., Wu, C., Kleinewietfeld, M., Kunder, S., & Hafler, D. A. (2012). Induction and molecular signature of pathogenic TH17 cells. *Nature immunology*, *13*(10), 991-999.

Lee, Y. K., Turner, H., Maynard, C. L., Oliver, J. R., Chen, D., Elson, C. O., & Weaver, C. T. (2009). Late developmental plasticity in the T helper 17 lineage. *Immunity*, *30*(1), 92-107.

Levin, A., Tonelli, M., Bonventre, J., Coresh, J., Donner, J.-A., Fogo, A. B., Fox, C. S., Gansevoort, R. T., Heerspink, H. J., & Jardine, M. (2017). Global kidney health 2017 and beyond: a roadmap for closing gaps in care, research, and policy. *The Lancet*, *390*(10105), 1888-1917.

Light, S. H., & Nagler, C. R. (2024). Regulation of immune responses to food by commensal microbes. *Immunological Reviews*, *326*(1), 203-218.

Linke, A., Tiegs, G., & Neumann, K. (2022). Pathogenic T-cell responses in immune-mediated glomerulonephritis. *Cells*, *11*(10), 1625.

Luckheeram, R. V., Zhou, R., Verma, A. D., & Xia, B. (2012). CD4+ T cells: differentiation and functions. *Journal of Immunology Research*, *2012*.

Ma, J., Wang, R., Fang, X., Ding, Y., & Sun, Z. (2011). Critical role of TCF-1 in repression of the IL-17 gene. *PLoS One*, *6*(9), e24768. https://doi.org/10.1371/journal.pone.0024768

Ma, J., Wang, R., Fang, X., & Sun, Z. (2012). beta-catenin/TCF-1 pathway in T cell development and differentiation. *J Neuroimmune Pharmacol*, *7*(4), 750-762. https://doi.org/10.1007/s11481-012-9367-y

Makino, Y., Kanno, R., Ito, T., Higashino, K., & Taniguchi, M. (1995). Predominant expression of invariant Vα14+ TCR α chain in NK1. 1+ T cell populations. *International immunology*, *7*(7), 1157-1161.

Mangani, D., Subramanian, A., Huang, L., Cheng, H., Krovi, S. H., Wu, Y., Yang, D., Moreira, T. G., Escobar, G., & Schnell, A. (2024). Transcription factor TCF1 binds to RORγt and orchestrates a regulatory network that determines homeostatic Th17 cell state. *Immunity*.

Martin, T., Mufson, E., & Mesulam, M. (1984). The light side of horseradish peroxidase histochemistry. *Journal of Histochemistry & Cytochemistry*, *32*(7), 793-793.

Maynard, C. L., & Weaver, C. T. (2008). Diversity in the contribution of interleukin-10 to T-cell-mediated immune regulation. *Immunological Reviews*, *226*(1), 219-233.

McGeachy, M. J., Bak-Jensen, K. S., Chen, Y., Tato, C. M., Blumenschein, W., McClanahan, T., & Cua, D. J. (2007). TGF-β and IL-6 drive the production of IL-17 and IL-10 by T cells and restrain TH-17 cell–mediated pathology. *Nature immunology*, *8*(12), 1390-1397.

Miller, J. F. (1961). Immunological function of the thymus. *The Lancet*, *278*(7205), 748-749.

Mills, K. H. (2023). IL-17 and IL-17-producing cells in protection versus pathology. *Nature Reviews Immunology*, *23*(1), 38-54.

Mohamed, O. N., Ibrahim, S. A., Saleh, R. K., Issa, A. S., Setouhi, A., Rabou, A. A. A., Mohamed, M. R., & Kamel, S. F. (2024). Clinicopathological characteristics and predictors of outcome of rapidly progressive glomerulonephritis: a retrospective study. *BMC nephrology*, *25*(1), 103.

Mukasa, R., Balasubramani, A., Lee, Y. K., Whitley, S. K., Weaver, B. T., Shibata, Y., Crawford, G. E., Hatton, R. D., & Weaver, C. T. (2010). Epigenetic instability of cytokine and transcription factor gene loci underlies plasticity of the T helper 17 cell lineage. *Immunity*, *32*(5), 616-627.

Nakayama, T., Hirahara, K., Onodera, A., Endo, Y., Hosokawa, H., Shinoda, K., Tumes, D. J., & Okamoto, Y. (2017). Th2 cells in health and disease. *Annual review of immunology*, *35*, 53-84.

Niroula, A., Sekar, A., Murakami, M. A., Trinder, M., Agrawal, M., Wong, W. J., Bick, A. G., Uddin, M. M., Gibson, C. J., & Griffin, G. K. (2021). Distinction of lymphoid and myeloid clonal hematopoiesis. *Nature medicine*, *27*(11), 1921-1927.

O'Garra, A., & Vieira, P. (2007). TH1 cells control themselves by producing interleukin-10. *Nature Reviews Immunology*, *7*(6), 425-428.

Odobasic, D., Gan, P.-Y., Summers, S. A., Semple, T. J., Muljadi, R. C., Iwakura, Y., Kitching, A. R., & Holdsworth, S. R. (2011). Interleukin-17A promotes early but attenuates established disease in crescentic glomerulonephritis in mice. *The American journal of pathology*, *179*(3), 1188-1198.

Ohkura, N., Hamaguchi, M., Morikawa, H., Sugimura, K., Tanaka, A., Ito, Y., Osaki, M., Tanaka, Y., Yamashita, R., & Nakano, N. (2012). T cell receptor stimulation-induced epigenetic changes and Foxp3 expression are independent and complementary events required for Treg cell development. *Immunity*, *37*(5), 785-799.

Ostmann, A., Paust, H.-J., Panzer, U., Wegscheid, C., Kapffer, S., Huber, S., Flavell, R. A., Erhardt, A., & Tiegs, G. (2013). Regulatory T cell–derived IL-10 ameliorates crescentic GN. *Journal of the American Society of Nephrology*, *24*(6), 930-942.

Palomares, O., Martin-Fontecha, M., Lauener, R., Traidl-Hoffmann, C., Cavkaytar, O., Akdis, M., & Akdis, C. (2014). Regulatory T cells and immune regulation of allergic diseases: roles of IL-10 and TGF-β. *Genes & Immunity*, *15*(8), 511-520.

Paquissi, F. C., & Abensur, H. (2021). The Th17/IL-17 axis and kidney diseases, with focus on lupus nephritis. *Frontiers in Medicine*, *8*, 654912.

Park, H., Li, Z., Yang, X. O., Chang, S. H., Nurieva, R., Wang, Y.-H., Wang, Y., Hood, L., Zhu, Z., & Tian, Q. (2005). A distinct lineage of CD4 T cells regulates tissue inflammation by producing interleukin 17. *Nature immunology*, *6*(11), 1133-1141.

Paust, H.-J., Song, N., De Feo, D., Asada, N., Tuzlak, S., Zhao, Y., Riedel, J.-H., Hellmig, M., Sivayoganathan, A., & Peters, A. (2023). CD4+ T cells produce GM-CSF and drive immune-mediated glomerular disease by licensing monocyte-derived cells to produce MMP12. *Science Translational Medicine*, *15*(687), eadd6137.

Perez, L. G., Kempski, J., McGee, H. M., Pelzcar, P., Agalioti, T., Giannou, A., Konczalla, L., Brockmann, L., Wahib, R., & Xu, H. (2020). TGF-β signaling in Th17 cells promotes IL-22 production and colitis-associated colon cancer. *Nature communications*, *11*(1), 2608.

Pot, C., Jin, H., Awasthi, A., Liu, S. M., Lai, C.-Y., Madan, R., Sharpe, A. H., Karp, C. L., Miaw, S.-C., & Ho, I. (2009). Cutting edge: IL-27 induces the transcription factor c-Maf, cytokine IL-21, and the costimulatory receptor ICOS that coordinately act together to promote differentiation of IL-10-producing Tr1 cells. *The Journal of Immunology*, *183*(2), 797-801.

Preissl, S., Fang, R., Huang, H., Zhao, Y., Raviram, R., Gorkin, D. U., Zhang, Y., Sos, B. C., Afzal, V., & Dickel, D. E. (2018). Single-nucleus analysis of accessible chromatin in developing mouse forebrain reveals cell-type-specific transcriptional regulation. *Nature neuroscience*, *21*(3), 432-439.

Qiu, X., Mao, Q., Tang, Y., Wang, L., Chawla, R., Pliner, H. A., & Trapnell, C. (2017). Reversed graph embedding resolves complex single-cell trajectories. *Nature methods*, *14*(10), 979-982.

Rasouli, J., Ciric, B., Imitola, J., Gonnella, P., Hwang, D., Mahajan, K., Mari, E. R., Safavi, F., Leist, T. P., & Zhang, G.-X. (2015). Expression of GM-CSF in T cells is increased in multiple sclerosis and suppressed by IFN-β therapy. *The Journal of Immunology*, *194*(11), 5085-5093.

Riedel, J.-H., Paust, H.-J., Krohn, S., Turner, J.-E., Kluger, M. A., Steinmetz, O. M., Krebs, C. F., Stahl, R. A., & Panzer, U. (2016). IL-17F promotes tissue injury in autoimmune kidney diseases. *Journal of the American Society of Nephrology*, *27*(12), 3666-3677.

Rossi, M., & Bot, A. (2013). The Th17 cell population and the immune homeostasis of the gastrointestinal tract. *International reviews of immunology*, *32*(5-6), 471-474.

Satija, R., Farrell, J. A., Gennert, D., Schier, A. F., & Regev, A. (2015). Spatial reconstruction of single-cell gene expression data. *Nature biotechnology*, *33*(5), 495-502.

Schmidt, T., Luebbe, J., Kilian, C., Riedel, J.-H., Hiekmann, S., Asada, N., Ginsberg, P., Robben, L., Song, N., & Kaffke, A. (2021). IL-17 receptor C signaling controls CD4+ Th17 immune responses and tissue injury in immune-mediated kidney diseases. *Journal of the American Society of Nephrology*, *32*(12), 3081-3098.

Schmidt, T., Luebbe, J., Paust, H.-J., & Panzer, U. (2018). Mechanisms and functions of IL-17 signaling in renal autoimmune diseases. *Molecular immunology*, *104*, 90-99.

Schnell, A., Littman, D. R., & Kuchroo, V. K. (2023). TH17 cell heterogeneity and its role in tissue inflammation. *Nature immunology*, *24*(1), 19-29.

Shao, Y., Saredy, J., Yang, W. Y., Sun, Y., Lu, Y., Saaoud, F., Drummer IV, C., Johnson, C., Xu, K., & Jiang, X. (2020). Vascular endothelial cells and innate immunity. *Arteriosclerosis, thrombosis, and vascular biology*, *40*(6), e138-e152.

Shevyrev, D., & Tereshchenko, V. (2020). Treg heterogeneity, function, and homeostasis. *Frontiers in immunology*, *10*, 3100.

Shi, Z., Das, S., Morabito, S., Miyoshi, E., & Swarup, V. (2022). Protocol for single-nucleus ATAC sequencing and bioinformatic analysis in frozen human brain tissue. *STAR protocols*, *3*(3), 101491.

Shouval, D. S., Biswas, A., Goettel, J. A., McCann, K., Conaway, E., Redhu, N. S., Mascanfroni, I. D., Al Adham, Z., Lavoie, S., & Ibourk, M. (2014). Interleukin-10

receptor signaling in innate immune cells regulates mucosal immune tolerance and anti-inflammatory macrophage function. *Immunity*, *40*(5), 706-719.

Soukou, S., Huber, S., & Krebs, C. F. (2021). T cell plasticity in renal autoimmune disease. *Cell and tissue research*, *385*(2), 323-333.

Spits, H., & Di Santo, J. P. (2011). The expanding family of innate lymphoid cells: regulators and effectors of immunity and tissue remodeling. *Nature immunology*, *12*(1), 21-27.

Stockinger, B., & Omenetti, S. (2017). The dichotomous nature of T helper 17 cells. *Nature Reviews Immunology*, *17*(9), 535-544.

Stuart, T., Srivastava, A., Madad, S., Lareau, C. A., & Satija, R. (2021). Single-cell chromatin state analysis with Signac. *Nature methods*, *18*(11), 1333-1341.

Su, H., Na, N., Zhang, X., & Zhao, Y. (2017). The biological function and significance of CD74 in immune diseases. *Inflammation Research*, *66*, 209-216.

Sun, L., Fu, J., & Zhou, Y. (2017). Metabolism controls the balance of Th17/T-regulatory cells. *Frontiers in immunology*, *8*, 1632.

Szabo, S. J., Kim, S. T., Costa, G. L., Zhang, X., Fathman, C. G., & Glimcher, L. H. (2000). A novel transcription factor, T-bet, directs Th1 lineage commitment. *Cell*, *100*(6), 655-669.

Tran, H. T. N., Ang, K. S., Chevrier, M., Zhang, X., Lee, N. Y. S., Goh, M., & Chen, J. (2020). A benchmark of batch-effect correction methods for single-cell RNA sequencing data. *Genome biology*, *21*(1), 12.

Treiner, E., Duban, L., Bahram, S., Radosavljevic, M., Wanner, V., Tilloy, F., Affaticati, P., Gilfillan, S., & Lantz, O. (2003). Selection of evolutionarily conserved mucosal-associated invariant T cells by MR1. *Nature*, *422*(6928), 164-169.

Turvey, S. E., & Broide, D. H. (2010). Innate immunity. *Journal of Allergy and Clinical Immunology*, *125*(2), S24-S32.

Valeri, M., & Raffatellu, M. (2016). Cytokines IL-17 and IL-22 in the host response to infection. *Pathogens and disease*, *74*(9), ftw111.

Van Loosdregt, J., & Coffer, P. J. (2018). The role of WNT signaling in mature T cells: T cell factor is coming home. *The Journal of Immunology*, *201*(8), 2193-2200.

Veldhoen, M., Hocking, R. J., Atkins, C. J., Locksley, R. M., & Stockinger, B. (2006). TGFβ in the context of an inflammatory cytokine milieu supports de novo differentiation of IL-17-producing T cells. *Immunity*, *24*(2), 179-189.

Wadwa, M., Klopfleisch, R., Adamczyk, A., Frede, A., Pastille, E., Mahnke, K., Hansen, W., Geffers, R., Lang, K., & Buer, J. (2016). IL-10 downregulates CXCR3 expression on Th1 cells and interferes with their migration to intestinal inflammatory sites. *Mucosal immunology*, *9*(5), 1263-1277.

Wang, F., Qi, Z., Yao, Y., Yu, G., Feng, T., Zhao, T., Xue, H. H., Zhao, Y., Jiang, P., Bao, L., & Yu, S. (2021). Exploring the stage-specific roles of Tcf-1 in T cell development and malignancy at single-cell resolution. *Cell Mol Immunol*, *18*(3), 644-659. https://doi.org/10.1038/s41423-020-00527-1

Weber, B. N., Chi, A. W.-S., Chavez, A., Yashiro-Ohtani, Y., Yang, Q., Shestova, O., & Bhandoola, A. (2011). A critical role for TCF-1 in T-lineage specification and differentiation. *Nature*, *476*(7358), 63-68.

Yang, X. O., Pappu, B. P., Nurieva, R., Akimzhanov, A., Kang, H. S., Chung, Y., Ma, L., Shah, B., Panopoulos, A. D., & Schluns, K. S. (2008). T helper 17 lineage differentiation is programmed by orphan nuclear receptors RORα and RORγ. *Immunity*, *28*(1), 29-39.

Yasuda, K., Takeuchi, Y., & Hirota, K. (2019). The pathogenicity of Th17 cells in autoimmune diseases. *Semin Immunopathol*, *41*(3), 283-297. https://doi.org/10.1007/s00281-019-00733-8

Yekelchyk, M., Li, X., Guenther, S., & Braun, T. (2024). Single-Nucleus ATAC-seq for Mapping Chromatin Accessibility in Individual Cells of Murine Hearts. In *Single Cell Analysis: Methods and Protocols* (pp. 245-257). Springer.

Yu, B., Zhang, K., Milner, J. J., Toma, C., Chen, R., Scott-Browne, J. P., Pereira, R. M., Crotty, S., Chang, J. T., & Pipkin, M. E. (2017). Epigenetic landscapes reveal transcription factors that regulate CD8+ T cell differentiation. *Nature immunology*, *18*(5), 573-582.

Zhang, J., He, Z., Sen, S., Wang, F., Zhang, Q., & Sun, Z. (2018). TCF-1 Inhibits IL-17 Gene Expression To Restrain Th17 Immunity in a Stage-Specific Manner. *J Immunol*, *200*(10), 3397-3406. https://doi.org/10.4049/jimmunol.1800193

Zhu, J., Yamane, H., Cote-Sierra, J., Guo, L., & Paul, W. E. (2006). GATA-3 promotes Th2 responses through three different mechanisms: induction of Th2 cytokine production, selective growth of Th2 cells and inhibition of Th1 cell-specific factors. *Cell research*, *16*(1), 3-10.

Zhu, Y., Wang, W., & Wang, X. (2015). Roles of transcriptional factor 7 in production of inflammatory factors for lung diseases. *Journal of translational medicine*, *13*, 1-13.

List of Abbreviations

Abbreviation	Meaning
µl	micro litre
A	Adenine
ANCA	Anti-neutrophil cytoplasmic antibodies
APC	Allophycocyanin
Aqua dest.	Distilled water (Aqua destillata)
ATAC	Assay for Transposase-Accessible Chromatin
B cell	B lymphocyte
BMC	Bone marrow cell
BSA	Bovine serum albumin
BUN	Blood urea nitrogen
BV421	Brilliant Violet 421
BV605	Brilliant Violet 605
BV650	Brilliant Violet 650
BV711	Brilliant Violet 711
C	Cytosine
C57BL	C57BL mouse strain
CCR6	C-C chemokine receptor type 6
CD	Cluster of Differentiation
cGN	Crescentic glomerulonephritis
cre	Cre recombinase
CXCR3	C-X-C chemokine receptor type 3
DNA	Deoxyribonucleic acid
DPBS	Dulbecco’s Phosphate Buffered Saline
dT	Deoxythymidine
DTT	Dithiothreitol
EDTA	Ethylenediaminetetraacetic acid
ELISA	Enzyme linked immunosorbent assay
ETOH	Ethanol
FACS	Flourescence activated cell sorting
FBS	Fetal bovine serum
FCS	Fetal calf serum

flox	flanked by LoxP
FOXP3	Forkhead box P3
G	Guanine
g	Grams
g	Relative centrifugal force
g/l	Grams per litre
GATA3	GATA-binding protein 3
GBM	Glomerular basement membrane
GEM	Gel bead in emulsion
GM-CSF	Granulocyte–macrophage colony-stimulating factor
GN	Glomerulonephritis
H_2O	Water
H_2O_2	Hydrogen peroxide
H_2SO_4	Sulfuric acid
HBSS	Hanks' Balanced Salt Solution
HCL	Hydrochloric acid
HEPES	4-(2-hydroxyethyl)-1-piperazineethanesulfonic acid
HRP	Horseradish peroxidase
IBD	Inflammatory bowel disease
IEL	Intraepithelial lymphocyte
Ig	Immunoglobulin
IL	Interleukin
IR	Infrared
LEF	Lymphoid enhancer-binding factor
MACS	Magnetic-activated cell sorting
MAIT	Mucosal-associated invariant T cell
MHC	Major histocompatibility complex
ml	Millilitre
mM	Millimolar
NaCl	Sodium chloride
$NaHPO_4$	Sodium mono hydrogen phosphate
ng/ml	Nanograms per millilitre
NTN	Nephrotoxic nephritis
PAS	Periodic acid–Schiff
PBS	Phosphate-buffered saline
PCR	Polymerase chain reaction

PE	Phycoerythrin
PFA	Paraformaldehyde
PMA	Phorbol 12-myristate 13-acetate
RM4-5	Clone designation for anti-CD4 monoclonal antibody
RNA	Ribonucleic acid
RPGN	Rapidly progressive glomerulonephritis
RT	Room temperature
RT	Reverse transcription
scRNA-seq	Single-cell RNA sequencing
T	Thymine
T cell	T lymphocyte
TAE	Tris–acetate–EDTA buffer
TCF-1	T cell factor 1
TGF-β	Transforming growth factor beta
Th1	T helper type 1 cell
Th17	T helper type 17 cell
Th2	T helper type 2 cell
TMB	3,3′,5,5′-Tetramethylbenzidine
TMBE	TMB substrate buffer
TNF-α	Tumor necrosis factor alpha
Treg	T regulatory cell
TSO	Template switch oligo
U	Uracil
UMAP	Uniform Manifold Approximation and Projection
UMI	Unique molecular identifier
UV	Ultraviolet
V450	Violet 450
WNT	Wingless/Integrated signaling pathway
YFP	Yellow flourescent protein
γδT cell	Gamma delta T cell

Curriculum Vitae

Excluded for data protection reasons.

List of Publications

Bartsch P, Kilian C, Hellmig M, Paust H-J, Borchers A, **Sivayoganathan A**, Enk L, Zhao Y, Shaikh N, Büttner H, Wong MN, Puelles VG, Wiech T, Flavell R, Huber TB, Turner J-E, Bonn S, Huber S, Gagliani N, Mittrücker H-W, Rohde H, Panzer U, Krebs C F (2022). Th17 cell plasticity towards a T-bet-dependent Th1 phenotype is required for bacterial control in Staphylococcus aureus infection. *PLoS Pathogens*, *18*(4), e1010430.

Engesser, J., Khatri, R., Schaub, D.P., Zhao, Y., Paust, H.J., Sultana, Z., Asada, N., Riedel, J.H., **Sivayoganathan, V**., Peters, A. and Kaffke, A., 2024. Immune profiling-based targeting of pathogenic T cells with ustekinumab in ANCA-associated glomerulonephritis.

Enk, L.U., Hellmig, M., Riecken, K., Kilian, C., Datlinger, P., Jauch-Speer, S.L., Neben, T., Sultana, Z., **Sivayoganathan, V**., Borchers, A. and Paust, H.J., 2024. Targeting T cell plasticity in kidney and gut inflammation by pooled single-cell CRISPR screening. *Science Immunology*, *9*(96), p.eadd6774.

Grünhagel B, Borggrewe M, Hagen SH, Ziegler SM, Henseling F, Glau L, Thiele RJ, Pujantell M, **Sivayoganathan V**, Padoan B, Claussen JM. Reduction of IFN-I responses by plasmacytoid dendritic cells in a longitudinal trans men cohort. Iscience. 2023 Nov 17;26(11).

Herrnstadt, G.R., Niehus, C.B., Ramcke, T., Hagenstein, J., Ehnold, L.I., Nosko, A., Warkotsch, M.T., Feindt, F.C., Melderis, S., Paust, H.J. and **Sivayoganathan, V**., 2023. The CCR6/CCL20 axis expands RORγt+ Tregs to protect from glomerulonephritis. *Kidney International*, *104*(1), pp.74-89.

Huang, M., Schnarre, A., Jauch-Speer, S.L., Lu, S., Liu, S., **Sivayoganathan, V**., Krebs, C.F., Huber, T.B., Zahner, G. and Tomas, N.M., 2023. Single-Nucleus Transcriptome Profiling of the Kidney Glomerulus Identifies Cell-Specific Responses in an Autoimmune Mouse Model of Membranous Nephropathy: SA-OR92. *Journal of the American Society of Nephrology*, *34*(11S), p.87.

Mueller, A., Zhao, Y., Cicek, H., Paust, H.J., **Sivayoganathan, A**., Linke, A., Wegscheid, C., Wiech, T., Huber, T.B., Meyer-Schwesinger, C. and Bonn, S., 2023. Transcriptional and clonal characterization of cytotoxic T cells in crescentic glomerulonephritis. *Journal of the American Society of Nephrology*, *34*(6), pp.1003-1018.

Paust, H.J., Song, N., De Feo, D., Asada, N., Tuzlak, S., Zhao, Y., Riedel, J.H., Hellmig, M., **Sivayoganathan, A**., Peters, A. and Kaffke, A., 2023. CD4+ T cells produce GM-CSF and drive immune-mediated glomerular disease by licensing monocyte-derived cells to produce MMP12. *Science Translational Medicine*, *15*(687), p. eadd6137

Sultana, Z., Khatri, R., Yousefi, B., Shaikh, N., Jauch-Speer, S.L., Schaub, D.P., Engesser, J., Hellmig, M., Piegsa, V., Hube, A. and **Sivayoganathan, V**., 2025. Spatiotemporal interaction of immune and renal cells controls glomerular crescent formation in autoimmune kidney disease. *Nature Immunology*, pp.1-12.

Eidesstattliche Erklärung/Affidavit

Eidesstattliche Versicherung:

Hiermit versichere ich an Eides statt, die vorliegende Dissertationsschrift selbst verfasst und keine anderen als die angegebenen Hilfsmittel und Quellen benutzt zu haben.

Sofern im Zuge der Erstellung der vorliegenden Dissertationsschrift generative Künstliche Intelligenz (gKI) basierte elektronische Hilfsmittel verwendet wurden, versichere ich, dass meine eigene Leistung im Vordergrund stand und dass eine vollständige Dokumentation aller verwendeten Hilfsmittel gemäß der Guten wissenschaftlichen Praxis vorliegt. Ich trage die Verantwortung für eventuell durch die gKI generierte fehlerhafte oder verzerrte Inhalte, fehlerhafte Referenzen, Verstöße gegen das Datenschutz- und Urheberrecht oder Plagiate.

Affidavit:

I hereby declare and affirm that this doctoral dissertation is my own work and that I have not used any aids and sources other than those indicated.

If electronic resources based on generative artificial intelligence (gAI) were used in the course of writing this dissertation, I confirm that my own work was the main and value-adding contribution and that complete documentation of all resources used is available in accordance with good scientific practice. I am responsible for any erroneous or distorted content, incorrect references, violations of data protection and copyright law or plagiarism that may have been generated by the gAI.

Hamburg, Oktober 2025

Ort, den | City, date

Unterschrift | Signature